Building in vitro human iPSC-derived motor neuron systems to explore cell autonomous mechanisms and modifiers of TDP-43 perturbation associated neurotoxicity

HARVARD
Kenneth C. Griffin

GRADUATE SCHOOL
OF ARTS AND SCIENCES

DISSERTATION ACCEPTANCE CERTIFICATE

The undersigned, appointed by the

Division of Medical Sciences

in the subject of Biological and Biomedical Sciences

have examined a dissertation entitled

Building in vitro human iPSC-derived motor neuron systems to explore cell autonomous mechanisms and modifiers of TDP-43 perturbation associated neurotoxicity

presented by Stanley P Gill Jr

candidate for the degree of Doctor of Philosophy and hereby certify that it is worthy of acceptance.

Signature: Wade Harper
Wade Harper (Oct 25, 2023 14:31 EDT)

Typed Name: Dr. J.Wade Harper

Signature: Mel Feany
Mel Feany (Oct 24, 2023 16:34 EDT)

Typed Name: Dr. Mel Feany

Signature: Rosalind A. Segal

Typed Name: Dr. Rosalind Segal

Signature: Susan Birren
Susan Birren (Oct 24, 2023 16:35 EDT)

Typed Name: Dr. Susan Birren

Date: October 24, 2023

This page intentionally left blank

Building in vitro human iPSC-derived motor neuron systems to explore cell autonomous mechanisms and modifiers of TDP-43 perturbation associated neurotoxicity

A dissertation presented

by

Stanley P Gill Jr

to

The Division of Medical Sciences

in partial fulfillment of the requirements

for the degree of

Doctor of Philosophy

In the subject of

Biological and Biomedical Sciences

Harvard University

Cambridge, Massachusetts

October 2023

Dissertation Advisors: Lee Rubin and Kevin Eggan Stanley P Gill Jr

Building in vitro human iPSC-derived motor neuron systems to explore cell autonomous mechanisms and modifiers of TDP-43 perturbation associated neurotoxicity

Abstract

Transactive Response DNA Binding Protein 43 (TDP-43) is a ubiquitously expressed nucleic acid transport and processing factor that is essential for normal cellular development and function. Disruptions to TDP-43 function in neurons, particularly in the form of aggregation in the cytoplasm, have been associated with the development of several neurodegenerative diseases, including Amyotrophic Lateral Sclerosis (ALS). Approximately 97% of ALS patients will develop hyper-phosphorylated, hyper-ubiquitinated inclusions of TDP-43 in spinal cord motor neurons. While experimental models of TDP-43 perturbation relevant to ALS have been actively studied by many groups, many of these models are non-human, non-neuronal, inefficient to generate, or a combination of those qualities. These shortcomings limit the efficacy of these cellular systems for use as platforms for future therapeutic development at scale. This dissertation describes the development of genetically engineered human induced pluripotent stem cell (iPSC)-derived motor neuron models of TDP-43 overexpression and mislocalization as well as implementation of these models to elucidate mechanisms of ALS-relevant neurodegenerative processes.

To begin, we demonstrate that these engineered motor neuron systems recapitulate key gain-of-function properties of TDP-43 perturbation upon induction, such as visible aggregation of TDP-43, re-localization of TDP-43 to the cytoplasm, and loss of cellular viability. We will then examine the physiologic effects of persistent cytoplasmic localization of TDP-43. Specifically, we will examine how cytoplasmic localization of TDP-43 changes the neuronal response to oxidative

stress as well as which transcriptomic pathways are modulated by this disease-associated re-localization. Furthermore, we will use similar assays to examine the effect of genetic knockout of a proposed modifier of TDP-43 neurotoxicity, Ataxin-2 (ATXN2). We will establish that ATXN2 knockout rescues the neurotoxic effect of TDP-43 overexpression as well as positively modulates the stress response of neurons to proteotoxic and oxidative stress.

In summary, this dissertation describes an efficient and expandable human iPSC-derived neuronal platform that provides insights to the mechanisms of neurodegeneration. These discoveries have the potential to be starting points for the design of future pharmacological and genetic treatments for ALS and other TDP-43 associated neurologic conditions.

Table of Contents

List of Figures

Chapter 1

Chapter 2

Chapter 3

Chapter 4

Appendix A (Supplementary Figures)

List of Tables

Acknowledgements

I would like to start by recognizing that this thesis doesn't happen without the support from everyone who is involved in any part of my life. To say it takes a village to raise a child (scientist) is truly an understatement; I have been extremely fortunate to have a lovely contingent of family, friends, teachers, mentors, and students that have helped this thesis come together. Even you, the person who is reading this work, who may not know who I am, is important to the story of this science and deserves to be recognized as such.

But since I don't know who you are and can't refer to you by name (sorry!), here's an incomplete listing of people I can talk about who deserve special recognition on the occasion of completing this scientific achievement.

Firstly, I'd like to thank my parents, Stanley (Sr.) and Miriam Gill. Their endless patience with my curiosity and perfectionism allowed me the space to get creative, make mistakes, and learn how to learn even if no one else around me wanted to do the thing I wanted to do. There was basically no way I was leaving their house without learning to think like an engineer and I'm very grateful for the subconscious notion they instilled in me that all things are systems, how a system works is important to know how to fix it, but not every system is logical. It really took me far in my personal and professional life to understand these things at a deep level. I would also like to thank my parents for introducing me to my younger siblings, Kyle and Lauren, who are different flavors of engineer than me, and, accordingly, different flavors of ridiculous. It has been an absolute treat watching all three of us grow together and I look forward to a future where we continue to squabble about equally inane premises as "a potato is a fruit, fight me" or holding decades long grudges over muffins or mac and cheese.

Here's also to my elementary, middle, and high school teachers, who I'm sure did not fully know what to do with this (often times, the only) black kid who was very energetic and took that competitive energy to the classroom because he was not athletic enough for the first 14 years of his life to feel physically empowered in a meaningful way. I imagine this must have been frustrating to some degree, but many of you did try (and succeed) at engaging with me and helping me focus and redirect that energy (big shoutout to my math and music teachers for that); I will forever appreciate that effort.

In my early school years, I found community with many fellows who had the capacity to be somewhat physical, but who would prefer to sit and nerd out about their own fantasies and interests. Some were about sports, some were about video games, some were about real history, some were about worlds based on other worlds that were a mix of the D&D 2nd edition monster manual and Star Wars. They all taught me an excitement for sharing an experience or a story and an uncontrollable desire for making it real for someone else. I wouldn't know for several years that this was likely a seed for my interest in science communication (and also Dungeon Master-ing and storytelling in general). For that and so much more, cheers to Erik, Scott, Emma, Trenton, Ryan, Tyler, Tim, Maria, Cameron, Nick, Brad, and Andrew for your lifetimes of friendship and support.

In 2010 I made the (some would say, bewildering), choice to move out of sunny Arizona to cold Massachusetts to do my undergraduate studies at MIT. I didn't have a proper winter coat my first winter, nor did I have an AC during the summer while living in a very humid brick building. I was ill prepared for the journey and survived off sheer force of will, Easy-Mac and whatever free food (except Pad Thai) that I could stumble into. It was there I learned that I could do hard things, and some things really did push me to my intellectual limits. Although there was quite a bit of darkness (literally and figuratively, I'm still not used to 3pm winter sunsets), I found fraternity

with a fraternity (Alpha Delta Phi's Lambda Phi Chapter, which I'm now proud to say recently transitioned to being a co-ed society), which was a consistent source of light and joy during my time in undergrad. For that I have to thank Jesus, Everett, Siraj, Brook, Bryan, Evan, Ryan, George, Andy, Alex, and Matt for everything from stairwell parties, all day south park binges, post-midnight food runs, and long bus rides for fried chicken.

From my MIT time I would also like to recognize my research mentors, Drs. Retsina Meyer, Daisuke Akazawa, Giovanni Traverso, and Andrew Bellinger, who took a chance on my undergraduate self who again, was very eager, but had no practical knowledge of how to be in a lab. Thank you for welcoming me into your research and teaching me the skills I needed to grow into being the scientist I am today.

After I graduated, before I started my new job at the Broad Institute (via Dana-Farber Cancer Institute, courtesy of Dr. William Hahn), I declared that a personal mission of mine was to make friends with my co-workers. Coming into working with Dr. Hahn's group and our close collaborators, the Broad's Genetics Perturbation Platform, with that mindset is the equivalent of knocking on a door to someone else's Thanksgiving party and being welcomed with drink, food, and open arms without question of where you came from. I couldn't have asked for a better place to train in becoming proficient in all things CRISPR, screening, tissue culture, assay development, and more. I'd like to acknowledge Drs. William Hahn, Paquita Vazquez, David Root, Glenn Cowley, and Colles Price for being my scientific mentors and advocates during my three years at Broad. A heartfelt thanks also goes to my many friends and colleagues in the lab, with whom I spent many days trading off DJ responsibilities in the tissue culture room while gushing about last weekend's Game of Thrones episode, shared nights in lab, threw many house parties with in Somerville back when it was cheaper to take an Uber Pool than to take the T, among other

shenanigans. It was truly a vibe being a crew of scientists in (mostly) their 20s and 30s trying to figure out how to live. For many adventures, and a music video, I thank Derek, Levi, Meghan, Matt, Jamie, Victor, Amy, Yenarae, Sasha, Grace, Will, Erin, Adrija, Andrew, and Gabe. Special thanks during my years at Broad also goes to my non-biologist roommate Sam, who I met when he started his PhD and gave a very good example of a graduate student that has good balance in their life (which encouraged me to go through with applying). I do not thank you for continuing to beat me at board games more often than I would like to admit, but I do treasure the many hours we spent as a crew with Sharon and Ningzhou doing pub trivia and playing those board games.

Another special honor from my post-MIT, pre-grad school goes to Mike Grenier, manager of the MIT Pubs, who, again, indulged my eagerness to contribute to community, and did not protest when I transcended from regular bar patron during trivia nights at the Thirsty Ear Pub to coordinator of the trivia festivities at the Thirsty Ear despite the fact that I was not yet a grad student. Running that show on and off stage for three years taught me how to find my voice and how to anticipate how people will interpret instructions, which turned out to be incredibly useful for things related to science like protocol writing and teaching. I'm also extremely thankful to Mike that he has allowed me to run the room from behind the bar by inviting me back as bar staff at both the Muddy Charles and The Thirsty Ear since the start of 2023. It is a full circle that I started studying for the GRE as a patron at the Muddy and now I'm writing part of my thesis there as staff.

For support during graduate school, I recognize the BBS Office: Anne, Danny, Kate, and Deirdre as well as the program faculty heads – Drs. Susan Dymecki, Tom Bernhardt, Davie Van Vactor, and Monica Colaiacovo - for just being a brick house of support for anything we wanted to do as a community. BBS is, in my opinion, one of the best run administrative units at Harvard

by a significant margin. Not enough credit is possible to give to these folks who give us the space to thrive while finding our way in science. When I accepted my offer to join BBS, I had no idea the depth of community that there was among the students and how welcoming it would feel. Even when I had struggles with the administrative beast of Harvard, I never had issues with BBS. I want to thank my main crew of cohort mates, Adrija (yes the same Adrija as a couple of paragraphs ago!), Irene, Alex, and Patrick; any student volunteer during my five total years with HPREP with a special shout out to Xavier, Marina, Eileen, Elizabeth, Leonard, and Gloria; the BBS Peer Mentors past and present with special thanks to my co-leads, Adrija and Han; and my co-committee members in the Therapeutics Graduate Program Steering Committee – Harry, Ben, Kim, Sean, Ahmad, Kyle, Morgan, and Hawa.

A big part of my graduate training, which BBS graciously gave me the space to do and the Therapeutics Program helped me coordinate, was an internship that I worked at Novartis Institutes for Biomedical Research. My time there was incredibly enriching and helped me solidify my career goals such that I can walk out of this PhD with a solid direction and a clear mind. Thank you, Matt, Reina, Benika, Jacob, Om, Zach, Bill, and everyone else from the Chemical Biology and Therapeutics team who supported our project or came to hang out for the happy hours. Your support for me at that time of my PhD meant more than you know.

At the lab and departmental level, I want to first thank my first advisor during my PhD Dr. Kevin Eggan. Your excitement and passion for science is infectious and always inspired me to get creative and do my best. From the former Eggan lab, I want to thank Ellen, Francesco, Irune, Kevin Smith, Dan, Aditi, Derek, Maura, and Joanie who were particularly helpful in the beginning of my scientific training. Secondly, I would like to extend gratitude to Dr. Lee Rubin for allowing me to join his group for the last bit of my PhD after the closure of the Eggan Lab. The Rubin lab really

went above and beyond to make me feel welcome, especially given the circumstances. For that I give special thanks to Kiwi, Will, Jane, Jiye, and Kelsey. I also extend special thanks to Kellie Liu, my undergraduate lab mentee who I had the pleasure of working with during my final full year to establish some of the final experiments of this work. Also in the Department of Stem Cell and Regenerative Biology, I had the pleasure of serving as the co-chair of our Diversity, Inclusion, Belonging and Equity committee. Despite its ups and downs, being a part of this group was an overall enlightening experience and I'm happy I was able to contribute at a high level. Many thanks and good luck to my co-chairs past and present, Sarah, Alana, Dani, and Ozge, for your prior or present effort in fighting the good fight for a more equitable and inclusive working environment.

Lastly, I give the final word of specifically named acknowledgement to my wife Ningzhou Shen. I won the lottery once by meeting you immediately before I applied to graduate school, and then won it again when I got accepted to a school that meant I didn't have to move away from you. I think I spent most of my luck there because you seem to do significantly better than me at games of chance, but I wouldn't have it any other way. Your support has been foundational in keeping me physically and mentally healthy during these years where I was hustling doing the work for this thesis. You are my forever partner, my teammate, my cheerleader who encourages me to spend money on taking care of myself rather than eating the expired food in our fridge, my occasional adversary at the board game table, and my love. I cannot thank you enough for that love and the opportunity to grow with you over the course of my PhD. I dedicate this thesis first to you, our cats Kiki and Ziggy, the memory of our hedgehog Arthur and our unborn child Alice, and our future adventures together.

To everyone (yes – even you, reader-who-I-might-not-know) thank you for being a part of this chapter of my life and thank you for appreciating these scientific discoveries. I hope you find what you need inside and outside of these pages.

This thesis is further dedicated to my great-great-great grandparents who lived in the age of slavery, and yet persevered to give all their descendants a drive to be excellent and build community that only got bigger with each generation. And finally, this work is dedicated to anyone who everyone who had to flex that resilience because the world's biases and prejudices about your heritage, color, or creed beat you down. I've felt that. I see you. I acknowledge how tired you are. We still matter. We must continue. We can do hard things!

"I dedicate this one right here to all my homies out there grindin', you know what I'm sayin', legally and illegally" – Lupe Fiasco, 2006

Chapter 1: Introduction

Amyotrophic Lateral Sclerosis (ALS)

Amyotrophic Lateral Sclerosis (ALS) – also known as Lou Gehrig's Disease or Motor Neuron Disease – is a rapidly progressing neurodegenerative disease that affects both upper (cortical) and lower (spinal cord) motor neurons. Patients often initially present with limb weakness, stiffness, and/or trouble speaking or swallowing that progresses into general paralysis and muscle wasting as the condition advances (Kiernan et al. 2011). This paralysis will progress until the patients are unable to speak, move or breathe without mechanical assistance. Most ALS patients will die from respiratory failure (Leigh et al. 2003; Wijesekera and Nigel Leigh 2009). The average survival time from diagnosis is approximately 2.67 years in North America (Xu et al. 2020a).

ALS is frequently billed as one of the top 5 most common neurodegenerative diseases alongside Alzheimer's Disease, Parkinson's Disease, Huntington's Disease, and Frontotemporal Dementia (FTD) (Lamptey et. al 2022). The mean age of onset is estimated to be anywhere from 40 – 63 years old depending on family history, with a slightly higher risk in men than women (Mehta et al. 2016; Xu et al. 2020a). ALS has an approximate global prevalence of 4 in 100,000 people (Xu et al. 2020a). Like the neurodegenerative conditions listed above, public awareness of ALS is quite high thanks to the visibility of some that were afflicted by the condition such as Lou Gehrig and Steven Hawking as well as initiatives such as the viral Ice Bucket Challenge in 2014 (Wicks 2014). However, there are only about 20 – 30,000 people in the US living with ALS at any given time (Mehta et al. 2022) compared to approximately 5 million patients with Alzheimer's (Hao and Friedman 2016). This qualifies ALS as a rare disease under the US Food and Drug Administration's (USFDA) Orphan Drug Act, which provides a variety of incentives for the development and approval of therapies indicated to treat the condition (Miller et al. 2021).

ALS is a heterogenous disease in its presentation and treatment regimens are highly personalized to the individual patient. Many pharmacological agents and assistive interventions can be employed to manage symptoms. Examples include anti-spasticity agents for limb stiffness such as baclofen (McClelland III et al. 2007), anticholinergics for excessive saliva production such as amitriptyline (Mercadante et al. 2023), motorized wheelchairs and/or limb braces for mobility, and voice banking so that the patient can continue to communicate vocally with the assistance of a computer after they lose the ability to efficiently speak. However, these symptomatic treatments are not disease-modifying.

There are currently seven USFDA approved drugs indicated for the treatment of ALS (Table 1.1). Three of these are alternative formulations of the same compound, Riluzole, which was the first drug approved for the condition in 1995 (Bensimon et al. 1994; Doble 1994). Of the remaining four, two are specifically indicated for the general treatment of ALS (Relyvrio (Paganoni et al. 2020a) and Radicava (Yoshino et al. 2006)), one – Qalsody – is an antisense oligonucleotide therapy specifically for *SOD1* mutant ALS (Smith et al. 2006), and the final drug – Nuedexta – is indicated for the treatment of pseudobulbar affect (frequent involuntary episodes of crying or laughing discordant with emotion that commonly occurs secondary to ALS and other neurologic conditions (Brooks et al. 2004; Green et al. 2018). Relyvrio and Qalsody were USFDA approved in 2022 and 2023 respectively. With the exception of Qalsody, which is only effective in ALS patients with an *SOD1* mutation which comprises only about 2% of all cases (Berdynski et. al 2022; Ling et al. 2013), the therapeutic mechanisms of the approved pharmacological interventions have yet to be fully elucidated. Although these treatments have been shown to be effective in increasing patient quality of life, none of them increase average patient survival for longer than 8 – 9 months (Paganoni et al. 2020b). There remains an unmet need to learn more

about the mechanisms of neurodegeneration associated with ALS so that a true disease-modifying therapy can be developed.

Table 2.1: Overview of the seven current pharmacological treatments for ALS

Compound(s)	Trade Name	Approval Year	Proposed Mechanism of Action
Riluzole	Rilutek	1995	Neurotoxicity blocker by inhibiting glutamatergic transmission by blocking presynaptic release of glutamate. Tiglutik is a thickened formulation for patients with difficulty swallowing the original oral pill formulation. Exservan is further optimized for patient delivery – it is an oral film placed on your tongue that will dissolve. All formats have similar pharmacology. Prolongs patient survival by 2 - 3 months on average (Bensimon et al. 1994; Doble 1994; Miller et al. 2012; Rothstein 1996; Wymer et al. 2023)
	Tiglutik	2018	
	Exservan	2019	
Dextromethorphan and Quinidine	Nuedexta	2010	Primarily indicated for the treatment of Pseudobulbar Effect, which occurs secondary to ALS in ~50% of patients. Dextromethorphan is a weak non-competitive NMDA-glutamate receptor antagonist; Quinidine Sulfate is a Cytochrome P450 inhibitor that increases dextromethorphan's bioavailability by blocking first-pass hepatic metabolism. Effectively suppresses episodes of situationally inappropriate emotion when no mood disorder is present. Also, may improve speech and/or have a positive impact on other bulbar functions - such as swallowing (Brooks et al. 2004; Fang et al. 2017; Green et al. 2018).
Edaravone	Radicava	2017 (IV), 2022 (Oral)	Reduces oxidative stress by scavenging free radicals. Reduces neuroinflammation. Reduces functional decline and improves patient quality of life but does not extend survival beyond treatment with Riluzole alone. (Abe et al. 2017; Cruz 2018; Johnson et al. 2022; Yoshino et al. 2006)
Sodium Penylbutyrate and Taurursodiol	Relyvrio	2022	Reduces neuronal cell death by lowering endoplasmic reticulum stress and mitochondrial dysfunction. Prolongs patient survival by about 6.5 months compared to Riluzole only treated placebo group (Del Signore et al. 2008; Kusaczuk 2019; Paganoni et al. 2020a; Paganoni et al. 2020b).
SOD1 Antisense Oligonucleotide	Qalsody/Tofersen	2023	Blocks pathogenic aggregation of SOD1 by reducing total SOD1 protein levels using an antisense oligonucleotide targeting *SOD1* mRNA. Only effective in *SOD1* Mutant patients (Blair 2023; Smith et al. 2006)

Furthermore, about 15% of ALS patients also experience degeneration of neurons in the prefrontal and temporal cortex, which may lead to a concurrent diagnosis of FTD (Ling et al. 2013; Ringholz et al. 2005). Many who study neurodegeneration have hypothesized that ALS and FTD are closely related conditions given this evidence of co-existence and the discovery of common genetic variants that are associated with the development of both conditions (Ling et al. 2013). Given this relationship, it stands to reason that understanding the mechanisms of neurodegeneration in ALS may also benefit therapeutic development for patients with FTD.

Genetic risk factors for ALS

There is no single distinct cause that drives the onset or progression of ALS. Broadly, ALS cases are classified as familial or sporadic. Roughly 10% of ALS cases are familial, usually following an autosomal dominant inheritance pattern (Ghasemi and Brown 2018; Laferriere and Polymenidou 2015). Within familial ALS, approximately 80% of cases can be explained by a mutation in one or more ALS-associated genes, the most common of which is *C9orf72* (40-50% of familial ALS cases) (Ghasemi and Brown 2018; Renton et al. 2011). The remaining 90% of ALS cases are sporadic, occurring without a family history. A genetic cause can be identified in about 10% of sporadic cases as well, with most cases remaining unexplained (Figure 1.1).

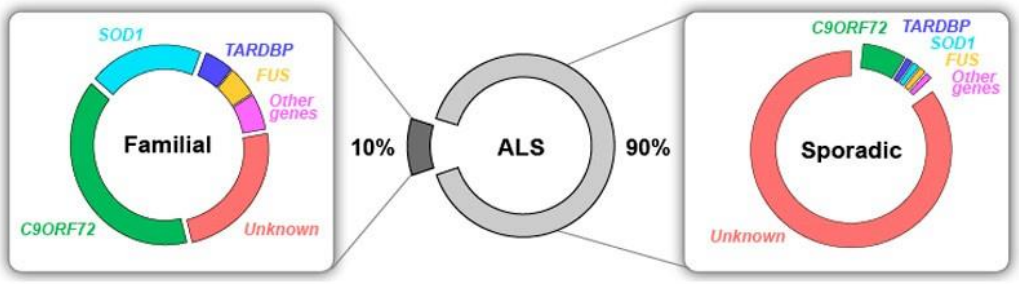

Figure 2.1: A Summary of the Genetics of ALS. Adapted from Laferriere and Polymenidou 2015.

At least 25 genes have been reproducibly associated with risk for ALS across several different functional areas including protein turnover, RNA processing, and cytoskeletal structure (Abel et al. 2012; Figure 1.2) While great strides have been made in the last 30 years to discover more genetic variants associated with risk for ALS, comparatively few studies have explored the mechanisms of why any given variant is pathogenic. Fewer still have hypothesized potential therapies for patients expressing these variants. This dissertation will focus on one ALS-associated gene in particular, *TARDBP*, which encodes Transactive Response DNA-binding Protein 43 (TDP-43).

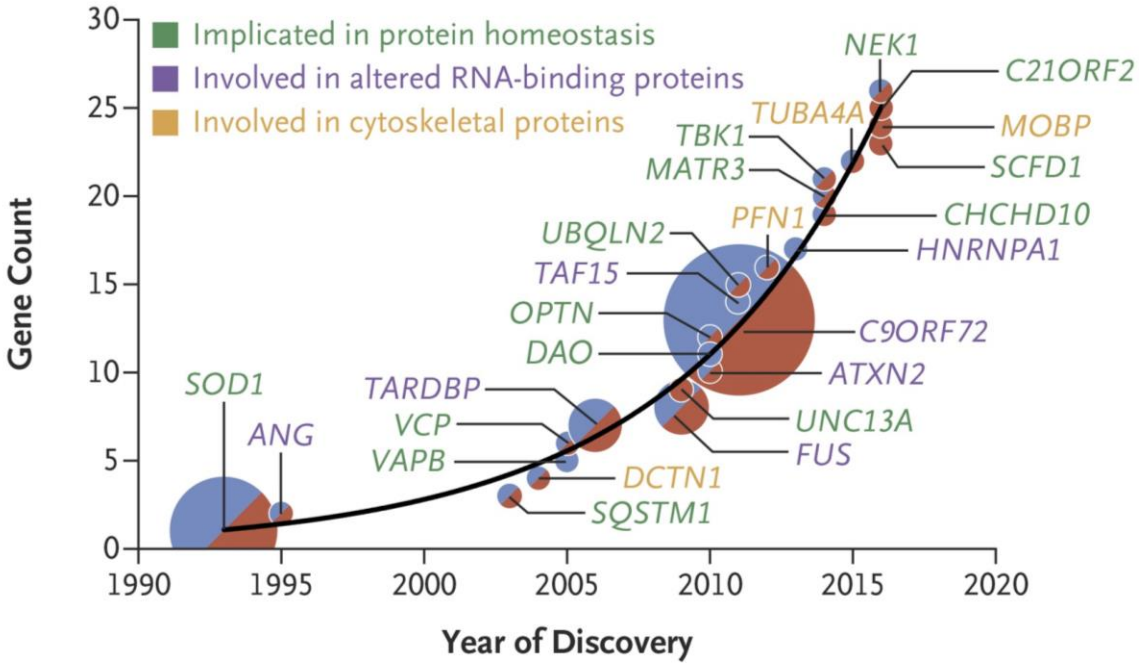

Figure 1.2: ALS Gene Discovery from 1990 – 2017. 25 genes are listed here across three different functional domains. Adapted from Brown and Al-Chalabi. 2017.

TDP-43 Structure and Function

TDP-43 was originally discovered as a transcriptional repressor that suppresses the expression of the gene *HIV-1* (Human immunodeficiency virus type 1 - Ou et al. 1995). It is now understood to be a ubiquitously expressed, multifunctional nucleic acid transport and processing

protein that is required for normal development (Buratti and Baralle. 2012; Kraemer et al. 2010). The protein contains a Nuclear Localization Sequence (NLS), a Nuclear Export Sequence (NES), two nucleic acid binding domains, and a C-terminal Glycine rich, relatively disordered region (Figure 1.3). Most of the clinically relevant TDP-43 mutations occur in this C-terminal disordered region (Buratti 2015).

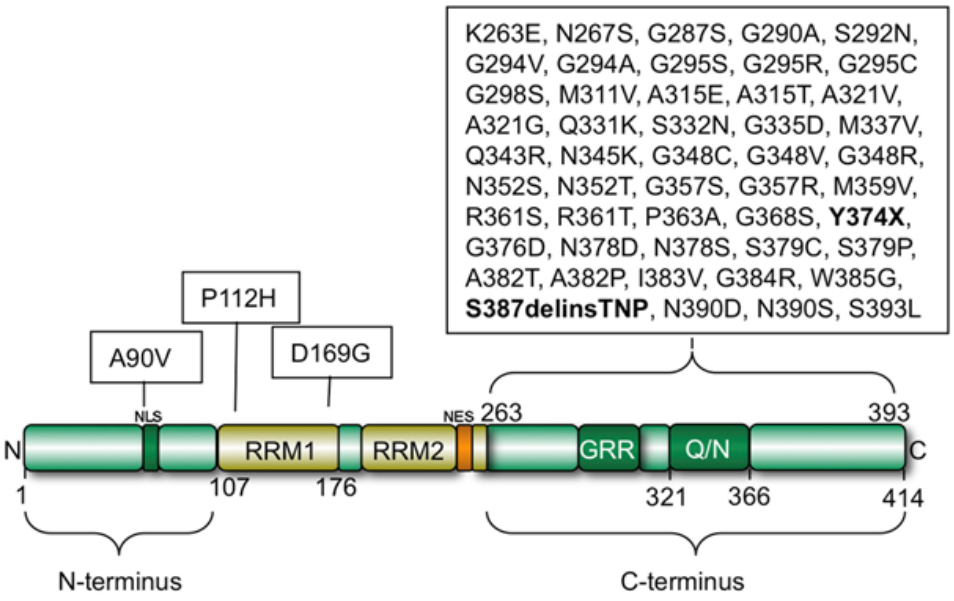

Figure 1.3: Structure of TDP-43 protein and known ALS patient mutations. RRM1 and RRM2 are the nucleic acid binding domains. Mutations are all missense mutations except for the bolded locations. Adapted from Buratti 2015.

Under normal conditions, TDP-43 is primarily localized to the nucleus, though a small amount will transiently be in the cytoplasm at any given moment as a function of its roles in RNA transport. In its role as an RNA binding and processing factor, TDP-43 is known to bind to UG-rich regions in transcripts representing over 4,000 genes, including its own (Sephton et al. 2011; Tollervey et al. 2011). TDP-43 also interacts with translation initiation machinery, elongation factors, and ribosomal subunits, suggesting that cytoplasmic TDP-43 plays a role in regulating translation (Birsa et al. 2020; Freibaum et al. 2010; Lee et al. 2021). As evidenced from its capacity to self-regulate, regulation of TDP-43 levels seems to be important to cellular health as both

knockdown and overexpression have profoundly negative effects in multiple cell types (Klim, et al. 2019; Lee et al. 2012; Nonaka et al. 2008; Winton et al. 2008a).

In multiple cell types, TDP-43 is also associated with the process of forming stress granules (Lin-Yesucevitz et al. 2010; Markmiller et al. 2018). Stress granules are small, membrane-less organelles that form in the cytoplasm in response to disturbances in cellular homeostasis. One primary function of stress granules is to gather proteins to illicit acute translational stalling as part of the adaptive cellular stress response (Kedersha and Anderson 2002). In response to cellular disturbances such as increased reactive oxygen species levels (Markmiller et. al 2021), proteotoxic stress (Klim et al. 2019), or physical damage (Sato et al. 2009), TDP-43 will exit the nucleus and co-localize with stress granule-associated proteins such as TIA-1 and G3BP1 (Lee et al. 2012; Markmiller et al. 2021) in the cytoplasm. After the stress is relieved, under normal conditions, TDP-43 will return to the nucleus (Klim et al. 2019; Sato et al. 2009). This suggests that transient cytoplasmic localization of TDP-43 plays an important role in the cellular stress response.

TDP-43 mutation, mislocalization, and aggregation in ALS

TARDBP mutation occurs in approximately 4% of familial ALS cases and 2% of sporadic ALS cases (Ghasemi and Brown 2018; Ingre et al. 2015). Although many of these mutations have limited experimental characterization, the results from the variants that have been characterized show similar functional effects. Mutations in TDP-43 are generally toxic upon knock-in or ectopic expression (Barmada et al. 2010; Johnson et al. 2008; Xu et al. 2010). While TDP-43 mutations generally do not change the proteins that TDP-43 interacts with (Freibaum et al. 2010), changes in transcript abundance of TDP-43 target RNAs have been observed in the context of these mutations (Klim et al. 2019). Alteration of transcript abundance in this fashion of certain factors is proposed as a contributing mechanism to neurodegeneration (Klim et al. 2019). ALS-associated mutations

also increase TDP-43's aggregation propensity, possibly by promoting misfolding and/or prion-like association of the disordered C-terminal region between proteins (Nonaka et al. 2009). This process is thought to be a driving cause for the formation of cytoplasmic TDP-43 aggregates that are hypothesized to be pathogenic.

Interestingly, *TARDBP* mutation is not required for TDP-43 mislocalization and aggregation in the cytoplasm. 97% of ALS patients will develop insoluble TDP-43 aggregates in degenerating motor neurons regardless of whether they have a *TARDBP* mutation or not (Ling et al. 2013). Mutation-independent mechanisms of TDP-43 aggregation have yet to be fully explored. As the cell attempts and fails to process these aggregates, TDP-43 becomes hyper-phosphorylated and hyper-ubiquitinated (Hasegawa et al. 2008; Neumann et al. 2006; Nonaka et al. 2016); staining for phosphorylated TDP-43 is a common method for determining aggregate presence. Cells will also attempt proteolytic cleavage of TDP-43, which results in the build-up of C-terminal fragments of varying size contained in these aggregates, which are also used as a biomarker for aggregating protein (Igaz et al. 2008; Xiao et al. 2015). Studies have been undertaken on the composition of these aggregates and found that they also contain nuclear pore complex proteins, nucleocytoplasmic transport machinery, translational processing components, and more (Chou et al. 2018). While there is still much to learn about the pathogenicity of TDP-43 aggregates, it is known that, in addition to depleting local functional TDP-43 levels, their presence negatively affects proteosome-mediated degradation (Riemenschneider et al. 2022) and autophagy (Ormeno et al. 2020; Torres et al. 2017), further limiting the cell's capacity to process and clear them.

Reasonably, dispersing TDP-43 aggregates has long been considered to be a potential therapy for ALS, though little headway has been made in developing a method to achieve this. Mechanisms driving the liquid-liquid phase separation of TDP-43 aggregates have been explored

by multiple groups (Babinchak et al. 2019; Mann et al. 2019; Suk and Rousseaux 2020), with the one hypothesis being that TDP-43 was more likely to phase separate and become insoluble if it was not bound to RNA or DNA (Mann et al. 2019). However, given that an equilibrium of bound and unbound TDP-43 is essential for TDP-43's ability to transport and process RNAs, simply forcing TDP-43 to assume the bound state more often is not a viable therapeutic strategy. Recruiting deubiquitinases (Hans et al. 2014), ubiquitin ligases to facilitate proteasome degradation (Tseng et al. 2023; Uchida et al. 2016), or phosphatases targeting TDP-43 (Eck et al. 2021; Liachko et al. 2016) have all shown promise *in vitro* in decreasing aggregate burden, however these methods and models do not explain nor treat the underlying cause driving why the aggregates formed.

Previously developed models of TDP-43 disruption for the study of neurodegeneration

Many *in vitro* and *in vivo* models have previously been interrogated to characterize and explain the effects of TDP-43 overexpression, knockdown, or persistent cytoplasmic localization (Barmada et al. 2010; Klim et al. 2019; Walker et al. 2015; Winton et al. 2008a; Wils et al 2010). Commonly used *in vitro* models include HEK293 (Human Embryonic Kidney), SHSY5Y (Human Neuroblastoma), and NSC-34 (Mouse Motor Neuron-like) immortalized cell lines engineered to contain an additional copy of TDP-43 wild-type or a mutant variant (Ding et al. 2021; Nonaka et al. 2008; Winton et al. 2008a). Similar to the effect of expressing of an ALS-associated TDP-43 mutant, wild-type TDP-43 overexpression alone is sufficient to drive the formation of cytoplasmic and nuclear TDP-43 aggregates and induce cell death (Xu et al. 2010). Expressing a TDP-43 variant with a non-functional Nuclear Localization Sequence (TDP-43ΔNLS) is also an established method for forcing cytoplasmic localization of the protein and inducing aggregate formation (Barmada et al. 2010; Winton et al. 2008a). While much has been learned about TDP-

43 proteinopathy from these models, their efficacy is limited for exploring cell autonomous effects that are specific to motor neurons. These mechanisms are important to understand particularly for studying the progression of ALS because it is a condition that preferentially affects motor neurons.

Primary neurons isolated from humanized TDP-43 mutant mice are also frequently employed in studying the biochemistry of TDP-43 perturbation (Alami et al. 2014; Barmada et al. 2010; Feiler et al. 2015). While examining interactions in a neuronal context is generally more applicable than a focus on other cell types, such models derived from mouse also carry the problem that the source organism is not human. ALS is a uniquely human disease – mice that these primary cultures are derived from do not get ALS or a condition that resembles this without the transgenic introduction of a human causal genetic variant (Fisher et al. 2023; Phillips and Rothstein 2015), which also functionally means that any *in vivo* study is better equipped to tackle mechanisms behind familial ALS rather than sporadic ALS. Additionally, discoveries of hypothesized ALS-relevant neurodegenerative mechanisms in primary and *in vivo* models have repeatedly failed to translate into viable human therapies (Fisher et al. 2023; Ittner et al. 2015). There remains an unmet need for better platforms on which ALS therapeutic discovery projects can be reliably built on.

To address these shortcomings, ALS patient-derived iPSCs differentiated into neurons are becoming an increasingly popular method of studying the disease. However, this is not without its drawbacks. Reprogramming iPSCs from patient skin or blood samples is a well-established, but labor-intensive process (Malik and Rao 2013). Until initiatives were established such as the Answer ALS consortium in 2016, which now maintains a cell bank of ALS patient-derived iPSCs available to procure for study (Baxi et al. 2022), the only way to acquire iPSCs was to have the necessary permissions, patient access, and equipment to derive them yourself. The cost of iPSC derivation and maintenance reagents are also substantially higher than commonly used cell culture

medias (for example, a bottle of mTESR Plus Basal Stem Cell Media used to maintain pluripotent stem cells is, at the time of this writing, $360 USD from Stem Cell Technologies, over ten times the cost of a standard bottle of Dulbecco's Modified Eagle Medium (DMEM) from Thermo Fisher Scientific, which costs about $30 USD), further limiting widespread use.

Neurons differentiated from induced pluripotent stem cells (iPSC) derived from patients harboring TDP-43 mutations may recapitulate aggregation phenotypes associated with ALS at baseline (Bilican et al. 2012; Burkhardt et al. 2012; Egawa et al. 2012; Zhang et al. 2013b). There are many different protocols for the derivation of neurons of different types from iPSCs (Giacomelli et al. 2022; Klim et al. 2019; Limone et al. 2023; Nehme et al. 2018; Xue et al. 2013; Zhang et al. 2013a). Several of these protocols rely on spontaneous differentiation of iPSCs followed by isolation of neurons or neural progenitor cells (Bossolasco et al. 2018; Liyang et al. 2014). These processes have relatively low efficiency in terms of the number of neurons generated and can take as long as 30 days or more to generate neurons stable enough to be used in additional experiments. Additionally, to increase experimental throughput, many groups in the past did not limit their studies to putative motor neurons – mixed neuron populations or cortical neuron models are still in use for the study of ALS-associated neurodegenerative mechanisms (Ma et al. 2022; Mennini et al. 2006; Wen et al. 2014). Similar to the drawback of using non-neuronal models, the efficacy of non-motor neuron studies to investigate cell autonomous mechanisms of motor neuron degeneration is limited. Recent advances in differentiation methods have made studying cultures of iPSC-derived motor neurons more tractable. I will explain the pros and cons of different motor neuron differentiation protocols later in this chapter.

Regardless of the experimental methods used to generate the models of TDP-43 proteinopathy, they broadly fall into two camps representing the hypothesized primary driver of

pathology – loss-of-function models centered around loss of TDP-43's splicing and processing functions in the nucleus and gain-of-function models centered around disruptions to essential cellular functions caused by the presence of the insoluble TDP-43 aggregates (Figure 1.4)

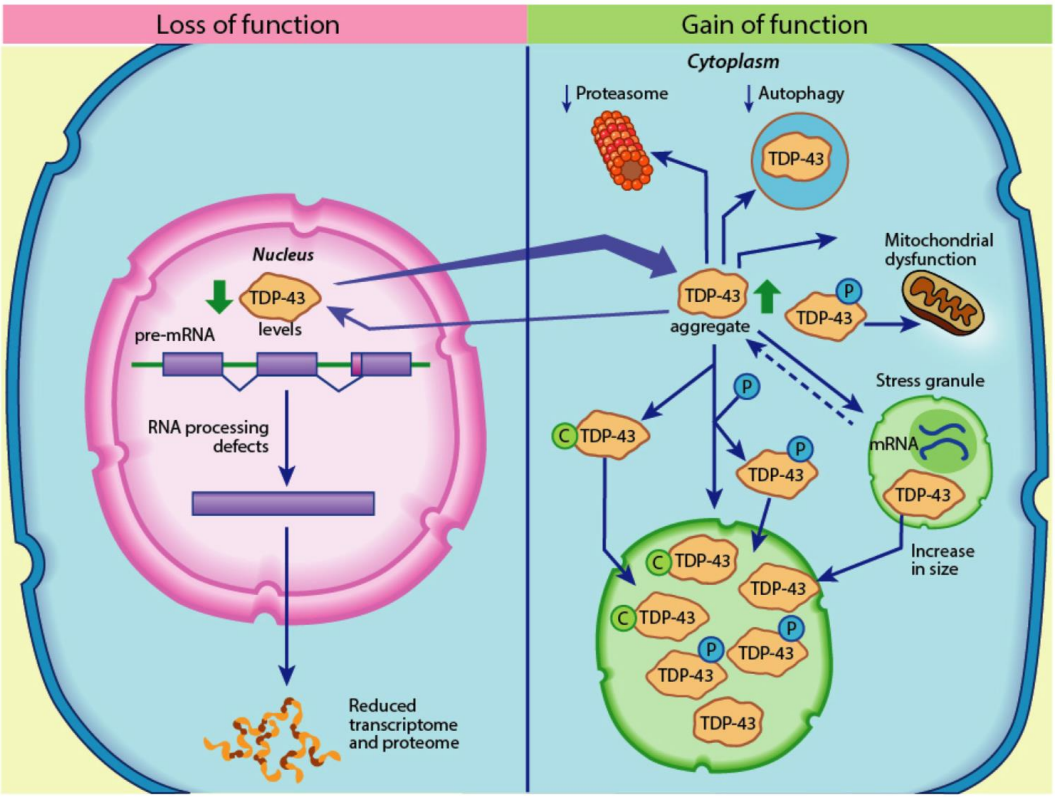

Figure 1.4: Overview of hypothesized loss-of-function and gain-of-function mechanisms of TDP-43 mediated neurodegeneration. The TDP-43 loss-of-function hypothesis states that TDP-43 depletion from the nucleus leads to RNA splicing and transport defects. The TDP-43 gain-of-function hypotheses center around aggregates of TDP-43 (which may begin as stress granules) disrupt cellular processes, including mitochondrial function and protein turnover. Adapted from de Boer et al. 2020

Hypothesized neurodegenerative mechanisms in TDP-43 Loss-of-Function Models

The primary purpose of developing TDP-43 loss-of-function models is to explore drivers of neurodegeneration that may be applicable in the case where much of the functional TDP-43 in the cell becoming trapped in the cytoplasmic aggregates, leaving its functions in the nucleus unable

to be completed. In other words, this is akin to the end state of ALS wherein there is evidence of near complete TDP-43 depletion from the nucleus. Experimental methods to develop these models often center around transient knockdown of TDP-43 (e.g., by siRNA) as persistent TDP-43 knockout is not tolerated in most conditions because it is an essential gene (Kraemer et al. 2010).

In recent years, the loss-of-function hypothesis as the primary driver of TDP-43 mediated neurodegeneration has gained traction due to the discovery and validation of several transcripts including *STMN2* (Klim et al. 2019; Melamed et al. 2019) and *UNC13A* (Ma et al. 2022), which have functional roles essential to human neurons and are mis-spliced to contain cryptic exons (exons that would generally not be included in the mature mRNA during normal conditions) in the context of TDP-43 mutation and knockdown that ablate the function of the translated protein. Furthermore, for *STMN2*, it was shown that knockout in mice was sufficient to induce motor neuropathy (Krus et al. 2022), further suggesting that loss of TDP-43 is a valid model for discovering factors that are essential to normal function of motor neurons which may be compromised in ALS.

Hypothesized neurodegenerative mechanisms in TDP-43 Gain-of-Function Models

The primary purpose of examining TDP-43 gain-of-function models is to explore the pathogenic mechanisms that may arise from the presence of the insoluble TDP-43 aggregates. Because aggregation of mislocalization of TDP-43 may occur before full depletion of TDP-43 from the nucleus at the end state (Nilaver and Urbanski 2023), these models may hold additional efficacy in exploring mechanisms of disease progression rather than only being powered to assess the terminal end state as loss-of-function models commonly are. Experimental models to explore these mechanisms are developed through expression of additional wild-type or mutant copy of TDP-43 *in vitro* or *in vivo*, examining animal models with a knock-in of an ALS-relevant mutation,

or interrogating iPSCs (and subsequently differentiated neurons from those iPSCs) that are reprogrammed from ALS patient tissue.

In addition to the effects of aggregates on protein turnover previously discussed earlier in this chapter, persistent cytoplasmic localization and aggregation of TDP-43 is also associated with mitochondrial dysfunction (Dafinca et al. 2021; Wang et al. 2019). Mitochondrial dysfunction may lead to motor neuron degeneration by sensitizing the neurons to calcium-mediated excitotoxicity (Aggad et al. 2014), increasing the generation of reactive oxygen species (Wang et al. 2019), and/or initiating intrinsic apoptotic pathways (Suzuki et al. 2011). It has additionally been established that both *C9orf72* expansion-associated ALS and TDP-43 mutations or aggregates may perturb mitochondrial membrane potential and/or reduce calcium buffering capacity of the cells, which are both processes that may activate pro-apoptotic signals, among other effects (Dafinca et al. 2020; Dafinca et al. 2021). TDP-43 aggregates may also localize to mitochondria and directly induce mitochondrial depolarization and/or defects in morphology and transport (Hong et al. 2012; Shan et al. 2010; Wang et al. 2013).

Some groups have also suggested that TDP-43's propensity to co-localize with stress granules may be a driver of neurodegeneration. The prevailing hypothesis is that the stress granules are the seeds on which larger aggregates form (Dewey et al. 2012; Fang et al. 2019). Additionally, compounds that reduced the number of stress granules *in vitro* in the context of oxidative stress were shown to reduce the number of TDP-43 aggregates in response to that same stress (Fang et al. 2019). This suggests that reducing the number of TDP-43-containing stress granules or otherwise modulating stress granule dynamics in the context of TDP-43 perturbation may be a potential therapeutic angle to explore.

ATXN2 Structure and Function

One protein that is also closely associated with stress granule formation that I will also be examining over the course of this dissertation is Ataxin-2 (ATXN2). ATXN2 contains an N-terminal like-Sm (Lsm) and an Lsm-associated domain (LsmAD), both of which are responsible for ATXN2's interaction with RNAs similar to other proteins that contain those domains (Lee et al. 2018; Nonhoff et al. 2007; Tharun 2009). ATXN2 also contains a poly-Q tract that is associated with the development of ALS in cases of intermediate expansion (27-33 repeats) (Hart and Gitler 2012) and directly correlated with the development of Spinal Cerebellar Ataxia Type 2 in cases of large expansions (33+ repeats). ATXN2 plays a role in a diverse set of cellular functions including mRNA stabilization (Yokoshi et al. 2014), miRNA mediated gene silencing (Su et al. 2011), translational activation (Lee et al. 2017; Lim and Allada 2013), and regulation of cellular growth and metabolism via the mTOR pathway (Bar et al. 2016; Lastres-Becker et al. 2008). In the context of stress granules, ATXN2, similar to TDP-43, co-localizes with stress granule machinery components (e.g., G3BP1) in response to many forms of stress including heat shock and oxidative stress (Nonhoff et al. 2007). Clip-seq analysis of ATXN2 RNA binding partners discovered that ATXN2 binds primarily to 3' Untranslated Regions of RNAs that contain the consensus motif AUUUN (Yokoshi et al. 2014). ATXN2 was found to interact with transcripts coding approximately 4000 different genes, including TDP-43 (Yokoshi et al. 2014). Examination of protein-protein interactions in iPSC-derived excitatory neurons also revealed a relationship between TDP-43 and ATXN2 (Pintacuda et al. 2021).

ATXN2 as a modifier of ALS-associated neurodegeneration

ATXN2 was first linked to TDP-43-associated toxicity from an initial discovery in a yeast two-hybrid screen that knockout of the yeast ortholog of ATXN2, *pbp1*, was sufficient to reduce

toxicity conferred by TDP-43 overexpression (Elden et al. 2010). Several years later, the same group also demonstrated that mice with transgenic TDP-43 overexpression – which generally only live for about 24 days (Wils et al. 2010) – would survive significantly longer (300+ days) in the context of an additional transgenic knockout of ATXN2 (Becker et al. 2017). The Eggan lab also independently performed and verified the results of this experiment (Figure 1.5). One hypothesized mechanism of why ATXN2 provides neuroprotection in the context of TDP-43 perturbation is that ATXN2 knockout may suppress the formation of pathogenic TDP-43 foci, which supports the stress granule seeding model of neurodegeneration mechanisms (Becker et al. 2017). However, this hypothesis has not been confirmed in a human-derived model system.

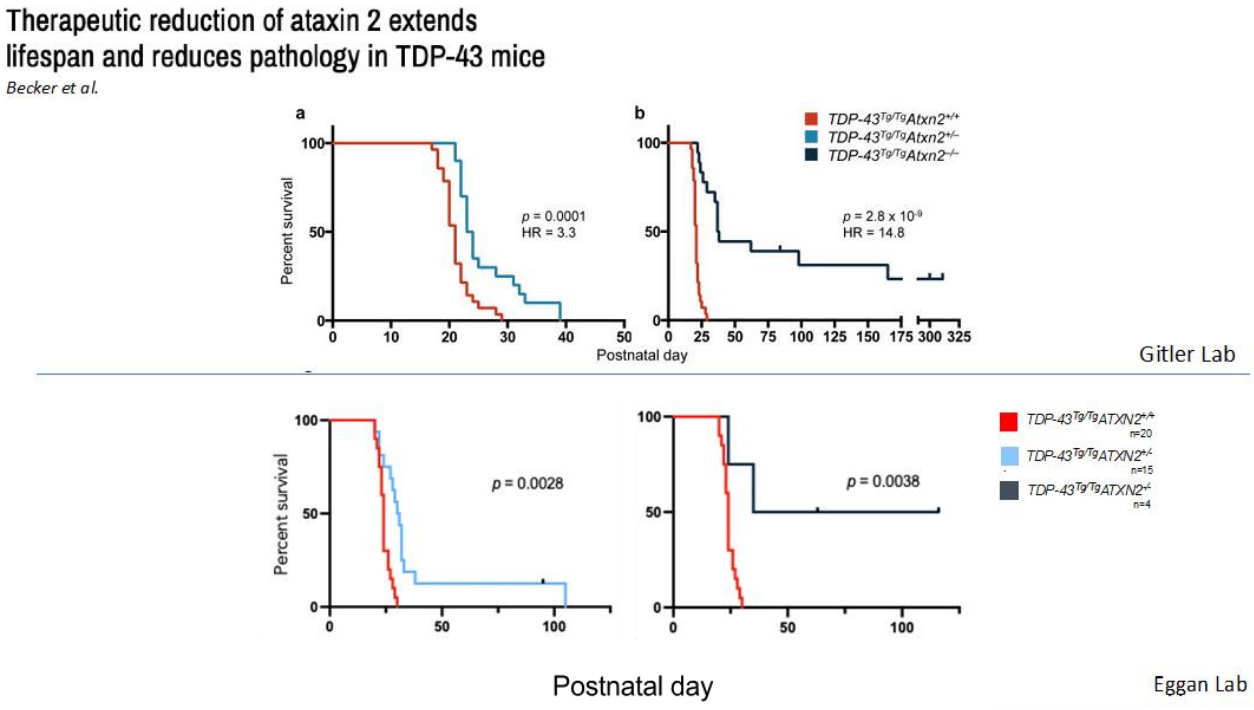

Figure 1.5: Transgenic ATXN2 knockout increases lifespan of TDP-43 overexpressing mice. The Eggan Lab was able to independently verify that TDP-43 overexpressing mice that would normally survive for about 24 days now survive at least 100 days with ATXN2 knockout. Reported p-values are output from the survdiff() R function, which performs a Cochran-Mantel-Haenszel method statistical test of the data input to generate the Kaplan-Meier Curves (Becker et al. 2017). Data from the Eggan Lab generated by Joanie Mok, Alexander Couto, and Alexander Dorr.

As previously stated, intermediate length ATXN2 poly-Q expansion repeats are associated with the development of ALS (Hart et al. 2012). One mechanistic hypothesis as to why this occurs is because cells harboring this intermediate expansion also have higher basal Caspase-3 activation, suggesting that they may be more susceptible to completing the process of apoptosis than a cell without that mutant expansion (Hart and Gitler 2012). Although this mechanism of pathogenesis is likely independent of its other roles as a modifier of disease in the context of TDP-43 disruption, this is further evidence that ATXN2 is likely a contributing factor to multiple reasons why neurodegeneration may begin and/or progress, which bolsters the value of understanding more about its neurobiological functions and relationships.

LiMoNes: A new protocol for differentiating iPSCs into spinal cord motor neurons

A key issue limiting the development of human stem cell-derived motor neuron models to study ALS is the efficiency of current protocols to generate these motor neurons. There is no accepted standard protocol for motor neuron differentiation, so it is a frequent occurrence that even papers contemporary to each other will cite drastically different methods of differentiation (Klim et. al 2019; Melamed et. al 2019; Vandoorne et al. 2019). Capitalizing on the discovery that overexpression of the transcription factor Neurogenin-2 (NGN2) is effective in accelerating development of stem cells into neurons (Zhang et al. 2013a), the Eggan lab developed a new differentiation protocol for rapid and efficient generation of spinal cord motor neurons, which we coined LiMoNes (**L**ower **I**nduced **Mo**tor **Ne**uron**s**) (Limone, et al. 2023). This method, similar to a method the group previously developed for rapid generation of upper cortical neurons (Nehme et al. 2018), combines overexpression of NGN2 with dual-SMAD inhibition (which directs iPSCs to develop towards the neuroectoderm lineage (Chambers et al. 2009)) and patterning morphogens – Retinoic Acid and Smoothened Agonist – that direct the cells to develop in a context as if they

were in the spinal cord (Amoroso et al. 2013). This strategy is effective in generating near pure cultures of motor neurons from iPSCs within the span of one week. As soon as halfway through the differentiation protocol, cells show high expression of motor neuron specific factors such as ChAT and HOXC6. Over 85% of cells on average from any given differentiation will stain positive for these and other markers of putative motor neurons such as Islet1 (Figure 1.6a, b). The levels of motor neuron specific factors in neurons derived using LiMoNes are on par with or higher than levels from neurons isolated from a different differentiation protocol that does not depend on NGN2 overexpression (Figure 1.6c). Furthermore, upon interrogation by single cell RNA sequencing, our group determined that neurons generated by the LiMoNes method contain markers for a diverse set of motor neuron subtypes that are found in the spinal cord, further cementing the value of the method in generating a physiologically relevant neuronal model to examine generalized spinal cord degeneration (Limone et al. 2023).

Motor neurons generated using this method are recoverable upon freeze-thawing immediately after differentiation, amenable to *in vitro* culture in all size formats that were tested (up to 10cm plates) and can be maintained in culture for over 40 days. Given the technical advantages in time, efficiency, and quality over other established motor neuron differentiation protocols, I chose to make the LiMoNes differentiation method my primary technique for generating motor neurons.

Dissertation Overview and Significance

This dissertation showcases the development and implementation of an engineered iPSC-derived human motor neuron system to validate previous findings about and discover novel mechanisms of ALS-relevant neurodegeneration. To date, little work has been done to examine cell autonomous mechanisms of neurodegeneration tied to a specific genetic perturbation in a

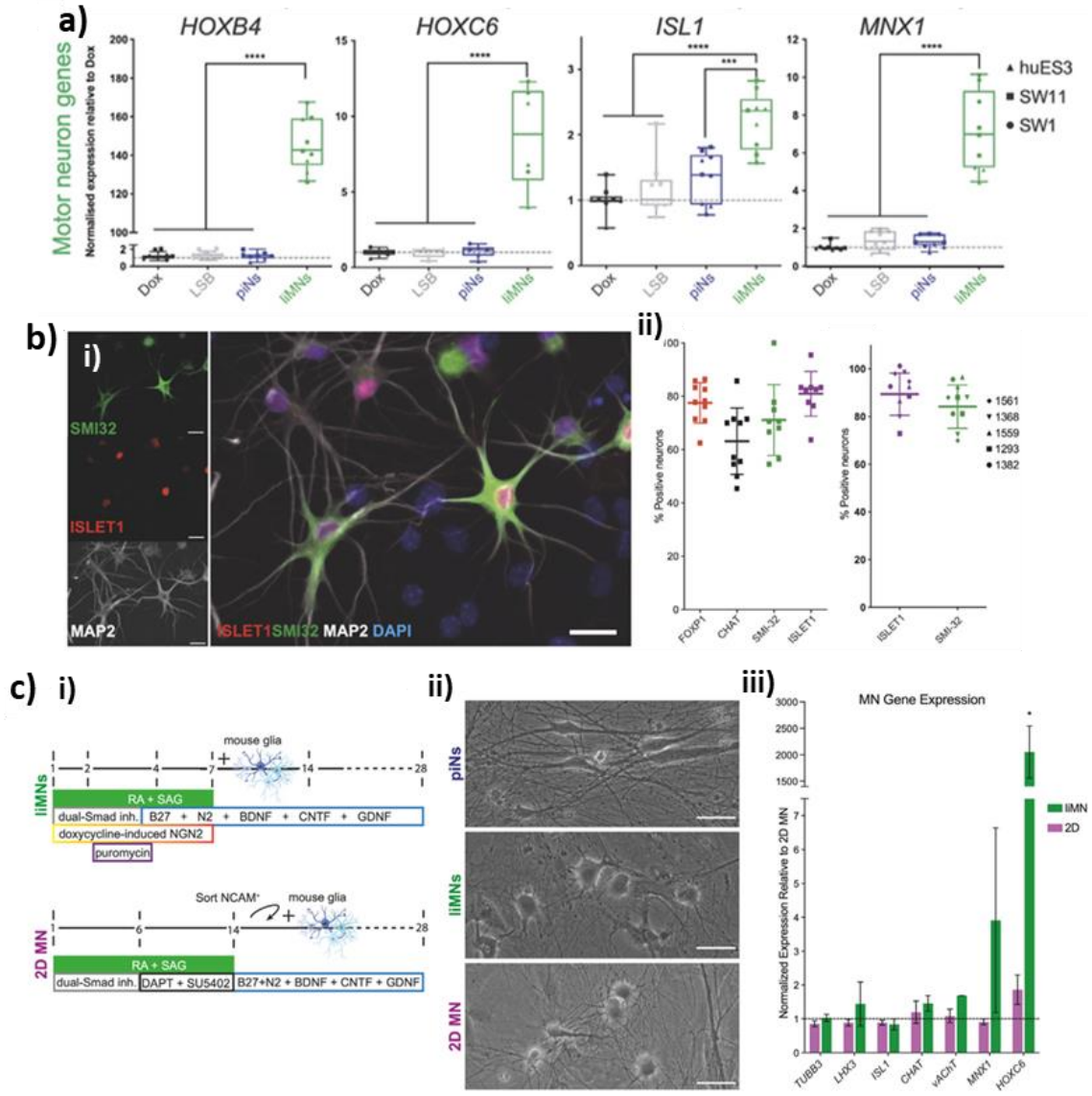

Figure 1.6: Using the LiMoNes method to generate motor neurons from hESCs. Adapted from Limone et al. 2023 **(a)** qPCR of select motor neuron specific genes at Day 4 of differentiation compared to other non-motor neuron specific differentiation protocols in three different cell lines. (three cell lines in n = 3 technical replicates each, p values from one-way ANOVA) **(b)** (i) Immunofluorescence of Day 30 neurons for motor neuron specific markers. Scale bar = 100µM. (ii) Quantification of percentage of culture that stains positive for each motor neuron marker. Tested in 5 different cell lines (n = 10). **(c)** (i) Schematic of the two different motor neuron protocols for comparison, the second being without NGN2 overexpression (ii) Brightfield images of neurons generated from the cortical neuron differentiation (piN) and two motor neuron differentiation protocols. Scale bar = 50µM. (iii) qRT-PCR quantification of motor neuron marker genes in liMNs compared to the 2D MN differentiation protocol (n = 3).

human motor neuron system. This work aims to fill that gap and contribute to our understanding of human motor neuron biology in neurodegenerative conditions, including how the effects of those conditions can be managed, so that we may be better positioned to initiate rationally designed therapeutic development programs for the treatment of ALS or other neurological diseases associated with TDP-43 proteinopathy.

My perturbation of choice to represent the neurodegenerative condition is TDP-43 overexpression via inducible expression from a bespoke vector that I generated for this purpose or constitutive expression as conferred by lentiviral infection on differentiated motor neurons. Given that TDP-43 perturbation by aggregation is the most common pathologic feature in ALS, I believe that models that faithfully represent this condition are excellent starting points for study. To that end, I will show that my models reproduce core aspects of TDP-43 proteinopathy and are amenable to be rapidly assayed for biochemical and phenotypical features correlated with neurodegeneration. In examining those features, I will explore the effect of TDP-43 perturbation though cytoplasmic restriction (TDP-43ΔNLS) as week as in the context of a potential rescue condition – knockout of the proposed neurotoxicity modifier ATXN2. The goal of these studies is, specifically in a human motor neuron system, to elucidate mechanisms in both TDP-43ΔNLS expression and ATXN2 knockout conditions that can be therapeutically leveraged to reduce the pathologic burden of TDP-43 dysregulation.

Chapter 2: Development of *in vitro* human iPSC-derived models of TDP-43 perturbation

Abstract

Transactive Response DNA-binding protein 43 (TDP-43) is a multifunctional nuclear protein ubiquitously expressed in all tissues. Although it is primarily nuclear, Amyotrophic Lateral Sclerosis (ALS) patients frequently present with cytoplasmic aggregates of TDP-43 in motor neurons upon post-mortem examination. Although only about 5% of all ALS patients have a *TARDBP* mutation (Ghasemi and Brown 2018; Ingre et al. 2015), which is known to cause these insoluble cytoplasmic aggregates, 97% of ALS patients will develop cytoplasmic, insoluble TDP-43 aggregates regardless of whether they have a mutation in *TARDBP* or not (Ling et al. 2013). This suggests that there are mutation-independent mechanisms that drive pathogenic aggregation of TDP-43. Most existing models to study TDP-43 proteinopathy *in vitro* are non-neuronal or non-human, limiting the efficacy of these models to elucidate cell autonomous mechanisms that may be contributing to neurodegeneration. In this chapter, I will show that I have built several *in vitro* models of TDP-43 proteinopathy by successfully incorporating an inducible TDP-43 variant construct or a constitutive TDP-43 variant lentivirus into iPSCs or differentiated motor neuron cultures as appropriate. These cell line models comprise an isogenic series beginning from a healthy male donor iPSC line, allowing for focus on the direct effects of TDP-43 overexpression-mediated proteinopathy without additional confounding variables of differing or uncharacterized genetic contexts. I will begin by showing proofs of concept that my expression systems work at the HEK293 and undifferentiated iPSC contexts. I will continue by showing that iPSC-derived motor neurons differentiated using the LiMoNes method (Limone et al. 2023) and harboring my custom expression systems can recapitulate core features of TDP-43 proteinopathy, including exploring questions about preferential motor neuron sensitivity to TDP-43 variants compared to other neuron types. These models fill a core need of the field for additional robust and expandable

models of TDP-43 proteinopathy. The result of these experiments is the generation of a scalable human iPSC-derived platform for *in vitro* neurodegeneration research that can be swiftly adjusted for implementation of exploring a variety of cellular mechanisms, a sampling of which will be explored in the following chapters of this dissertation.

Introduction

Transactive Response DNA-binding protein 43 (TDP-43) is a nuclear protein ubiquitously expressed in all tissues and required for normal development (Buratti and Baralle. 2012; Kraemer et al. 2010). TDP-43 is involved in a variety of cellular processes including RNA transport, splicing, and translational regulation (Birsa et al. 2020; Freibaum et al. 2010; Lee et al. 2021; Sephton et al. 2011). TDP-43 is of particular interest to the study of Amyotrophic Lateral Sclerosis (ALS) because 97% of ALS patients will exhibit cytoplasmic, insoluble aggregates of TDP-43 in motor neurons upon post-mortem examination (Ling et al. 2013). Given that there are few available therapies for the treatment of ALS, there is a need for better models of the disease that can be interrogated to learn more about mechanisms of neurodegeneration that may be therapeutically tractable for future treatment development.

TDP-43 proteinopathy and associated neurodegenerative effects can be readily induced by overexpression of TDP-43 *in vitro* and *in vivo* (Wils et al. 2010; Xu et al. 2010). However, most of the existing models of TDP-43 proteinopathy to date are non-human or non-neuronal (Ding et al. 2021; Nonaka et al. 2008; Wils et al. 2010; Winton et al. 2008a). This presents a challenge to investigating cell autonomous motor neuron-centered mechanisms of neurodegeneration because other models simply do not represent this context. Experimental validation and perspective in a motor neuron system is particularly important for ALS because it is a condition that preferentially affects motor neurons over other cell types (Ragagnin et al. 2019). Given the failure of recent

therapies derived from discoveries in other models to translate into successful clinical trials (Fisher et al. 2023), it seems rational that one approach to bolster the success and discovery rate of therapeutic, disease-relevant mechanisms is to build and explore a model that is more physiologically relevant to the condition being researched. This is especially relevant for ALS research because it is a uniquely human condition – all model organisms available for the study of the disease are derived using our knowledge of genetic mutations associated with familial ALS (Fisher et al. 2023; Phillips and Rothstein 2015). Without these transgenic modifications, commonly used non-human model organisms will not develop sporadic ALS.

To meet this challenge, we developed a bespoke inducible vector system for the overexpression of TDP-43 from the AAVS1 safe harbor locus (Smith et al. 2007). Expressing from AAVS1 has an advantage over transient transfections or lentiviral mediated transfection as it allows for stable expression while mitigating the likelihood of randomly silencing another gene through random integration (Smith et al. 2007). This is important to consider in ALS because the genetic landscape (in terms of modifiers and causal genes) is still an active area of discovery. In order to clearly define the parameters of my engineered TDP-43 perturbation model, I desired a system wherein everything else was as close to the original genetic context as possible except for my designed change of TDP-43 variant expression. Furthermore, genetic integration in this fashion results in a stable cell line after antibiotic selection, which is advantageous for distribution of reagents I generate during this study. I will show that this inducible expression system is active in HEK293, iPSCs, and iPSC-derived motor neurons as well as exhibit that TDP-43 expressed in this fashion leads to decrease in cell viability and induces cytoplasmic re-localization of TDP-43, both of which are characteristic features of the TDP-43 mediated neurodegeneration condition.

Results

TDP-43 overexpression is achievable in HEK293s using a custom inducible vector system

The first goal in building a system for interrogating TDP-43 proteinopathy was to achieve inducible overexpression of the protein in iPSCs. At the time this project was conceived, there was no commercially available all-in-one Tet-On inducible vector plasmid for recombination to the AAVS1 safe harbor locus. The plasmids that were available either were not inducible (which was undesirable because constitutive overexpression of TDP-43 is toxic) or required a second transduction to acquire the rtTA protein needed for the function of the Tet-On inducible system (Das et al. 2016). Thus, I set on a path to create a new system, derived from components from the AAVS1-Neo-m2rtTA plasmid procured through Addgene (DeKelver et al. 2010), pLIX_403 – an inducible lentiviral vector from the Broad Institute's Genetic Perturbation Platform DNA vector collection – and a collection of TDP-43-YFP fusion cDNAs also procured from Addgene (Elden et al. 2010). Using PCR, blunt-end cloning, and gateway cloning techniques, I was able to generate the plasmid and verify presence of my inserts using Sanger Sequencing. I then electroporated the cells to deliver this vector alongside a TALEN targeting AAVS1 to achieve stable recombination of my vector (Hockemeyer et al. 2009; Lombardo et al. 2011). I selected for successful transductants using Neomycin resistance conferred by the plasmid. I first examined the properties of TDP-43 expressed in this fashion using an easy to transfect line – HEK293 (Figure 2.1). I was able to establish that, upon induction with doxycycline, I could get robust expression of TDP-43:YFP by western blot and qRT-PCR in both the TDP-43:YFP and TDP-43ΔNLS:YFP conditions (Figure 2.1a, c). I used flow cytometry to establish that the TDP-43 construct I expressed was readily targetable by an siRNA against TDP-43 by showing that YFP expression was ablated upon treatment with siTDP-43 (Figure 2.1b). These facts established that I could successfully get

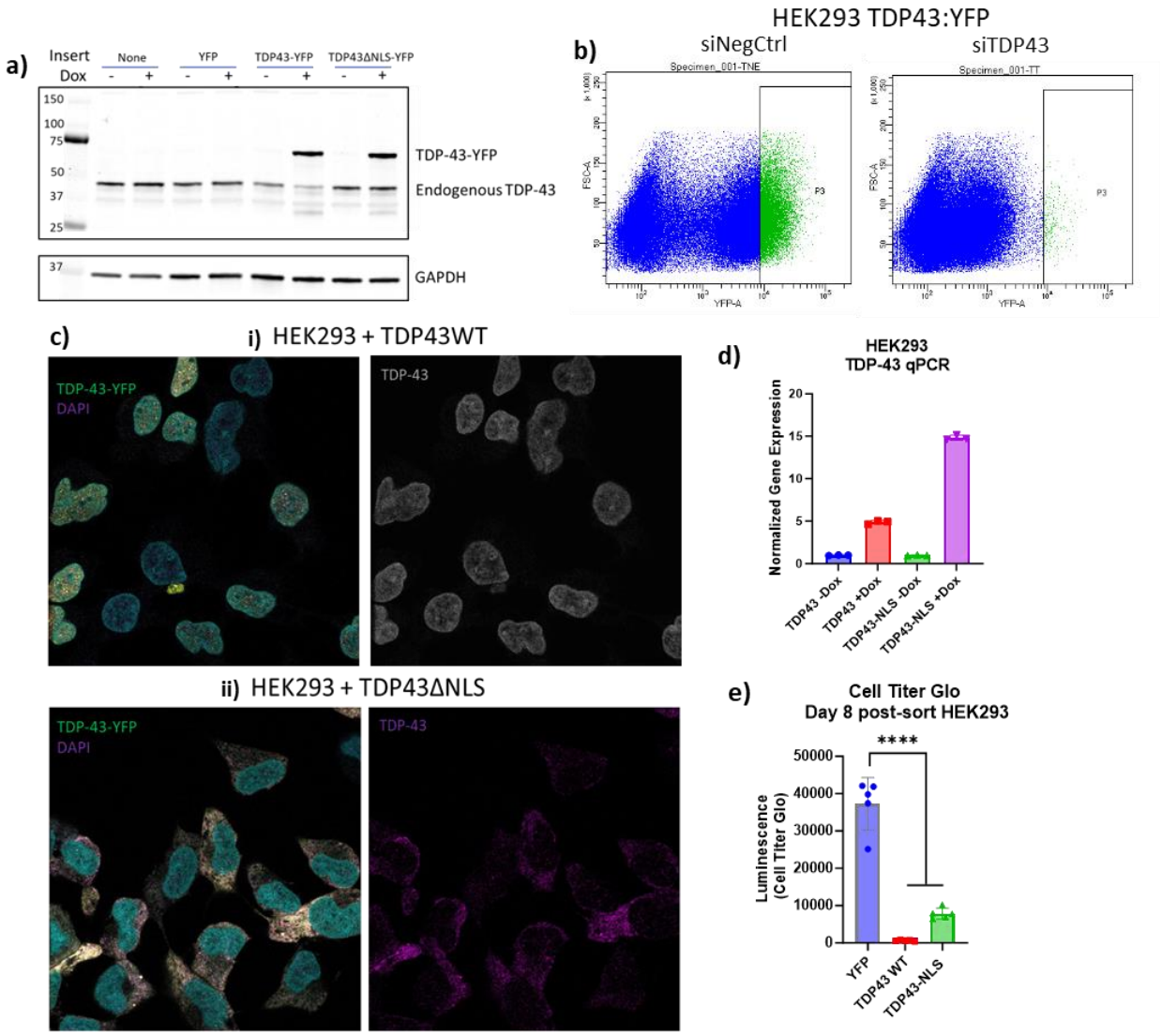

Figure 2.1: Inducible TDP-43 vector characterization in HEK293 cells. (a) Whole cell western blot of engineered cells with and without doxycycline **(b)** YFP Flow Cytometry results of HEK293 cells harboring inducible TDP-43:YFP treated with doxycycline concurrent with siRNA knockdown of TDP-43 for 48 hours **(c)** Immunofluorescence of HEK293 cells expressing TDP-43:YFP (i) or TDP-43ΔNLS:YFP (ii) for DAPI and YFP (left image of each set) or total TDP-43 (right image of each set) **(d)** qRT-PCR results of engineered cells with and without Doxycycline using primers targeting TDP-43 (n = 3 technical replicates) **(e)** Cell Titer Glo viability experiment luminescent results 8 days after plating YFP+ FACS sorted HEK293 cells harboring YFP, TDP-43:YFP, or TDP-43ΔNLS:YFP inducible systems treated with doxycycline for 24 hours pre-sort. Significance calculated by t-tests of pairwise comparisons between YFP and each of TDP-43:YFP and TDP-43ΔNLS:YFP (**** = $p<0.0001$) (n = 5 biological replicates).

expression of a TDP-43 construct that enhanced the levels of bona-fide TDP-43 expression upon treatment with doxycycline.

I additionally showed that the visible YFP fusion tag was localized to the nucleus upon expression of TDP-43:YFP (Figure 2.1c-i) and to the cytoplasm upon expression of TDP-43ΔNLS:YFP (Figure 2.1c-ii). I also noted that TDP-43ΔNLS:YFP expression had the capacity to drive clearance of endogenous TDP-43 from the nucleus as can be seen when immunostaining for total TDP-43 (Figure 2.1c-ii), which has been previously reported to occur in TDP-43ΔNLS engineered systems (Winton et al. 2008a). Lastly, I was able to establish that expression of TDP-43:YFP or TDP-43ΔNLS:YFP led to a decrease in cell viability as measured by Cell Titer Glo (Figure 2.1e). Taken together, these observations firmly support that the inducible vector system I created robustly expresses TDP-43, localizes to the expected location, and is toxic upon overexpression as expected.

TDP-43 overexpression is achievable in iPSCs using the inducible vector system

After establishing the proof of concept that I could get inducible expression of TDP-43 in HEK293 cells, I moved to generate engineered iPSCs also using the co-electroporation method of the AAVS1 TALEN with the donor inducible vector template. The iPSC line I chose to engineer was the healthy patient line 11a. To ensure sufficient enrichment in the culture of cells successfully transduced with the inducible system vector, I also performed single cell cloning after the initial antibiotic selection. I nominated clones for continued study based on whether the visible YFP tag was detectable upon imaging (Figure 2.2a) and biochemical confirmation of TDP-43 overexpression (Figure 2.2b). The result was that I was able to generate 2 - 3 clones for each expression condition (e.g., TDP-43, TDP-43ΔNLS) that I use at various points throughout the study.

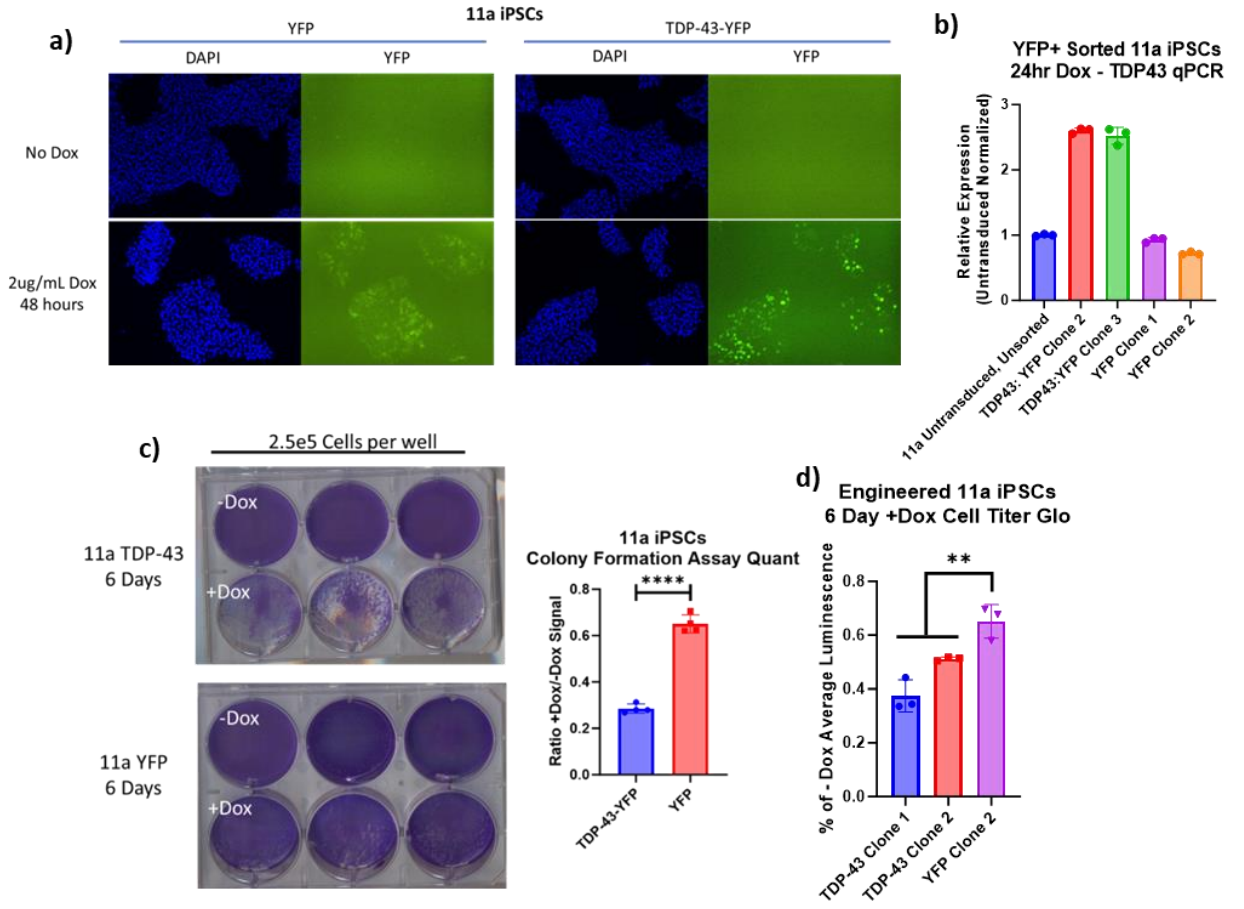

Figure 2.2: Inducible TDP-43 vector characterization in iPSCs (a) Fluorescent Imaging of iPSCs harboring inducible YFP or TDP-43:YFP 48 hours with or without exposure to doxycycline. Cells were fixed and counterstained with DAPI. **(b)** qRT-PCR results of YFP+ FACS sorted iPSCs using primers targeting TDP-43 (n = 3 technical replicates) **(c)** Colony Formation Assay plate pictures and quantification to assess viability of iPSCs after induction of TDP-43 overexpression. These plates show that after six days, there is substantially reduced viability of TDP-43:YFP expressing iPSCs compared to YFP expressing iPSCs. Significance calculated using a t-test (****= $p<0.0001$) (n = 3 biological replicates) **(d)** Cell Titer Glo viability measurement of engineered iPSCs after exposure to Doxycycline to induce TDP-43 overexpression, also for 6 days. Significance calculated using t-tests compared to the YFP sample (** = $p<0.01$) (n = 3 biological replicates).

Similar to HEK293s, I also assessed the viability of iPSCs after induction of TDP-43 overexpression. I showed that by a colony formation viability assay (Figure 2.2c) and by Cell Titer Glo comparison (Figure 2.2d) that viability of TDP-43:YFP expressing iPSCs was significantly

lower than YFP only expressing iPSCs after six days in culture. These data show that the inducible system of TDP-43 expression was continuing to function as intended in iPSCs. This paved the way for continued study in motor neurons derived from these engineered iPSCs.

Inducible TDP-43 overexpression persists upon differentiation into motor neurons

I generated motor neurons from the previously engineered iPSCs using the LiMoNes method (Limone et al. 2023; Figure 2.3a). To facilitate NGN2 overexpression, I infected the engineered iPSC cultures with an NGN2 lentivirus to generate a stable inducible NGN2 line that could be used for subsequent differentiations. After differentiation and a five-day incubation for the culture to mature and stabilize, I assessed the neurons to confirm visibility of the YFP fusion tag (Figure 2.3b) and biochemical detection of TDP-43 using qRT-PCR (Figure 2.3c) and western blot (Figure 2.3d). For this western blot method, I used a cellular fractionation kit to chemically separate each cellular compartment so they can be individually assessed for the presence of protein. Using this, I was able to show that TDP-43 is detectable in the cytoplasmic fraction upon overexpression, further confirming that TDP-43 overexpression using my inducible vector system is a viable method for modeling TDP-43 proteinopathy.

One caveat of using the engineered inducible TDP-43 system I developed is that both NGN2 expression and expression of the inducible plasmid payload are controlled by doxycycline. Because the only copy of rtTA is on the inducible TDP-43 plasmid and not on the NGN2 plasmid, there is an advantage in coupling expression of the two constructs as it ensures the composition of the neuronal culture after differentiation still expresses the TDP-43 variant in a majority of cells. iPSCs that may have silenced the vector will fail to differentiate and be selected out in the differentiation process. However, this means that it is not possible to decouple TDP-43 variant

expression from the differentiation process, which means I need an alternative method to explore how established motor neurons may react to a TDP-43

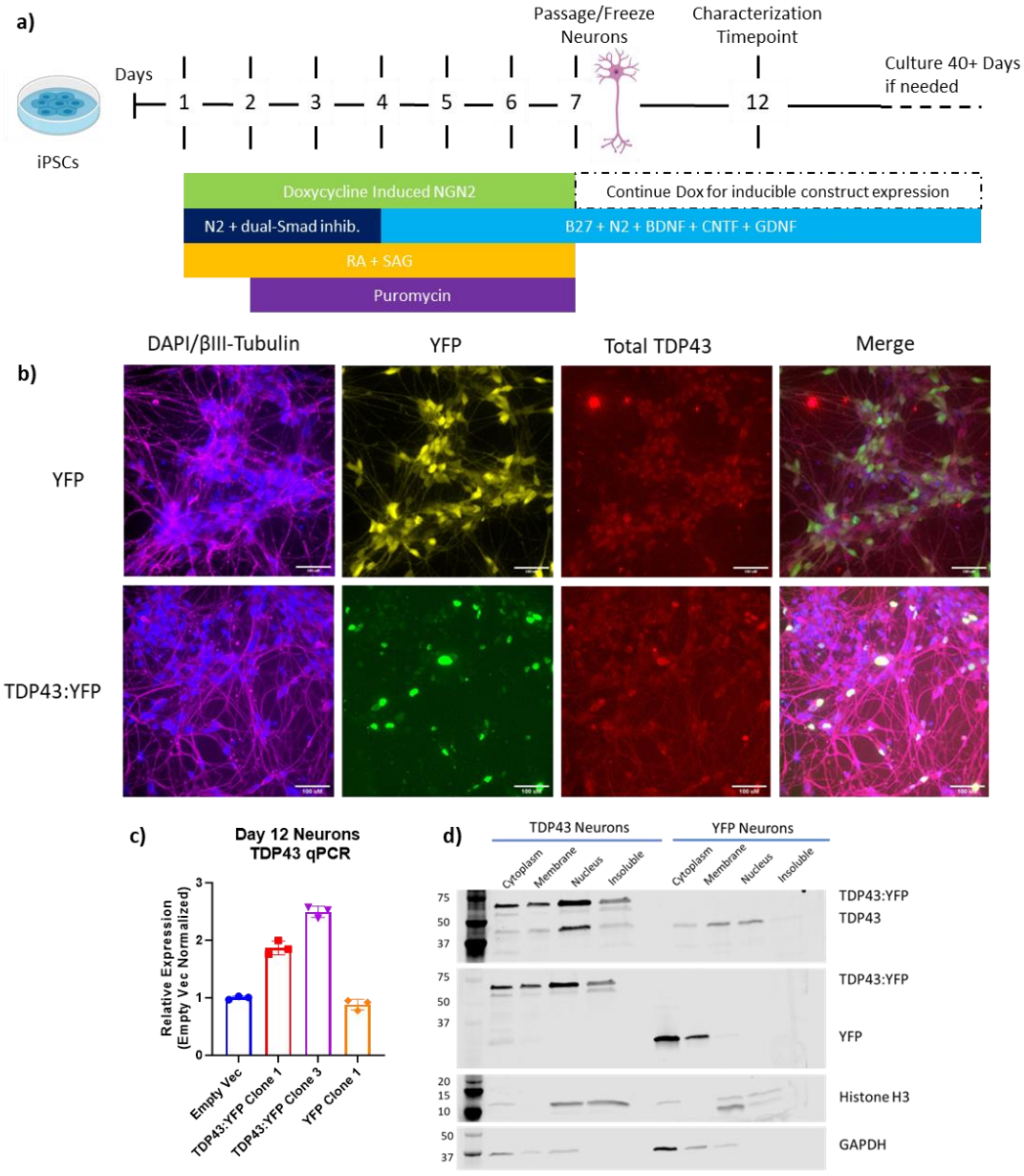

Figure 2.3: Differentiation and characterization of motor neurons derived from engineered iPSCs (a) Timeline of LiMoNes differentiation protocol **(b)** Confocal images of motor neurons derived from engineered iPSCs immunostained for total TDP-43 and the neuronal cytoskeletal marker βIII-Tubulin. Scale bars are 100uM **(c)** qRT-PCR of motor neurons five days with primers targeting TDP-43 (n = 3 technical replicates) **(d)** Cellular fractionation western blot of motor neurons. Note the presence of TDP-43 in the cytoplasmic and insoluble fractions upon overexpression.

perturbation. To meet this challenge, I also cloned a constitutive lentivirus plasmid with the same TDP-43 variant cDNA used in the inducible plasmid system (Figure 2.4). This alternative construct was similarly able to express TDP-43:YFP and YFP as observed by microscopy (Figure 2.4b) and western blot (Figure 2.4c) when used to infect motor neurons that were not previously engineered to harbor a TDP-43:YFP or YFP expression construct.

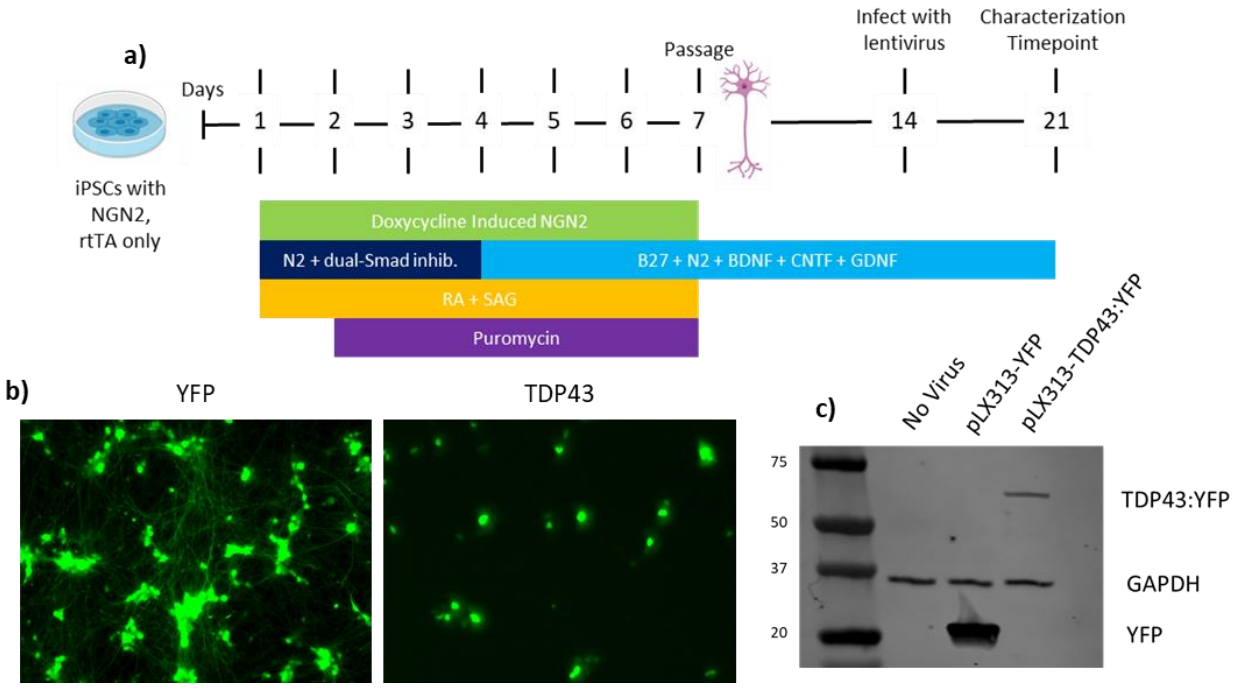

Figure 2.4: Testing TDP-43 lentivirus as an alternative expression system in motor neurons **(a)** Timeline of motor neuron differentiation and infection **(b)** YFP channel images of two neuronal cultures infected with pLX313-YFP and pLX313-TDP-43:YFP accordingly **(c)** Western blot of neuronal cultures seven days after infection with either pLX313-YFP or pLX313-TDP-43:YFP, confirming expression of the lentivirally delivered constructs.

Overexpression of TDP-43 is sufficient to induce death in iPSC-derived motor neurons

The final test in assessing this model of engineered iPSCs before going on to deploy it to explore questions of neurodegenerative mechanisms was to verify that expression of TDP-43:YFP was toxic to motor neurons as it had been to HEK293s (Figure 2.1) and iPSCs (Figure 2.2).

Unfortunately, a first pass attempt at differentiating the engineered iPSCs and then continuing to culture them for up to 28 days did not yield positive results (Supplementary Figure 2.1). I hypothesized that this may be because TDP-43 overexpression could be killing a significant population of the TDP-43 perturbed cells much earlier than anticipated. To investigate this possibility, I developed a short-term differentiation viability assay, wherein I assessed differentiating cultures of iPSCs using Cell Titer Glo every day for the second half of the differentiation protocol (i.e., after the cells have already committed to a neuronal identity and begin to express markers of putative motor neurons (Figure 1.6)). Using this assay, I was able to observe that at every point during the 2nd half of the differentiation, TDP-43:YFP expressing cells had significantly lower viability than expected compared to YFP expressing control differentiations (Figure 2.5a-ii). The largest magnitude of viability decrease occurred between days 5 and 6. To control for the possibility that this was a technical artifact of differing degrees of NGN2 or inducible vector transduction, I used immunofluorescence to assess the number of differentiable cells at Day 2 of the differentiation protocol in the TDP-43:YFP and YFP engineered cultures. I found the levels to be comparable (Supplementary Figure 2.2), suggesting that the viability effect seen in the short-term differentiation assay results was indeed a biological effect. To further validate the toxic effect of TDP-43 overexpression in motor neurons, I also infected un-engineered motor neurons with lentivirus containing the constructs for TDP-43:YFP or YFP and cultured the neurons for 28 additional days. Upon measurement by Cell Titer Glo, I observed that there was also a decrease in viability in neuron cultures that had been transduced with TDP-43:YFP compared to those transduced with YFP alone (Figure 2.5b-ii). These observations together continue to support the notion that I have developed a robust human neuronal platform to

investigate mechanisms of neurodegeneration that are relevant in the context of TDP-43 proteinopathy.

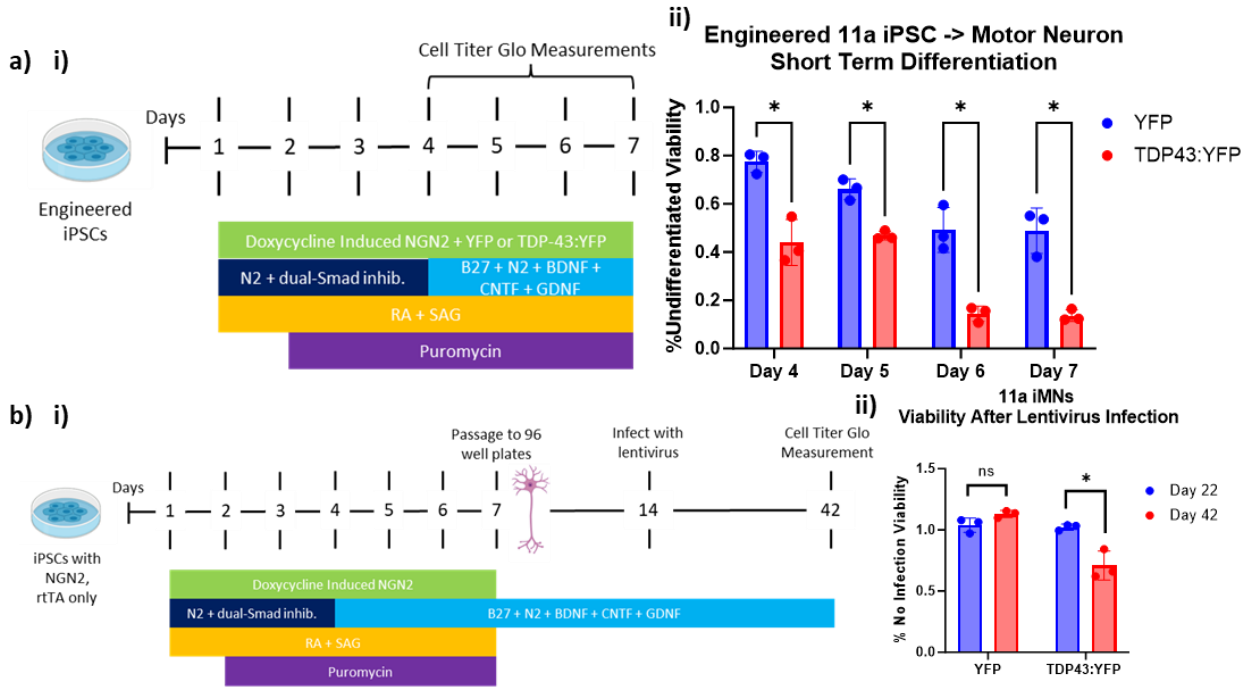

Figure 2.5: TDP-43 overexpression in motor neurons is toxic in the short-term and long-term **(a)** Assessment of inducible TDP-43 toxicity in a short-term differentiation assay of engineered iPSCs converting to motor neurons. (i) Experimental timeline (ii) Results. Significance calculated using a t-test for each pairwise comparison (* = $p<0.05$) (n = 3 biological replicates) **(b)** Assessment of TDP-43 overexpression toxicity as conferred by a lentivirus infecting established motor neurons (i) Experimental timeline (ii) Results. Significance calculated using a t-test for each pairwise comparison (* = $p<0.05$) (n = 3 biological replicates).

Motor and cortical neurons are more sensitive to TDP-43 perturbations than unenriched neuronal cultures

Although it is very clear through the physiological course of ALS that motor neurons are profoundly affected in the condition, it remains an open question what the mechanisms of this specificity are. Given that familial ALS mutations are heritable, it stands to reason that tissue specific mutation in motor neurons to acquire TDP-43 mutation is an unlikely explanation for the

sensitivity of motor neurons to the proteinopathy compared to other cell types. Using the neuronal platform I generated, we can begin to make progress towards discovering what some of these sensitivity mechanisms may be by assessing whether cultures of motor neurons compared to other iPSC-derived neuronal cultures are preferentially sensitive to TDP-43 perturbation by wild-type overexpression or cytoplasmic mutant expression. By taking advantage of the lentiviral-mediated expression of TDP-43, I have established models of TDP-43 proteinopathy in different neuronal differentiation contexts and assessed the viability of the cultures using Cell Titer Glo (Figure 2.6).

From this investigation, I concluded that motor neurons displayed a particular sensitivity to expression of TDP-43ΔNLS after 14 days compared to two differentiation methods not enriched for a particular neuron subtype (Zhang et al. 2013a), which would be expected from previous work indicating that cytoplasmic TDP-43 expression is neurotoxic to neurons after an extended period of time (Winton et al. 2008a, Barmada et al. 2010). 14 days was not sufficient to see toxicity of wild-type TDP-43, but this would be in line with my previous results in Figure 2.3 and Figure 2.5. If a significant driver of neurotoxicity is cytoplasmic TDP-43 expression and the cytoplasmic TDP-43 expression driven by TDP-43ΔNLS is more severe than by overexpressing the wild-type nuclear version, I would expect for toxic effects to occur at a later timepoint, as I observed in the previously presented viability experiments (Figure 2.5). The average observed viability loss in motor neurons in the presence of TDP-43ΔNLS was larger than in cortical neurons, though cortical neurons showed a statistically significant viability difference to both TDP-43 and TDP-43ΔNLS lentivirus (Figure 2.6b). This is not entirely surprising however given that TDP-43 proteinopathy in cortical neurons has also been linked to Frontotemporal Dementia (Ling et al. 2013). Sensitivity of cortical neurons to TDP-43 disruption as well supports the notion that this method of TDP-43 perturbation could be a viable strategy for examining cell autonomous mechanisms in both the

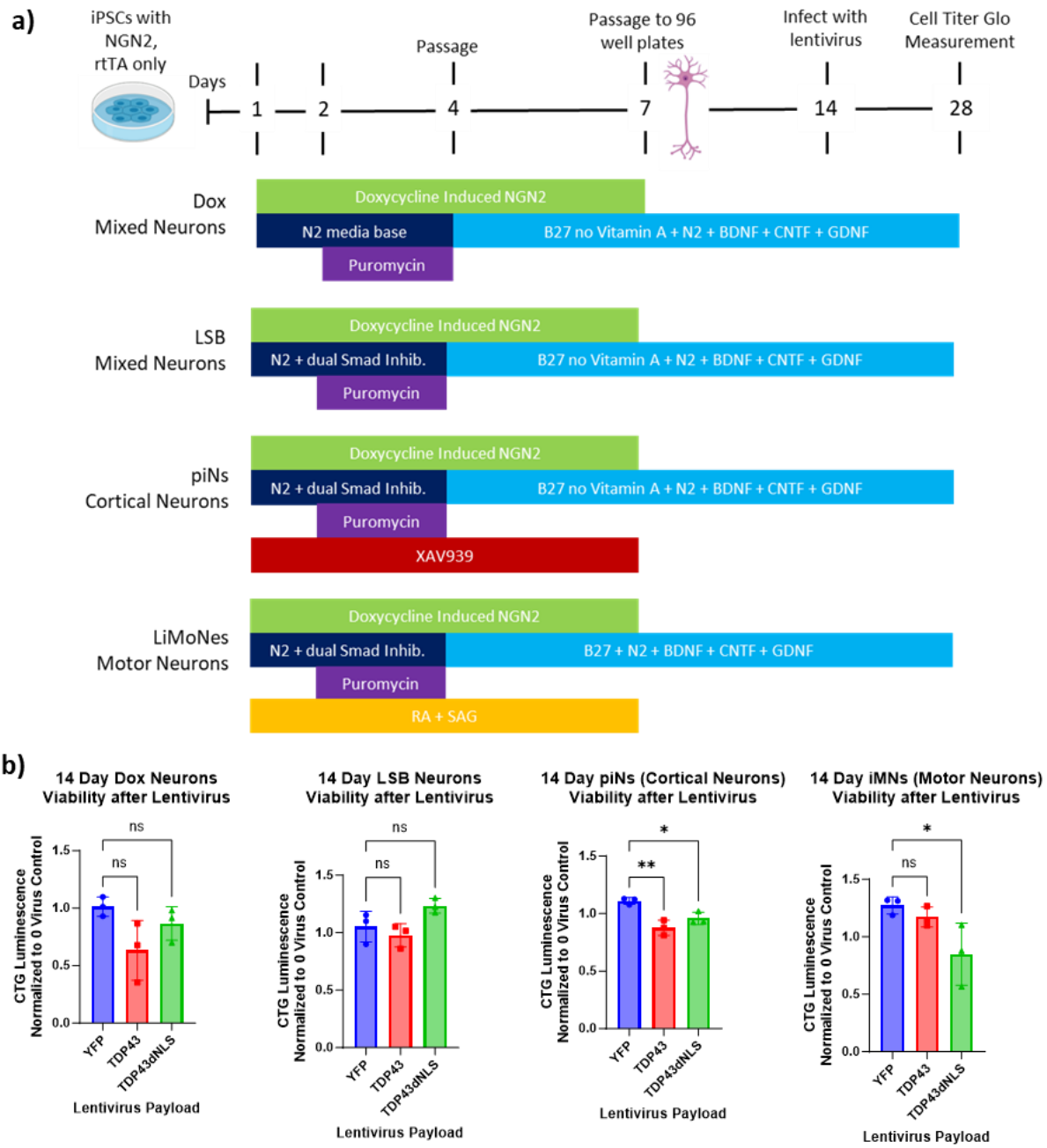

Figure 2.6: Motor and Cortical neurons are more sensitive to TDP-43 perturbation than mixed neuron differentiations (a) Experimental overview and summary of differentiation methods **(b)** Viability results as measured by Cell Titer Glo 14 days after infection with lentivirus. Significance calculated using a one-way ANOVA with Dunnett's multiple comparisons test for pairwise relationships (* = $p<0.05$; **= $p<0.01$) (n = 3 biological replicates).

motor neuron context for the treatment and study of ALS-specific drivers or cortical neuron context for the treatment and study of FTD-specific factors. For the remainder of this study, I will focus on motor neurons as I continue to explore ALS-specific neurodegenerative mechanisms and modifiers.

Discussion

In this chapter I sought to establish a human iPSC-derived neuronal platform for the continued study of TDP-43 perturbation-associated neurodegeneration. I developed and characterized two different methods for generating this engineered cellular platform of TDP-43 proteinopathy, an inducible vector driven method that expresses TDP-43 as the neurons differentiate and develop (Figure 2.3) and a lentiviral vector that can deliver TDP-43 after the core differentiation procedure is complete (Figure 2.4). These systems have an advantage over previously developed *in vitro* systems in that they exist in a context that is both neuronal and representative of a condition where the core perturbation is TDP-43 proteinopathy without any additional uncharacterized confounding factors that may influence the study, such as would be a concern in examining TDP-43 mutant harboring iPSC-derived neurons. Indeed, characterizing the effects of TDP-43 proteinopathy in the absence of *TARDBP* mutations is important given that most ALS patients develop TDP-43 aggregates without a mutation (Ling et al. 2013).

I was able to show that motor neurons derived using both methods described faithfully represent many features of the TDP-43 proteinopathy condition including viability loss upon TDP-43 perturbation and biochemical evidence of overexpression (Figures 2.3, 2.4, and 2.5). One feature that I did not show in this chapter is the propensity of overexpressed TDP-43 to form spontaneous cytoplasmic aggregates. Although I showed evidence of cytoplasmic translocation of TDP-43 upon overexpression (Figure 2.3d), my engineered TDP-43 overexpression neurons do

not generally form visible TDP-43 cytoplasmic foci without an additional stressor that drives the formation of TDP-43 containing stress granules (Becker et al. 2017). Taking a closer look at the qRT-PCR data from Figure 2.1, we observe that expression of TDP-43 mRNA in the TDP-43ΔNLS is nearly three-fold higher than in the wild-type TDP-43. In the next chapter, I will show that TDP-43ΔNLS expressing neurons do undergo spontaneous formation of cytoplasmic TDP-43 foci at baseline. Taken together, this suggests that wild-type TDP-43 overexpression may simply not be meeting the threshold for forming spontaneous aggregates that evade the cell's endogenous protein turnover machinery (e.g., autophagy or proteasome mediated degradation). The fact that TDP-43 also has the capacity to bind to and regulate the levels of its own transcript (Sephton et al. 2011) lends credence to a potential ability of cells to self-regulate nuclear overexpression of the protein, which would support why a wild-type TDP-43 overexpression model, being primarily nuclear, would not necessarily achieve as high levels of expression, even given a similar transduction rate of the delivery vector (Figure 2.2).

One caveat of the design of the inducible vector system I designed is that expression of TDP-43 cannot be decoupled from expression of NGN2 in the LiMoNes differentiation paradigm. This understandably raises questions about toxicity conferred by TDP-43 in this manner being truly relevant to adult-onset neurodegeneration as opposed to representing a model of neural development instead. Because the lentivirus experiment in Figure 2.5b gave similar results to the viability experiment using the inducible vector system in the short-term, I believe that the effects of TDP-43 overexpression as captured by the inducible system are still relevant. Additionally, there continues to be robust expression of the engineered TDP-43 construct after differentiation is complete – the neurons do not seem to be compensating for the overexpression by successfully downregulating the levels of endogenous TDP-43 production during the developmental process,

which one may expect of surviving cells (Figure 2.3c). I will also show in the following chapters that the majority of motor neurons in the differentiated culture are YFP+ after passaging, in part because the rtTA required for Doxycycline activation of both the NGN2 and inducible TDP-43 construct is located only on the inducible TDP-43 plasmid. Taken together, I believe these cellular models that I have generated are very relevant to the continued study of TDP-43 proteinopathy-associated mechanisms.

Lastly, these cellular models represent a key advantage of building platforms using the LiMoNes protocol. The fact that this protocol does not require an enrichment step to pull motor neurons from the culture as previous protocols had means that the LiMoNes differentiation method and models built on it are much more amendable to large scale, high throughput experiments. Previously, performing high throughput compound or genetic screens would not be feasible on motor neurons. Now that these models can be generated at scale in a week's time, the potential for screening assay development is within reach.

Materials and Methods

Cell Culture Conditions – HEK293 and iPSCs

HEK293 cells were maintained in Dulbecco's Modified Eagle Medium (DMEM) supplemented with 10% Tet System Approved Fetal Bovine Serum (FBS) (Takara #631368) to facilitate culture with inducible vector system components. Media was changed every 3 – 4 days and cells were passaged using Trypsin (Gibco #25200056) as needed. Cells were maintained in a 37℃, 5% CO_2 incubator.

The 11a iPSC line was derived from a biopsy from a 37-year-old healthy male patient as previously described in Boulting et al. 2011. iPSCs were maintained in mTESR1 or mTESR Plus (Stem Cell Technologies #85850, #100-0276) on Matrigel (Corning #354277) or Geltrex (Gibco #A1413201) coated tissue culture plates. Matrigel coatings were prepared by diluting 600uL of concentrate (prepared according to the dilution factor on the certificate of analysis for that lot of reagent) diluted in 24mL of DMEM/F12. Geltrex coatings were prepared by diluting thawed Geltrex 1:100 in Minimal Essential Media (MEM – Gibco #11095080). Coated plates were cured at 37℃ for at least one hour and the coating media was aspirated immediately prior to cell addition. Media was changed every 1 – 2 days (mTESR1) or 2 – 3 days (mTESR plus). Cells were passaged using Accutase (Stem Cell Technologies #07920) as needed. On thaw and passage, media was also supplemented with 10uM Rock Inhibitor (Y-27632 – Stemgent #04-0012) to facilitate adherence and survival. Cells were maintained in a 37℃, 5% CO_2 incubator.

When needed, aliquots of HEK293s or iPSCs were cryopreserved using CryoStor® CS10 Freeze Media (BioLife Solutions #210502) and stored in -80℃ or vapor phase liquid nitrogen.

Molecular Cloning of Plasmid Vectors

AAVS1-Neo-TRE-DEST-m2rtTA

All DNA components used to create the new inducible vector system were procured through Addgene. AAVS1-Neo-m2rtTA was a gift from Rudolf Jaenisch (Addgene plasmid # 60843; http://n2t.net/addgene:60843; RRID:Addgene_60843). pLIX_403 was a gift from David Root (Addgene plasmid # 41395; http://n2t.net/addgene:41395; RRID:Addgene_41395). Upon receipt of bacterial stabs, AAVS1-Neo-m2rtTA bacteria were amplified in an overnight LB media suspension culture at 37℃; pLIX_403 bacteria were amplified in a similar culture at 30℃. Plasmids were purified the next day Qiagen HiSpeed Plasmid Midi Prep kits (Qiagen #12643). The identity of each plasmid was confirmed using Sanger Sequencing provided by Genewiz (now Azenta Life Sciences) with the following sequencing primers: AAVS1-Neo Seq-Fwd: 5' – GGGATTAGATAAATGCCTGCTC – 3'; AAVS1-Neo Seq-Rev: 5' – CATGAGTGGGAGGAATGAGC – 3'; TRE Region Seq-Fwd: 5' – GAACGTATGTCGAGGTAGGC – 3'; TRE Region Seq-Rev: 5' – CGGTCTATGCTGTACTGTCG – 3'.

Modification of AAVS1-Neo-m2rtTA was performed via restriction enzyme digestion with EcoRV (New England Biolabs #R0195) followed by treatment with Alkaline Calf Intestinal Phosphatase (CIP – New England Biolabs #M0525). The opened vector was then isolated on a 1% agarose gel containing Ethidium Bromide and purified using the Qiagen Gel Extraction Kit (Qiagen #28704). Blunt-end ligation of a PCR product containing the Tet-inducible promoter and Gateway™ cloning insert sites from pLIX_403 was then performed to complete the base vector assembly. PCR primers used to target pLIX_403 were as follows: Forward Primer: 5' – CCGCGAATCGATATGTCGAG – 3'; Reverse Primer: 5' – GATCCTTAGTGGTGGTGGTG – 3'. Primers were treated with T4 Polynucleotide Kinase (New England Biolabs #M0201) before

commencing the PCR reaction. PCR reactions were performed using the Phusion High-Fidelity PCR Master Mix Kit with GC Buffer (New England Biolabs #M0532) according to manufacturer's instructions at an annealing temperature of 58°C for 30 cycles. Ligations of the PCR product to the opened AAVS1-Neo-M2rtTA plasmid were performed using Blunt/TA Ligase Master Mix (New England Biolabs #M0367) according to manufacturer's instructions.

Ligations were transformed to ccdB survival 2 $T1^R$ competent cells (Invitrogen #A10460) and resultant plasmids were purified using Qiagen Spin Miniprep kits (Qiagen #27104). Plasmids were screened for correct orientation of insertion using Sanger Sequencing provided by Genewiz with the following sequencing primers: AAVS1-Neo Seq-Fwd: 5' – GGGATTAGATAAATGCCTGCTC – 3'; AAVS1-Neo Seq-Rev: 5' – CATGAGTGGGAGGAATGAGC – 3'; TRE Region Seq-Fwd: 5' – GAACGTATGTCGAGGTAGGC – 3'; TRE Region Seq-Rev: 5' – CGGTCTATGCTGTACTGTCG – 3'; pCAG-F (for rtTA): 5' – GCAACGTGCTGGTTATTGTG – 3'. Upon identification of a successfully generated clone, the construct was again amplified in ccdB survival 2 $T1^R$ competent cells and purified as a midi prep batch of the final cloned construct using the Qiagen HiSpeed Plasmid Midi Prep kits. The end result of this effort is the destination vector on which the cDNAs of interest were expressed in – AAVS1-Neo-TRE-DEST-M2rtTA (Supplementary Figure 2.3).

TDP-43 and TDP-43ΔNLS Entry Clones and insertions into AAVS1 directed vector

All cDNAs were procured as plasmids from Addgene. pcDNA3.2 YFP was a gift from Aaron Gitler (Addgene plasmid # 84910 ; http://n2t.net/addgene:84910 ; RRID:Addgene_84910) pcDNA3.2 TDP-43 YFP was a gift from Aaron Gitler (Addgene plasmid #84911; http://n2t.net/addgene:84911; RRID:Addgene_84911). pcDNA3.2 TDP-43 NLS1 YFP was a gift

from Aaron Gitler (Addgene plasmid # 84912; http://n2t.net/addgene:84912; RRID:Addgene_84912). Upon receipt of bacterial stabs, each bacterial sample was amplified in an overnight LB media suspension culture at 37°C and plasmids from each were purified the following day using Qiagen Spin Mini Prep Kits. The identity of each plasmid was confirmed using Sanger Sequencing by Genewiz with the following sequencing primers: CMV-fwd: 5' – CGCAAATGGGCGGTAGGCGTG – 3'; EGFP-N-Rev 5' – CGTCGCCGTCCAGCTCGACCA – 3'

The cDNAs in the procured pcDNA3.2 backbones are flanked by Gateway cloning sites. A BP Clonase reaction (Invitrogen #11789-020) was performed according to manufacturer's instructions to transfer YFP, TDP-43:YFP, and TDP-43ΔNLS each to their own pDONR221 Entry Vector backbone. DNA from the BP reaction was transformed to Stbl3 Chemically Competent Bacteria Cells (Invitrogen #C7373-03) under manufacturer's recommended conditions and purified using Qiagen Spin Miniprep kits (Qiagen #27104) to generate the Gateway cloning entry vectors for each of my constructs of interest. Successful transfer of the cDNA insert was verified by Sanger Sequencing provided by Genewiz using the EGFP-N-Rev 5' – CGTCGCCGTCCAGCTCGACCA – 3' sequencing primer.

An LR Clonase (Invitrogen #11791-020) reaction was then performed according to manufacturer's instructions using each of the generated entry vector plasmids with AAVS1-Neo-TRE-DEST-m2rtTA as the destination vector. DNA from the LR reaction was also transformed to Stbl3 Chemically Competent Bacteria under manufacturer's recommended conditions and purified using Qiagen Spin Miniprep kits. Successful transfer of the cDNA insert was verified by Sanger Sequencing provided by Genewiz using the following sequencing primers: TightTRESeq-Fwd: 5' – GTGGGAGGCCTATATAAGCAG – 3'; EGFP-N-Rev 5' – CGTCGCCGTCCAGCTCGACCA

– 3'; V5Seq-Rev: 5' – TTTGGGATTGGCTTTCTGC – 3'. Once a plasmid for each condition was successfully isolated, a Midi prep was performed using the Qiagen HiSpeed Midiprep Kit to purify a large amount of the plasmid to facilitate electroporation.

pLX_313 Lentivirus Vectors

Similar to AAVS1-Neo-TRE-DEST-m2rtTA, pLX_313 is also a Gateway cloning destination vector. The base pLX_313 empty vector was obtained by request from the Broad Institute Genetic Perturbation Platform. This plasmid DNA sample was transformed to ccdB survival 2 $T1^R$ competent cells, amplified, and re-purified using a Qiagen Spin Mini Prep kit. Using the same LR Clonase procedure and subsequent transformation as described above, pLX_313-YFP, pLX_313-TDP-43:YFP, and pLX_313-TDP-43ΔNLS:YFP were generated from the entry clones previously used in creating the inducible AAVS1 plasmids. Successful cloning was verified using Sanger Sequencing provided by Genewiz or Psomagen using the EGFP-N-Rev 5' – CGTCGCCGTCCAGCTCGACCA – 3' sequencing primer**.**

Generation of stable engineered cell lines

HEK293 with AAVS1-inducible inserts

HEK293 cells were co-electroporated with the AAVS1-targeting inducible gene insert plasmid and a plasmid encoding an AAVS1 TALEN at a mass ratio of 5 donor vector to 1 nuclease using the Invitrogen Neon™ Transfection system. The conditions for electroporation were 1100V, 20ms pulse width, 2 pulses. Following electroporation, positive transductants were selected by culturing in DMEM + 10% Tet-Free FBS described above supplemented with 200ug/mL G-418 (Neomycin analog – Gibco #10131035)

iPSCs with AAVS1-inducible inserts

iPSCs were co-electroporated with the AAVS1-targeting inducible gene insert plasmid and a plasmid encoding an AAVS1 TALEN at a mass ratio of 5 donor vector to 1 nuclease using the Invitrogen Neon™ Transfection system. The conditions for electroporation were 1050V, 30ms pulse width, 2 pulses. Following electroporation, positive transductants were selected by culturing in mTESR1 or mTESR Plus as described above supplemented with 500ug/mL G-418.

Following selection, single cell clones were generated by plating the cells at a limiting dilution to achieve substantial separation between growing colonies (e.g. 500 cells total plated on a 10cm tissue culture dish). Culture media was supplemented with 1uM Rock Inhibitor for up to one week to increase viability of the sparse culture. Once the colonies were visible under the microscope, they were manually scraped from the plate using a pipette and transferred to a 24 well culture dish for continued outgrowth. Clones were expanded up to a 6-well culture before cryopreservation and subsequent evaluation.

Neuronal Differentiation Protocols

Prior to all differentiations, iPSCs were infected with lentivirus containing TetO-NGN2-Puro at approximately 2 MOI in a 6 well tissue culture dish. Cells were expanded and cryopreserved prior to the first differentiation.

LiMoNes Motor Neuron Differentiation

Adapted from Limone et al. 2023. iPSCs were plated in their desired format and grown until at least 80% confluent. Media changes each day were performed as follows. Day 1: N2 Media Base – DMEM/F12 Media (Gibco #11320033), 1X GlutaMAX (Gibco #35050061), 0.3% (v/v) Glucose (Sigma-Aldrich #G7021 – dissolved in PBS before addition), 1X N2 Supplement (Life Technologies #17502048) – supplemented with 4ug/mL Doxycycline (Sigma Aldrich #D9891 –

dissolved in water), 200nM LDN-193189 (Stemgent #04-0074-02 – dissolved in DMSO), 10µM SB-431542 (Tocris #1614 – dissolved in DMSO), 2µM Retinoic Acid (Sigma Aldrich #R2625 – dissolved in DMSO), and 2µM Smoothened Agonist (SAG – Stem Cell Technologies #73412 – dissolved in DMSO). Day 2 and 3: N2 Media Base supplemented with 4µg/mL Doxycycline, 5µg/mL Puromycin (Gibco #A11138-03), 100nM LDN-193189, 10µM SB-431542, 1µM Retinoic Acid, 1µM SAG. Day 4: NBM/B27+ Media Base – Neurobasal Media (Gibco #21103049), 1X GlutaMAX, 1X MEM Non-Essential Amino Acids (NEAA – Gibco #11140050), 1X N2 Supplement, 1X B27 Plus Supplement (Gibco #A3582801) – supplemented with 4µg/mL Doxycycline, 5µg/mL Puromycin, 1µM Retinoic Acid, 1µM SAG, 10ng/mL recombinant Brain Derived Neurotrophic Factor (BDNF – R&D Systems #11166-BD – dissolved in 0.1% (w/v) BSA-PBS), 10ng/mL recombinant Ciliary Neurotrophic Factor (CNTF – R&D Systems #257-NT – dissolved in 0.1% (w/v) BSA-PBS), and 10ng/mL recombinant Glial Cell Line-derived Neurotrophic Factor (GDNF – R&D Systems #212-GD – dissolved in 0.1% (w/v) BSA-PBS). Day 5 and 6: NBM/B27+ Media Base supplemented with 4µg/mL Doxycycline, 5µg/mL Puromycin, 1µM Retinoic Acid, 1µM SAG, 10ng/mL BDNF, 10ng/mL CNTF, 10ng/mL GDNF, and 1µM EdU (Invitrogen #A10044 – dissolved in DMSO). Day 7: Freshly differentiated neurons are passaged using Accutase in Day 5 differentiation media supplemented with 10uM Rock Inhibitor or cryopreserved in CryoStor CS10 as desired. Destination plates for passaged neurons are prepared as follows: plates are coated with Poly-D-Lysine (Gibco #A3890401) at 4°C overnight. Coated plates are then washed three times with PBS, coated with Natural Mouse Laminin (Gibco #23017015) diluted 1:200 in PBS and cured at 37°C for at least two hours. Plates are washed three times with PBS before neurons are seeded. Neurons thawed from frozen are plated using the same procedure as if they were freshly passaged Day 9+: Media is gently removed (i.e., without the use

of a vacuum aspirator), and slowly replaced with NBM/B27+ Media Base supplemented with 4µg/mL Doxycycline if needed to maintain expression of inducible vector insert, 10ng/mL BDNF, 10ng/mL CNTF, 10ng/mL GDNF, and 1µM EdU.. For maintenance of neuronal cultures, half-media changes are performed with the Day 9+ media every 2 – 3 days.

Dox Mixed Neuron Differentiation

Adapted from Limone et al. 2023 and Zhang et al. 2013a. iPSCs were plated in their desired format and grown until at least 80% confluent. Media changes each day were performed as follows: Day 1: N2 Type 2 Media Base – DMEM/F12, 1X GlutaMAX, 1X NEAA, 0.5% (v/v) Glucose, 0.5X N2 Supplement – supplemented with 2µg/mL Doxycycline. Day 2 and 3: N2 Type 2 Media Base supplemented with 2µg/mL Doxycycline and 5µg/mL Puromycin. Day 4 thru 7: NBM/B27noVitA Media Base – Neurobasal Medium, 1X GlutaMAX, 1X NEAA, 0.5% (v/v) Glucose, 1X B27 Supplement without Vitamin A (Gibco #12587010) – supplemented with 2µg/mL Doxycycline, 10ng/mL BDNF, 10ng/mL CNTF, and 10ng/mL GDNF. Cells were passaged 1:2 to a new Matrigel or Geltrex coated plate on Day 4 using the Day 4 – 7 media recipe additionally supplemented with 10µM Rock Inhibitor. On Day 7 neurons were passaged to plates coated with Poly-D-Lysine and Laminin as described in the previous section using the Day 4 – 7 media recipe additionally supplemented with 10µM Rock Inhibitor or cryopreserved using CryoStor CS10. For maintenance of differentiated neuronal cultures, half-media changes were performed with the Day 4+ media every 2 – 3 days beginning from Day 9.

LSB Mixed Neuron Differentiation

Adapted from Limone et al. 2023. This differentiation protocol is the same as the Dox mixed neuron differentiation protocol outlined above, but with the addition of 200nM LDN-

193189 and 10µM SB-431542 on Day 1; 100nM LDN-193189 and 10µM SB-431542 on Days 2 and 3.

piN Cortical Neuron Differentiation

Adapted from Nehme et al. 2018 and Limone et al. 2023. This differentiation protocol is the same as the LSB differentiation protocol outlined above, but with the addition of 4µM XAV939 (Stem Cell Technologies #72672) on Day 1 and 2µM XAV939 on Days 2 thru 7.

Lentivirus Production and Infection

Lentivirus was produced according to a protocol provided by the Broad Institute RNAi Consortium. HEK293T cells (maintained the same as HEK293) were used as the packaging cells. For 10cm plate virus production runs, HEK293T cells were seeded on 10cm plates at $3.8*10^5$ cells/mL (10mL per plate) for 24 hours. The plasmid transfection mixture is prepared as follows for each 10cm plate: 9µg psPAX2 packaging plasmid (gift from Didier Trono (Addgene plasmid # 12260 ; http://n2t.net/addgene:12260 ; RRID:Addgene_12260)), 0.9µg VSV-G envelope plasmid (gift from Didier Trono (Addgene plasmid # 12259 ; http://n2t.net/addgene:12259 ; RRID:Addgene_12259)), 9µg pLX vector of choice, and OPTI-MEM (Gibco #31985062) added to achieve a total volume of 225µL. The transfection reagent – TransIT-LT1 (Mirus Bio #MIR2300) – was diluted in OPTI-MEM by adding 54µL TransIT-LT1 to 36µL OPTI-MEM for a total volume of 90µL per 10cm plate. Each tube of diluted TransIT-LT1 was added to each of the plasmid transfection mix dropwise, gently mixed, and incubated at room temperature for 30 minutes. The final transfection mixes were then added to each cell plate and returned to the incubator overnight. The next day, the media was changed to 15mL viral harvest media – DMEM + 30% Tet System FBS – and incubated overnight. Each day for the following two days, virus-containing media was

harvested from the plate. On the first day, the harvested media is replaced with the same volume of fresh viral harvest media. The plates were discarded after the second harvest on the second day. Harvested lentivirus was concentrated 100-fold using Lenti-X Concentrator (Takara #631232) according to manufacturer's instructions. Approximate titers were determined by inoculating cells at a range of volumes and assessing percentage infection by fixing the neurons using 4% Paraformaldehyde 7 days after infection and using flow cytometry for YFP+ cells.

For reported experiments, plated cells to be infected were inoculated with lentivirus directly into freshly changed culture medium to achieve MOI ≈ 1 according to the results of the titration. Cells were incubated for 48 hours before the next media change, at which point culture maintenance proceeds as previously described for that cell type.

Representative pictures of TDP-43ΔNLS expression via lentivirus are provided in Supplementary Figure 2.4.

FACS and Flow Cytometry

Cells were prepared for flow cytometry sorting or analysis by resuspending freshly a freshly passaged cell sample in sorting buffer (PBS with 1mM EDTA, 15mM HEPES, 1% (w/v) BSA). Support for FACS experiments was provided by the Department of Stem Cell and Regenerative Biology Flow Cytometry Core. Live-cell sort experiments were conducted using a BD FACS Aria II+. For fixed cell flow cytometry experiments, analysis was performed using a BD LSR II or BD Symphony A5.

RNA Extraction and qRT-PCR

RNA extractions from cultured cells were performed using the Qiagen RNEasy Plus Mini Kit (Qiagen #74134). QIAshredder columns (Qiagen #79656) were used for homogenization of

harvested cultures prior to RNA purification. cDNA generation was performed using the iScript (Bio-Rad #1708890) or iScript Advanced (Bio-Rad #172037) cDNA Synthesis kits with 500ng RNA input. qRT-PCR was performed using the generated cDNA reactions diluted 1:4 and combined according to manufacturer's instructions with iTaq™ Universal SYBR® Green Supermix (Bio-Rad #1725124). Primers used were as follows: GAPDH-Fwd: 5' – TTGTCAAGCTCATTTCCTGGTATG – 3; GAPDH-Rev: 5' – TTCTCTTGTGCTCTTGCTGG – 3'; TDP-43 1: 5' – CAGCTCATCCTCAGTCATGTC – 3'; TDP-43 2: 5' – GATGGTGTGACTGCAAACTTC – 3'. Samples were run as technical triplicates with an additional no template control. Reactions were performed on a Bio-Rad CFX96 Real-Time PCR Detection System using the following protocol: 1 step of 95℃ 30s followed by 95℃ 5s, 60℃ 30s for 40 Cycles.

Western Blots

Whole cell western blots

Protein was extracted from cultured cells using RIPA buffer (Thermo Scientific #89900) supplemented with 1X Halt™ Protease/Phosphatase Inhibitor Cocktail (Thermo Scientific #78440). Cells were incubated in a suspension of RIPA buffer on ice for 10 minutes before centrifugation at maximum speed for 20 minutes followed by collection of the protein containing supernatant. Protein was quantified using the Pierce™ BCA Protein Assay Kit according to manufacturer's instructions (Thermo Scientific #23225). Absorbance of the quantification plate at 562nM was read using a Cytation3 plate reader. 10µg of protein from each sample was resuspended in Blue Loading Buffer enriched with DTT as the reducing agent (Cell Signaling Technology #7722). Diluted samples were boiled for 5 minutes at 95℃ before being loaded to Bio-Rad Mini-PROTEAN TGX 4 – 20% pre-cast gels (Bio-Rad #4561094). Precision Plus Protein

Dual Color Standards (Bio-Rad #1610374) was used as the molecular weight ladder. Gels were run using Tris/Glycine/SDS Running Buffer (National Diagnostics #EC-870) at 200V for 40 minutes. Gels were transferred to a PVDF membrane using the iBlot 2 Dry Transfer system. Membranes were cut to size and blocked for 1 hour in LI-COR Intercept® Blocking Buffer at room temperature (LI-COR #927-60001). Primary antibodies were then diluted as appropriate in 5% (w/v) BSA-TBS-T (Tris Buffered Saline with 0.1% (v/v) Tween 20) and added to the membranes to incubate at 4°C overnight. Primary antibodies utilized were Rabbit anti-TDP43 (G400) (Cell Signaling #3448S) at 1:1000 dilution and Mouse anti-GAPDH (Millipore Sigma #MAB374) at 1:1000 dilution. The next day, membranes were washed with TBST, incubated with LI-COR anti-rabbit and anti-mouse IRDye secondary antibodies suspended in Blocking Buffer supplemented with 0.1% (v/v) Tween 20 and 0.01% (w/v) SDS for 1 hour and then washed again with TBST before being visualized on the LI-COR Odyssey Imager.

Cellular Fractionation Western Blots

Subcellular protein fractionations were performed using the Subcellular Protein Fractionation Kit for Cultured Cells (Life Technologies #78840) according to manufacturer's instructions. After the fractions were isolated, the same procedure was followed as the whole cell western blot for BCA quantification of the protein, running the gel, and analyzing the membrane. Primary antibodies used were Rabbit anti-TDP43 (G400) at 1:1000 dilution, Mouse anti-GAPDH at 1:1000 dilution, Mouse anti-HistoneH3 (96C10) (Cell Signaling #3638) at 1:1000 dilution and Chicken anti-GFP (Abcam #ab13970) at 1:5000 dilution. When needed for sequential blotting, I also used Restore Plus Western Blot Stripping Buffer (Thermo Scientific #46430) to gently remove the previous antibodies from the membrane. To complete this, the membrane was washed 3 times with PBS, coated with stripping buffer at room temperature with gentle shaking for 30 minutes,

washed again 3 times with PBS, then re-blocked with Intercept Blocking Buffer before adding the primary antibody mix as previously described.

Immunofluorescence and Imaging

All immunofluorescence, including confocal imaging, was performed in Perkin Elmer 96-well PhenoPlates. Cells to be stained were fixed with 4% Paraformaldehyde for 20 minutes at room temperature or overnight at 4°C. Fixed cells were briefly washed with PBS and then coated with a blocking and permeabilization buffer comprised of 0.1% (v/v) Triton X-100-PBS (Sigma Aldrich #T8787) and 10% Normal Donkey Serum (Jackson ImmunoResarch Laboratories #017-000-121) for one hour at room temperature. Primary antibodies were then added diluted in the stated blocking/permeabilization buffer and incubated overnight at 4°C. The following day, the plate was washed three times with PBS and the Alexa-Fluor conjugated secondary antibodies were added diluted 1:1000 in PBS for one hour in the dark. Two PBS washes were performed followed by incubation with 1µg/mL DAPI (Invitrogen #D3571) for 5 minutes in the dark. After two additional PBS washes, the plates were imaged or stored at 4°C until imaging. Primary antibodies used in the studies in this chapter are Rabbit anti-TDP43 (G400) at 1:100 dilution, Mouse anti-Tuj1/βIII-Tubulin at 1:100 dilution (R&D Systems #MAB1195) and/or Rabbit anti-NGN2 (Abcam #ab109236) at 1:100 dilution. Imaging was performed using either the Zeiss LSM 700 (for high magnification confocal microscopy), the Molecular Devices IXM (for high throughput confocal microscopy), or the Nikon Eclipse Ti. Live cell images of neurons expressing YFP conferred by lentivirus were captured with a Nikon Eclipse TE2000-S.

Colony Formation Assays

iPSCs were plated at 250,000 cells per well in a 6 well tissue culture plate using standard methods. 24 hours after plating, media was supplemented with 2 (Figure 2.2) or 4µg/mL (Supplementary Figure 2.5) Doxycycline for half of the plate each. Cells were maintained in media with or without doxycycline on the regular feeding schedule for 6 additional days. On the final day, cells were fixed with ice-cold methanol for 10 minutes on ice and stained with a 0.5% Crystal Violet solution comprised of water and 25% methanol (VWR #BT144750) with gentle shaking for at least 20 minutes at room temperature. Plates were scanned using a conventional flat screen paper scanner to capture images. Crystal Violet levels were quantified after imaging using 10% Acetic Acid (v/v in water) extraction by coating the wells with the solution, gently shaking for at least 30 minutes, and then measuring the absorbance of samples from each well at 570nM using a Cytation3 plate reader.

Cell Titer Glo Viability Assays

For HEK293, iPSC and neuron viability assays iPSCs or neurons were plated on 96 well tissue culture plates at 5,000 cells per well (HEK293), 10,000 cells per well (iPSCs), or 30,000 cells per well (Neurons) per standard culture methods. HEK293s and iPSCs began 2µg/mL Doxycycline treatment for selected wells 24 hours after plating. Neurons were infected with a YFP, TDP-43:YFP, or TDP-43ΔNLS:YFP lentivirus 7 days after plating. After an additional 6 days (HEK293, iPSCs), 14 Days (Neurons Figure 2.6), or 28 days (Neurons Figure 2.5), cells were assayed using Cell Titer Glo 2.0 reagent according to manufacturer's instructions (Promega #G9243). Luminescent readings were captured using a Cytation3 plate reader.

For the short-term differentiation assay, NGN2 infected iPSCs were plated on 96 well tissue culture plates at 10 – 20,000 cells per well per standard culture methods. LiMoNes motor neuron differentiation commenced 24 hours after plating until the captured timepoints listed. There was a

separate 96 well plate for each time point. Undifferentiated samples were exposed to the same differentiation media as the rest of the plate without Doxycycline, Puromycin, or EdU. On each read day reported, one plate was assayed using Cell Titer Glo 2.0 reagent according to manufacturer's instructions. Luminescent readings were captured using a Cytation3 plate reader.

Additional Acknowledgements

Menglu Qian provided key reagents and initial protocols for the electroporation protocol that was optimized to generate the stable HEK293 and iPSC lines. Kevin Smith and the Harvard Center for Biological Imaging provided access to and support for using the LSM700 confocal microscope. Michelle Sauer provided support for using the Molecular Devices IXM confocal microscope. Live cell FACS sorting performed by Joyce LaVecchio and Nema Kheradmand at the Harvard Stem Cell and Regenerative Biology Flow Cytometry Core. Kellie Liu assisted with lentivirus production and characterization and performed the multi-differentiation TDP-43 sensitivity experiment in Figure 2.6 under my supervision.

Chapter 3: Elucidating effects of cytoplasmic TDP-43 on the health and function of human motor neurons

Abstract

Transactive Response DNA-binding protein 43 (TDP-43) is a multifunctional nucleic acid binding protein ubiquitously expressed in all tissues. Although it is primarily nuclear, Amyotrophic Lateral Sclerosis (ALS) patients frequently present with cytoplasmic aggregates of TDP-43 in motor neurons on post-mortem examination. Although only about 5% of all ALS patients have a *TARDBP* mutation (Ghasemi and Brown 2018; Ingre et al. 2015), which is known to cause these insoluble cytoplasmic aggregates, 97% of ALS patients will develop cytoplasmic, insoluble TDP-43 aggregates regardless of whether they have a mutation in *TARDBP* or not (Ling et al. 2013). This suggests that there are mutation-independent mechanisms that drive pathogenic aggregation of TDP-43 which have yet to be fully elucidated. In this chapter, I demonstrate that I can use induced pluripotent stem cell (iPSC)-derived motor neurons in conjunction with inducible expression of a cytoplasmically locked variant of TDP-43, TDP-43ΔNLS, to establish a model on which we can discover what these mutation-independent mechanisms of TDP-43 aggregation driven neurodegeneration could be. I will show that cytoplasmic TDP-43 fundamentally changes the cellular response to stress by causing the cell to exhibit more signs of stress at baseline as measured by a higher increase in the basal number of stress granules and TDP-43 aggregates. I will then explore several potential mechanisms, including changes in synaptic structure and apoptotic priming, that could be driving this increase in basal stress level by interrogating transcriptomic changes during TDP-43ΔNLS expression using bulk RNA-sequencing. Overall, I will establish that this cellular platform can substantively contribute to mechanistic discovery efforts for neurodegeneration that have the potential to be therapeutically actionable and relevant for a broad population of ALS patients.

Introduction

Transactive Response DNA-binding protein 43 (TDP-43) is a nucleic acid binding protein involved in several cellular processes including RNA splicing, nucleocytoplasmic transport of RNAs, and translational regulation (Birsa et al. 2020; Freibaum et al. 2010; Lee et al. 2021; Sephton et al. 2011). Although most of TDP-43 is localized to the nucleus at any given time, one striking feature of TDP-43's localization dynamics is that it a large amount of TDP-43 will become temporarily cytoplasmically localized in response to a cellular stress such as free radical exposure via an oxidative stress (Markmiller et al. 2021), transient proteasome inhibition (Klim et al. 2019), or axonal injury (Sato et al. 2009). This suggests that transient cytoplasmic localization of TDP-43 may be beneficial for cells, particularly neurons, in the short-term as part of the canonical response to internal or environmental stress.

In contrast, it has also been established that persistent cytoplasmic localization of TDP-43, even in models that did not focus on whether this cytoplasmic localization caused spontaneous aggregation, is detrimental to cellular health and function (Barmada et al 2010, Walker et al 2016, Zamani et al. 2022). We additionally know that when TDP-43 does aggregate by virtue of being in the cytoplasm that these aggregates tend to disrupt protein turnover machinery (Ormeno et al. 2020; Riemenschneider et al. 2022; Torres et al. 2017) and destabilize essential functions of the mitochondria (Aggad et al. 2014; Dafinca et al. 2021; Hong et al. 2012; Shan et al. 2010; Wang et al. 2019; Wang et al. 2013). However, these observations to date have only been described in non-human systems, most of which did not focus on motor neurons. Given that TDP-43 re-localization and aggregation occurs in 97% of all Amyotrophic Lateral Sclerosis (ALS) patients (Ling et al. 2013), exploring when and how cytoplasmic TDP-43 becomes detrimental to motor neuron health,

particularly in a human system, is very likely to be informative when developing therapeutic strategies to attenuate and mitigate the pathogenic effect of cytoplasmic TDP-43 or its aggregates.

One hypothesis of how TDP-43 aggregates may begin to form centers around the propensity of TDP-43 to co-localize with stress granules (Dewey et al. 2012; Fang et al. 2019). Because of the link between TDP-43 localization and stress onset, I was also interested in examining the relationship between cytoplasmic TDP-43 and stress granules to examine if the presence of TDP-43 in the cytoplasm changed how neurons respond to stress and/or drove the cell to assume a more stressed state as though cytoplasm TDP-43 could be a signal to the cell that it needed to drive pathways related to the stress response, even if a stress was not present.

This chapter will describe the process of establishing the human *in vitro* iPSC-derived motor neuron system described in Chapter 2 for the study of neurodegeneration as conferred by cytoplasmic TDP-43 via expression of the TDP-43ΔNLS variant. I will then show that this model is powered to phenotypically explore how the number of stress granules changes in response to an acute oxidative stress when TDP-43ΔNLS is expressed. Finally, I will showcase and discuss data from RNA sequencing of TDP-43ΔNLS motor neurons compared to TDP-43 wild type overexpressing motor neurons to examine what cellular processes could be preferentially disrupted in the TDP-43ΔNLS condition that may merit further study for ALS therapeutic development.

Results

Inducible TDP-43ΔNLS expression is achievable in motor neurons

Using the same methods as described in Chapter 2, I was able to electroporate the 11a healthy control iPSC line with my AAVS1-Neo-TRE-TDPΔNLS:YFP-rtTA plasmid and select and screen for successful transductants. I then differentiated those engineered iPSCs into motor neurons using the LiMoNes method (Limone et al. 2023) and characterized the resultant cultures

by immunofluorescence (Figure 3.1a), cellular fractionated western blots (Figure 3.1b), and qRT-PCR (Figure 3.1c). As expected, I was able to achieve robust expression of the TDP-43ΔNLS construct and it successfully induces a high level of expression of TDP-43 in the cytoplasm. Of particular note is that partial nuclear clearance of TDP-43 can be observed by immunofluorescence, which is supported by the results in HEK293 (Figure 2.1; Winton et al. 2008a).

Inducible TDP-43ΔNLS expression represents a TDP-43 gain of function model because its expression does not induce changes in splicing of STMN2

To better contextualize the cellular state that the TDP-43ΔNLS model represents, I decided to examine whether the cytoplasmic clearance seen by eye in the immunofluorescence images was sufficient to induce splicing defects similar to TDP-43 loss of function models (Klim et al. 2019, Melamed et al. 2019). The sentinel mRNA that I used for this analysis was *Stathmin-2* (*STMN2*), which had previously been shown to experience cryptic exon inclusion in the context of TDP-43 knockdown that truncates the protein (Klim et al. 2019; Melamed et al. 2019). I hypothesized that if TDP-43ΔNLS:YFP as expressed from my inducible vector system was sufficient to drive complete clearance of TDP-43, then I would observe a marked increase in the amount of cryptic *STMN2* mRNA in neurons expressing TDP-43ΔNLS:YFP compared to YFP. Upon examination by qRT-PCR, I did not observe a significant increase of cryptic *STMN2* mRNA in the TDP-43ΔNLS line (Figure 3.2). I also did not observe a substantive decrease in full length *STMN2* mRNA levels (Supplementary Figure 3.1). This suggests that the model of TDP-43ΔNLS I have is more akin to a gain of function model of TDP-43 as I could establish cytoplasmic localization of TDP-43 (Figure 3.1a, b) but did not exhibit signs of splicing defects, which is a core feature of the TDP-43 loss of function model.

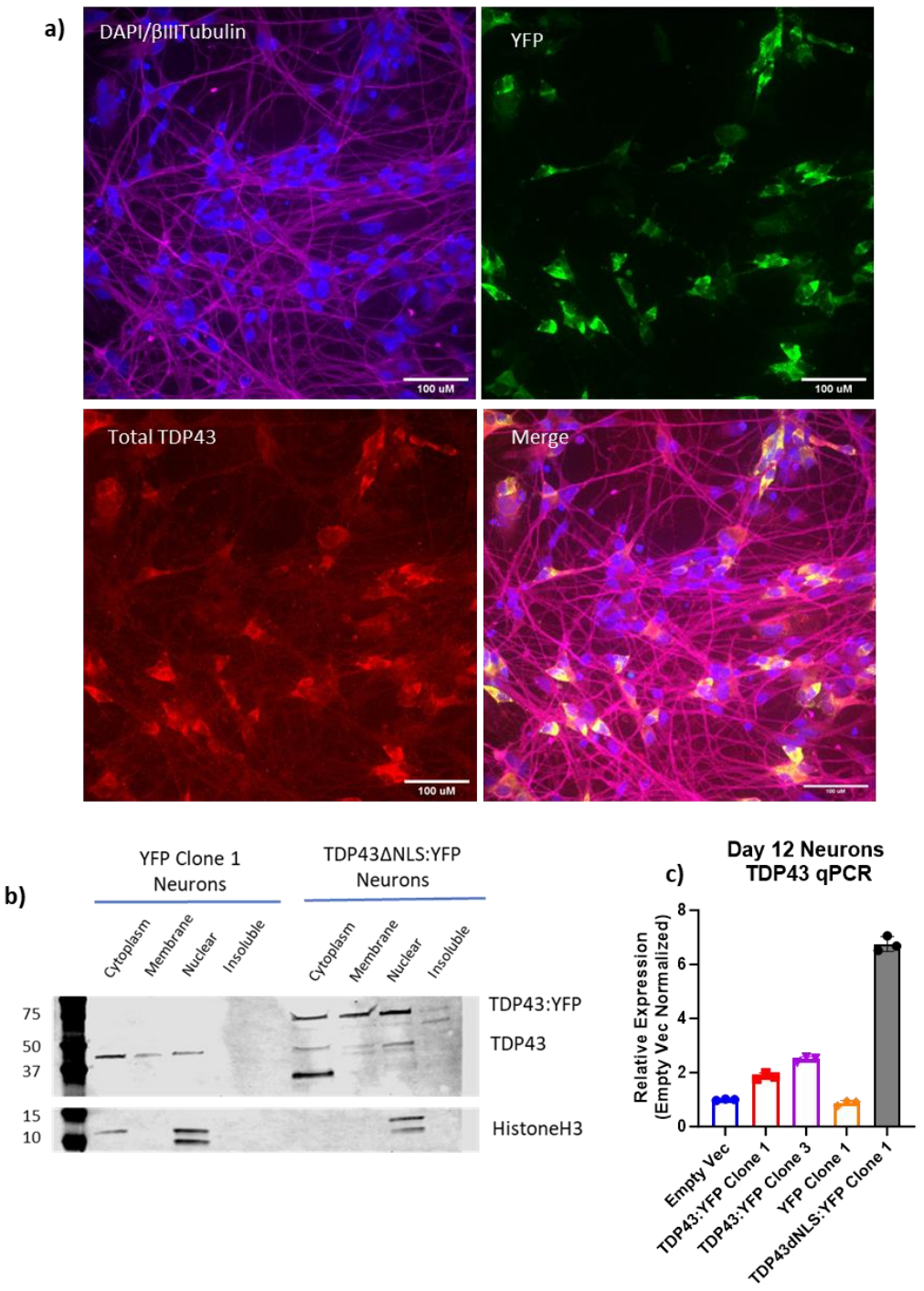

Figure 3.1: Expression and characterization of inducible TDP-43ΔNLS:YFP in engineered iPSC-derived motor neurons (a) Representative immunostained confocal images of fixed motor neurons 12 days after initiation of differentiation **(b)** Subcellular fractionated western blot of YFP and TDP-43ΔNLS:YFP motor neurons 12 days after initiation of differentiation **(c)** qRT-PCR of Day 12 neurons harboring different inducible constructs, now including TDP-43ΔNLS:YFP (n = 3 technical replicates).

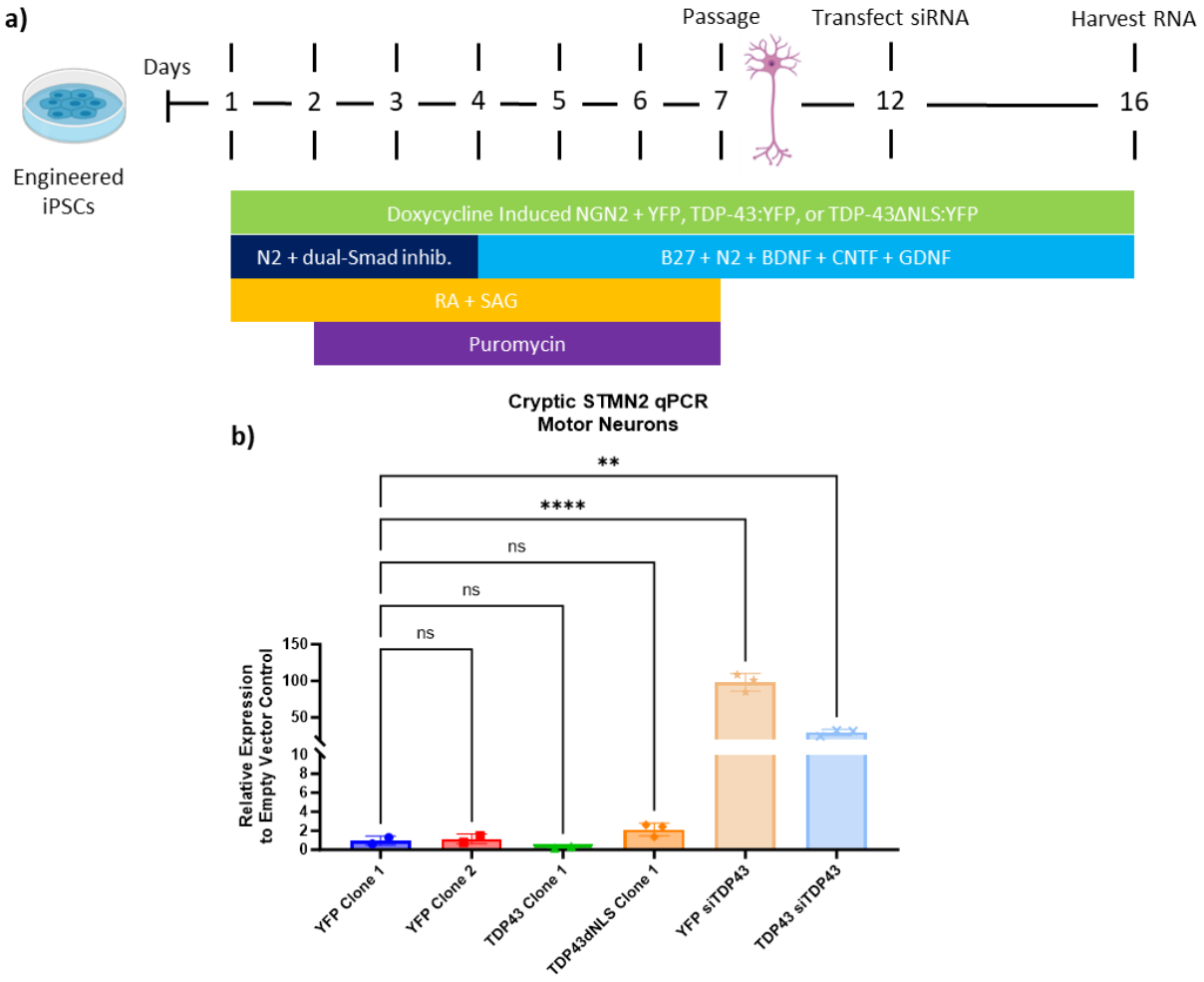

Figure 3.2: Expression of TDP-43ΔNLS does not lead to an increase in cryptic STMN2 splicing (a) Experimental schematic, including siRNA treatment timeline of positive controls **(b)** Expression of cryptic *STMN2* levels as determined by qRT-PCR in motor neurons. Significance calculated Significance calculated using ANOVA with Šídák's multiple comparisons test (** = $p<0.01$; **** = $p<0.001$) (n = 3 technical replicates).

TDP-43ΔNLS expression is neuroprotective during the short-term differentiation assay

As a final characterization step for the TDP-43ΔNLS model, I sought to see how the expression of cytoplasmic TDP-43 affected neuronal viability in the short-term using the short-term differentiation assay initially described in Figure 2.5. I observed that in this context, TDP-43ΔNLS:YFP expression seems to be protective – cells expressing this construct do not experience the same viability loss that developing neurons expressing wild-type TDP-43 do (Figure 3.3). This

seems in line with the observed function of cytoplasmic TDP-43 in response to a cellular stress. In those contexts as well, cytoplasmic TDP-43 was not immediately detrimental to cellular health; those models showed short-term recovery of TDP-43 localization after the stress was alleviated. This suggests that during the acute stress phase, cytoplasmic TDP-43 may be exerting a protective function, which may also manifest itself in looking at a less than seven-day assay like the short-term differentiation assay is. The following results will begin to make inroads on what some of those short-term protective and long-term pathogenic mechanisms may be.

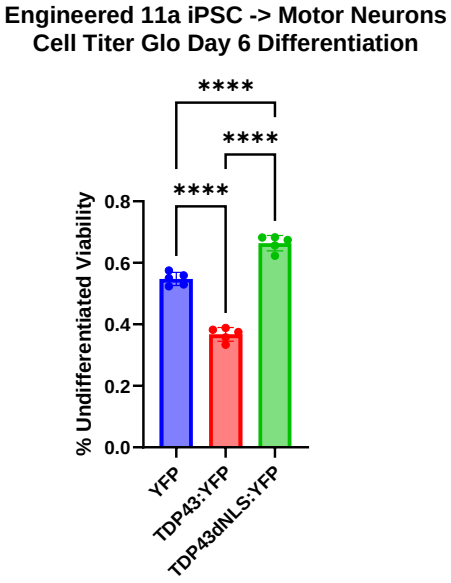

Figure 3.3: TDP-43ΔNLS expression in the short-term does not result in viability loss in motor neurons. Using the short-term differentiation assay outlined in Figure 2.5, TDP-43ΔNLS:YFP developing motor neurons do not experience a viability drop around Day 6 like the TDP-43 wild-type expressing motor neurons do. Significance calculated using ANOVA with Šídák's multiple comparisons test (**** = $p<0.001$) (n = 3 biological replicates).

Presence of cytoplasmic TDP-43 increases number of baseline TDP-43 containing stress granules, but abrogates stress-induced stress granule increase in the context of oxidative stress

To examine how cytoplasmic TDP-43 could potentially be protective or pathogenic, I decided to explore how cytoplasmic TDP-43 changed motor neurons' response to stress. Because a neuron, by virtue of being a post-mitotic cell that is generally not replaceable, must be

particularly well equipped to handle stress, it stands to reason that modulations in how the stress response progresses may be detrimental to the health of the neuron in the long-term. Given that presence of stress granules is a proxy for the cell invoking stress-related cellular processes (the number of stress granules goes up when the cell is experiencing a stress, as the name suggests) and that stress granules have been hypothesized to be the seed for pathogenic TDP-43 aggregation (Dewey et al. 2012; Fang et al. 2019) , I decided to examine how expression of TDP-43ΔNLS:YFP changed the number of stress granules in response to an acute oxidative stress, sodium arsenite exposure, which is a common modality used in the field (Becker et al 2017; Nonhoff at al 2007) (Figure 3.4). To perform this analysis, I developed an analysis pipeline in the Columbus imaging software to identify puncta in cells that could correspond to aggregates of TDP-43 or the stress granule assembly protein G3BP1 (Figure 3.4b, c)

I observed that in the presence of cytoplasmic TDP-43, motor neurons did not show an increase in stress granules when a stress was applied unlike in the context of no transgene expression or expression of wild-type TDP-43:YFP (Figure 3.4d). However, the basal number of stress granules observed in the TDP-43ΔNLS, unstressed condition was higher than the unstressed

Figure 3.4: TDP-43ΔNLS expression in the context of oxidative stress increases the baseline number of stress granules while decreasing the magnitude of stress-responsive increases in total and TDP-43-containing stress granule number (a) Experimental Outline **(b)** Representative confocal images of stressed and unstressed neurons **(c)** Representative monochrome YFP channel image of the analysis procedure. Circles represent aggregates identified by the analysis procedure. **(d)** Results of stress granules per neuron image analysis by captured field in each neuron line. n = 44 ~ 80. Significance calculated using ANOVA with Šídák's multiple comparisons test (* = $p<0.05$; ** = $p<0.01$; **** = $p<0.001$) **(e)** Results of TDP-43 aggregates per neuron images analysis by captured field in each neuron line. n = 43 ~ 80. Significance calculated using ANOVA with Šídák's multiple comparisons test **(f)** Results of TDP-43 containing stress granules per neuron images analysis by captured field in each neuron line. n = 38 ~ 80. Significance calculated using ANOVA with Šídák's multiple comparisons test (** = $p<0.01$).

Figure 3.4 (Continued)

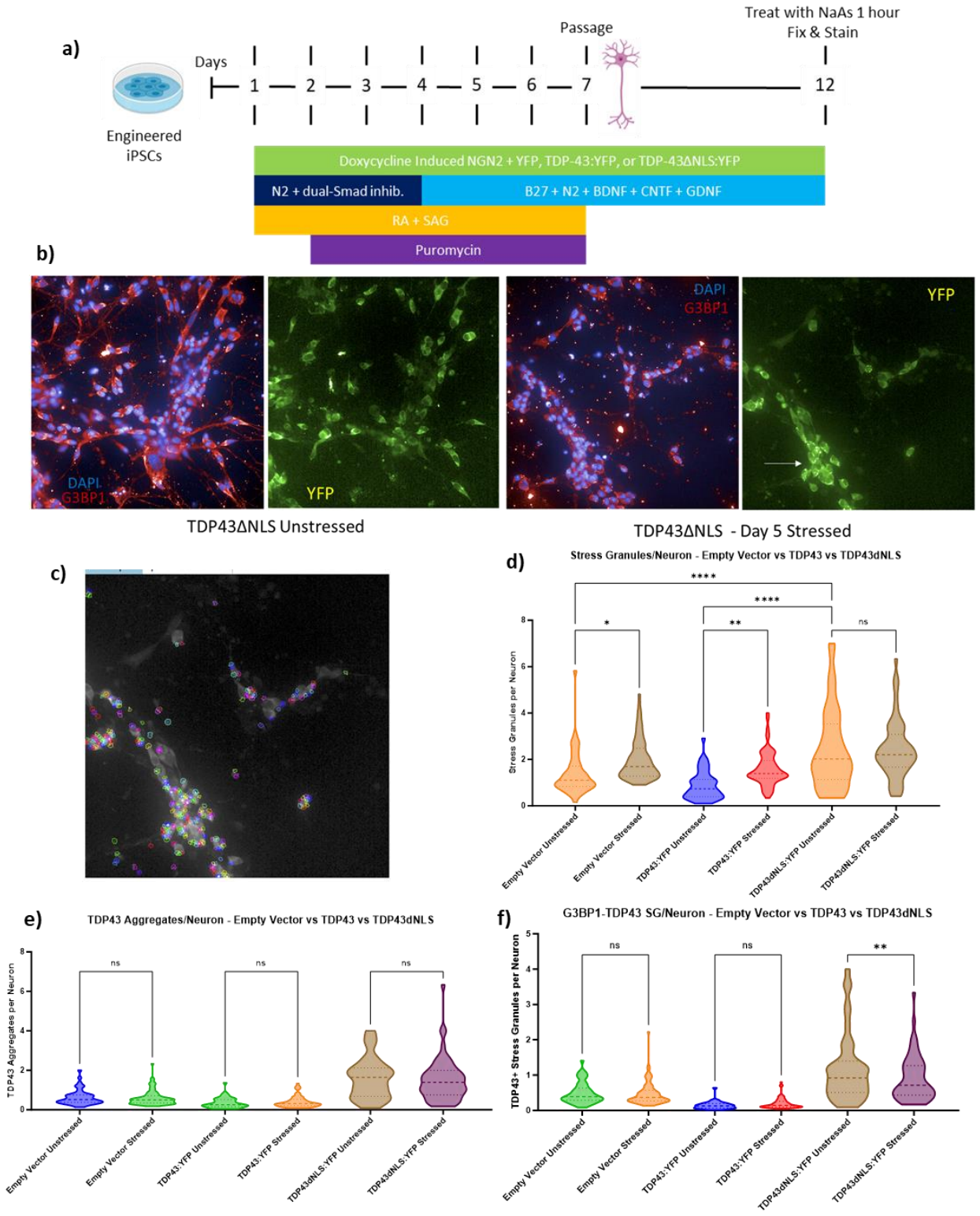

state in the other genetic contexts. The same relationship held from the perspective of total number TDP-43 aggregates (stress granule localization agnostic) (Figure 3.4e).

In interrogating the number of TDP-43 positive stress granules, I noted that although sodium arsenite oxidative stress generally only resulted in a modest increase of TDP-43 positive stress granules in the no transgene or TDP-43:YFP expression conditions, there was a decrease in TDP-43 positive stress granules in response to the oxidative stress application in the context of TDP-43ΔNLS:YFP (Figure 3.4f). Taken together, these observations capture the dual-role of cytoplasmic TDP-43 in short-term protection but suggest a potential longer-term harm to cellular health. From the observation of a decrease in the amount of TDP-43 positive stress granules in the short term, it is possible that the presence of cytoplasmic TDP-43 may be acting as a modifier of its own stress granule aggregation, sequestering excess cytoplasmic TDP-43 out of stress granules during a stress event such that anything that is not needed may be turned over by endogenous processes. However, given that the total number of stress granules in the unstressed condition is higher in the TDP-43ΔNLS line than the others also suggests that the neurons may be assuming a more basally stressed state. It is reasonable to expect that the effect of a perceived chronic stress, wherein the result could be longer than usual translational stalling of mRNAs trapped in stress granules, may not be healthy for the cell in the long-term.

Transcriptomic analysis of TDP-43ΔNLS motor neurons reveals changes in pathways implicated in synapse structure, apoptosis, and the cellular stress response

To further explore the effects of persistent cytoplasmic TDP-43 localization could be, we performed RNA sequencing on Day 12 (from the start of differentiation) motor neurons containing the inducible TDP-43ΔNLS:YFP, TDP-43:YFP, and YFP constructs. We examined the differential expression of genes in the TDP-43ΔNLS condition compared to the TDP-43 condition to

determine what genes and pathways could be specifically implicated in characterizing the cellular state where TDP-43 is primarily cytoplasmic, not just when TDP-43 is perturbed versus when it is not (Figure 3.5a). For example, in this comparison, if a genetic factor was driving motor neuron toxicity because of TDP-43 overexpression, but was agnostic to TDP-43 localization, then by design it would not score as a strong hit in this analysis.

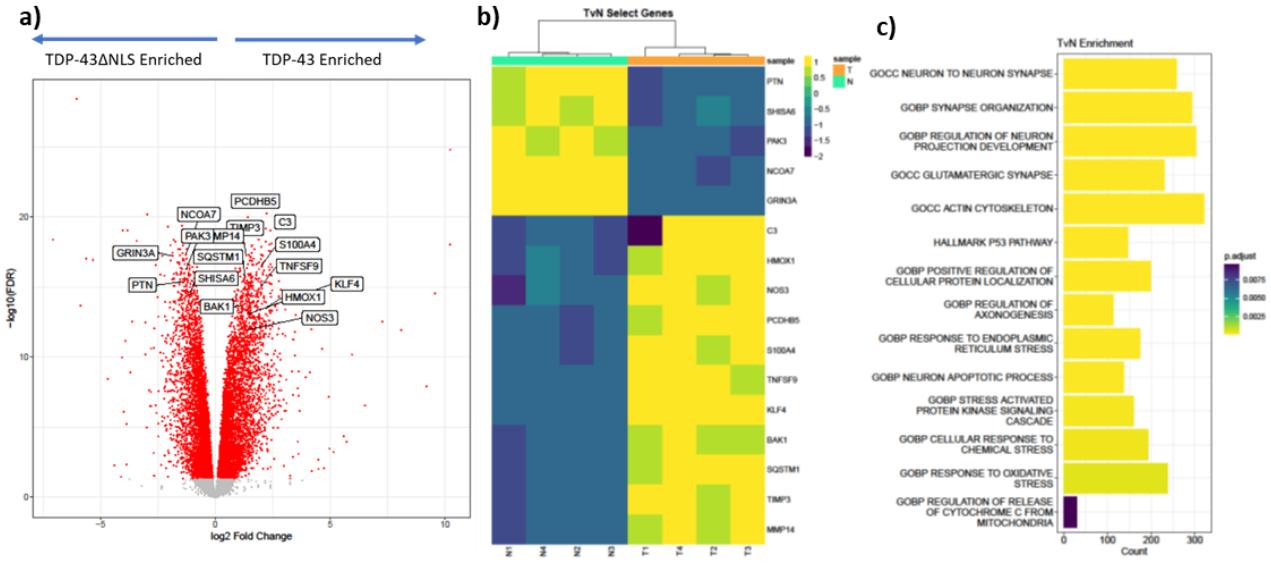

Figure 3.5: Transcriptomic effects of TDP-43ΔNLS expression compared to wild-type TDP-43 in motor neurons (a) Volcano plot of differentially expressed genes from RNA sequencing. Highlighted dots represent genes that pass a FDR < 0.05 significance threshold for discovery. **(b)** Heatmap of select genes related to synapse organization, apoptosis, and the neuronal oxidative stress response discovered as significant in the RNAseq experiment. Each column represents a replicate sample submitted for sequencing. T = TDP-43; N = TDP-43ΔNLS **(c)** Pathway over-enrichment analysis results of differentially expressed genes in TDP-43ΔNLS motor neurons compared to wild-type TDP-43 overexpressing motor neurons.

We identified 95 transcripts that were enriched in the TDP-43ΔNLS condition above a log2 fold change threshold of 2 compared to wild-type TDP-43 and 272 transcripts by the same standard that were enriched in the wild-type TDP-43 condition. A selection of genes of particular interest to neurobiological functions are presented in the heat map in Figure 3.5b. We also performed an over enrichment analysis using all genes called as significantly differentially expressed and discovered

several pathways perturbed in the cytoplasmic versus wild-type TDP-43 comparison including factors related to synapse organization, apoptosis, and response to oxidative, chemical, and endoplasmic reticulum stress (Figure 3.5c). From what we understand about the effect of cytoplasmic TDP-43 in other non-human systems, it is reassuring that some similar mechanisms previously hypothesized to influence cytoplasmic TDP-43 pathogenesis, such as by eliciting changes in mitochondria and driving ER stress (Dafinca et al. 2021), are represented in this analysis.

Discussion

In this chapter I sought to establish in iPSC-derived motor neuron model of persistent cytoplasmic TDP-43 expression and examine the features of that model to learn more about mechanisms of neurodegeneration in the motor neuron context that may be driven by cytoplasmic TDP-43 localization. My motor neurons differentiated from iPSCs engineered to contain the inducible TDP-43ΔNLS construct were able to express TDP-43 localized to the cytoplasm in such a fashion that seems to be most representative of a gain-of-function TDP-43 model. Similar to the effect in HEK293s presented in Figure 2.1, I was delighted to observe that TDP-43ΔNLS expression in motor neurons retained the ability to form spontaneous cytoplasmic aggregates and induce partial clearance of nuclear TDP-43. I believe a new model with these features is of particular benefit to the field because a model that has both a consistently high level of TDP-43 in the cytoplasm and has the propensity to form spontaneous aggregates (Figure 3.1; Figure 3.4) may represent a cellular state similar to patients during the course of ALS as opposed to at the end stage where TDP-43 is completely evacuated from the nucleus like loss of function models emulate. While examining models of the end stage of disease is fruitful and beneficial, there may be more opportunities for novel and unique therapeutic mechanism discovery when examining a mid-stage

or progression model that a TDP-43ΔNLS motor neuron expression model such as the one I have made would be powered to find. To date, no such *in vitro* human motor neuron model had previously been described.

This model of cytoplasmic TDP-43 expression is additionally unique in that it seems to show propensity to recapitulate both effects of cytoplasmic TDP-43 that are short-term neuroprotective (Figure 3.3; Figure 3.4f) and potentially detrimental to cell health in the long term (Figure 3.4d). This further bolsters the potential of model could for use in deeper mechanistic study of neurodegeneration since there is evidence of both protective and harmful effects co-existing induced by cytoplasmic TDP-43. Relatedly, this also increases the power of the RNAseq dataset as that may be powered to nominate pathways and genes are associated with both acute protection and chronic toxicity. Indeed, when diving deeper into the sequencing data, this is what we can begin to observe. For example, at the gene level, *BAK1*, a pro-apoptotic gene that localizes the mitochondria (Chittenden et al. 1995), is called as being enriched in the wild-type TDP-43 overexpression condition compared to the TDP-43ΔNLS, implying that expression of this gene goes down when TDP-43ΔNLS is expressed, which could suggest a decrease in pro-apoptotic signaling when cytoplasmic TDP-43 is present at high levels. This could be a potential mechanism of acute neuroprotection given that I have chosen to examine the neurons at a relatively young age of 12 days old counting from differentiation start.

To give an example of a potential long-term negative effector being upregulated by cytoplasmic TDP-43, the RNAseq data also calls expression of *Shisa6*, a transmembrane protein that interacts with auxiliary components of AMPA receptors (Klaassen et al. 2016), as enriched in the TDP-43ΔNLS condition. *Shisa6* has been reported to play a role in protecting AMPA receptors from desensitization and stabilization of AMPARs during periods of high synaptic activity

(Klaasen et al. 2016). It has also been established that glutamate mediated excitotoxicity can be driven by overactive AMPA receptors that do not undergo desensitization (Guo and Ma 2021; Jensen et al. 1998). This suggests that upregulating a receptor stabilizing factor like *Shisa6* may be involved in facilitating neurotoxicity mediated cell death in certain conditions. Thus, upregulation of this factor by cytoplasmic TDP-43 expression may be detrimental to neuronal health as it may predispose the motor neuron to excitotoxicity mediated neurodegeneration.

However, within these pathway categories, there are also genes with similar degrees of fold change differential expression that have the opposite effect. The fact that certain pathways were determined to be differentially over-enriched in the transcriptome in response to TDP-43 perturbation does not imply that all the enriched factors support the same phenotype. For example, a known ALS gene, *SQSTM1* which encodes the protein p62, is linked to neuroprotection and decrease in protein aggregation when upregulated as well as ER stress and ER stress-mediated apoptosis when inhibited (Fecto et al. 2011; Jiang et al. 2020). Contrary to the anti-apoptotic effect of *BAK1* downregulation, TDP-43ΔNLS drives *SQSTM1* expression down, which would ostensibly be pro-apoptotic. In the synaptic structure category, expression of *PAK3* – which has been linked to axon guidance and synapse maturation processes (Boda et al. 2004; Lesnick et al. 2008) – was shown to be upregulated in the TDP-43ΔNLS condition, which in contrast to the effect of *Shisa6*, could be neuroprotective as loss-of-function variants of *PAK3* have been linked to defects in dendritic spine dynamics and synaptic plasticity (Duarte et al. 2020).

These competing observations create a complex image of cytoplasmic TDP-43's effects that merits further study, perhaps over multiple timepoints of cellular age to determine if the effects associated with neuroprotection wane over time but the effects associated with potential drivers of neurotoxicity do not. It is also possible that some of these effects identified may have epistatic

relationships, for instance driving anti-apoptotic signaling may not matter if the effects of excitotoxicity mediated neurodegeneration are too large. This motor neuron model of TDP-43ΔNLS is well tuned to be used for future mechanistic studies to evaluate these relationships.

In general, it seems that cytoplasmic TDP-43 presence drives the cell to assume a more stressed state regardless of whether a stressor is present or not. This is supported by the stress granule analysis (Figure 3.4) and the activation of genes such as *NCOA7* that are modulated to respond to and protect from the effects of exogenous stressors (Figure 3.5; Finelli et al. 2016; Volkert and Crowley 2020). This suggests that a potential therapeutic angle of mitigating the damage done by cytoplasmic TDP-43 may be to modulate other features of stress response pathways so as to prevent the neurons from aberrantly activating them to negative consequence. In truth, hypothesis is already in part supported though what is known about the recently approved drug Relyvrio as it is hypothesized to increase survival of ALS patients by decreasing ER-mediated stress (Del Signore et al. 2008; Kusaczuk 2019). More study is needed to determine whether additional modulation of different stress sensors, signal transducers, or other pathway components can be leveraged into therapeutic treatments.

Materials and Methods

iPSC Cell Culture Conditions

The 11a iPSC line was derived from a biopsy from a 37-year-old healthy male patient as previously described in Boulting et al. 2011. iPSCs were maintained in mTESR1 or mTESR Plus (Stem Cell Technologies #85850, #100-0276) on Matrigel (Corning #354277) or Geltrex (Gibco #A1413201) coated tissue culture plates. Matrigel coatings were prepared by diluting 600uL of concentrate (prepared according to the dilution factor on the certificate of analysis for that lot of

reagent) diluted in 24mL of DMEM/F12. Geltrex coatings were prepared by diluting thawed Geltrex 1:100 in Minimal Essential Media (MEM – Gibco #11095080). Coated plates were cured at 37℃ for at least one hour and the coating media was aspirated immediately prior to cell addition. Media was changed every 1 – 2 days (mTESR1) or 2 – 3 days (mTESR plus) and cells were passaged using Accutase (Stem Cell Technologies #07920) as needed. On thaw and passage, media was also supplemented with 10uM Rock Inhibitor (Y-27632 – Stemgent #04-0012) to facilitate adherence and survival. Cells were maintained in a 37℃, 5% CO_2 incubator.

When needed, iPSCs were cryopreserved using CryoStor® CS10 Freeze Media (BioLife Solutions #210502) and stored in -80℃ or vapor phase liquid nitrogen.

Methods for generating the AAVS1-Neo-TRE-TDP-43ΔNLS-rtTA plasmid and subsequent generation of the 11a-TRE-TDP-43ΔNLS iPSC line are described in the Materials and Methods section of Chapter 2. iPSCs harboring the inducible vector system components (including empty vector control transductants that contain rtTA but no additional transgene) were maintained in mTESR1 or mTESR Plus supplemented with 500µg/mL G-418 (Neomycin analog – Gibco #10131035).

LiMoNes Motor Neuron Differentiation

Adapted from Limone et al. 2023. Prior to all differentiations, iPSCs were infected with lentivirus containing TetO-NGN2-Puro at approximately 2 MOI in a 6 well tissue culture dish. Cells were expanded and cryopreserved prior to the first differentiation.

NGN2-infected iPSCs were plated in their desired format and grown until at least 80% confluent. Media changes each day were performed as follows. Day 1: N2 Media Base – DMEM/F12 Media (Gibco #11320033), 1X GlutaMAX (Gibco #35050061), 0.3% (v/v) Glucose

(Sigma-Aldrich #G7021 – dissolved in PBS before addition), 1X N2 Supplement (Life Technologies #17502048) – supplemented with 4ug/mL Doxycycline (Sigma Aldrich #D9891 – dissolved in water), 200nM LDN-193189 (Stemgent #04-0074-02 – dissolved in DMSO), 10µM SB-431542 (Tocris #1614 – dissolved in DMSO), 2µM Retinoic Acid (Sigma Aldrich #R2625 – dissolved in DMSO), and 2µM Smoothened Agonist (SAG – Stem Cell Technologies #73412 – dissolved in DMSO). Day 2 and 3: N2 Media Base supplemented with 4µg/mL Doxycycline, 5µg/mL Puromycin (Gibco #A11138-03), 100nM LDN-193189, 10µM SB-431542, 1µM Retinoic Acid, 1µM SAG. Day 4: NBM/B27+ Media Base – Neurobasal Media (Gibco #21103049), 1X GlutaMAX, 1X MEM Non-Essential Amino Acids (NEAA – Gibco #11140050), 1X N2 Supplement, 1X B27 Plus Supplement (Gibco #A3582801) – supplemented with 4µg/mL Doxycycline, 5µg/mL Puromycin, 1µM Retinoic Acid, 1µM SAG, 10ng/mL recombinant Brain Derived Neurotrophic Factor (BDNF – R&D Systems #11166-BD – dissolved in 0.1% (w/v) BSA-PBS), 10ng/mL recombinant Ciliary Neurotrophic Factor (CNTF – R&D Systems #257-NT – dissolved in 0.1% (w/v) BSA-PBS), and 10ng/mL recombinant Glial Cell Line-derived Neurotrophic Factor (GDNF – R&D Systems #212-GD – dissolved in 0.1% (w/v) BSA-PBS). Day 5 and 6: NBM/B27+ Media Base supplemented with 4µg/mL Doxycycline, 5µg/mL Puromycin, 1µM Retinoic Acid, 1µM SAG, 10ng/mL BDNF, 10ng/mL CNTF, 10ng/mL GDNF, and 1µM EdU (Invitrogen #A10044 – dissolved in DMSO). Day 7: Freshly differentiated neurons are passaged using Accutase in Day 5 differentiation media supplemented with 10uM Rock Inhibitor or cryopreserved in CryoStor CS10 as desired. Destination plates for passaged neurons are prepared as follows: plates are coated with Poly-D-Lysine (Gibco #A3890401) at 4°C overnight. Coated plates were then washed three times with PBS, coated with Natural Mouse Laminin (Gibco #23017015) diluted 1:200 in PBS and cured at 37°C for at least two hours. Plates were washed

three times with PBS before neurons are seeded. Neurons thawed from frozen are plated using the same procedure as if they were freshly passaged Day 9+: Media was gently removed (i.e., without the use of a vacuum aspirator), and slowly replaced with NBM/B27+ Media Base supplemented with 4µg/mL Doxycycline if needed to maintain expression of inducible vector insert, 10ng/mL BDNF, 10ng/mL CNTF, 10ng/mL GDNF, and 1µM EdU. For maintenance of neuronal cultures, half-media changes are performed with the Day 9+ media every 2 – 3 days.

siRNA Transfection of Motor Neurons

Adapted from the procedure previously described in Klim et al. 2019. For each well of a 6-well plate of motor neurons transfected, 9µL Lipofectamine RNAiMAX Transfection Reagent (Invitrogen #13778075) was diluted in 150µL of OPTI-MEM (Gibco #31985062). Separately, Negative Control and TDP-43 targeting siRNAs were diluted in 150µL OPTI-MEM such that the final per well concentration of transfected siRNA was 60nM. These mixtures were combined and incubated at room temperature for 30 minutes. Following incubation, the combined mixture was added to neurons fed with fresh media immediately prior to transfection. Neurons were maintained following transfection according to standard method described in the previous section. The siRNAs used were the Invitrogen *Silencer*™ Select Negative Control No. 1 (Invitrogen #4390843) and siTDP-43 acquired from the same *Silencer*™ Select collection (Invitrogen # 4392420-s23831).

RNA Extraction and qRT-PCR

RNA extractions from cultured cells were performed using the Qiagen RNEasy Plus Mini Kit (Qiagen #74134). QIAshredder columns (Qiagen #79656) were used for homogenization of harvested cultures prior to RNA purification. cDNA generation was performed using the iScript (Bio-Rad #1708890) or iScript Advanced (Bio-Rad #172037) cDNA Synthesis kits with 500ng

RNA input. qRT-PCR was performed using the generated cDNA reactions diluted 1:4 and combined according to manufacturer's instructions with iTaq™ Universal SYBR® Green Supermix (Bio-Rad #1725124). Samples were run as technical triplicates with an additional no template control. For experiments presented in Figure 3.1, reactions were performed on a Bio-Rad CFX96 Real-Time PCR Detection System in a 96-well format using the following protocol: 1 step of 95℃ 30s followed by 95℃ 5s, 60℃ 30s for 40 Cycles. For experiments presented in Figure 3.2 and Supplementary Figure 3.1, reactions were performed on an Applied Biosciences QuantStudio 6 in a 384-well format using Fast SYBR Green Master Mix (Life Technologies #4385614) with the following protocol: 1 step of 95℃ 20s followed by 95℃ 1s, 60℃ 20s for 40 cycles.

The following primers were used where applicable: GAPDH-Fwd: 5' – TTGTCAAGCTCATTTCCTGGTATG – 3; GAPDH-Rev: 5' – TTCTCTTGTGCTCTTGCTGG – 3'; TDP-43 1: 5' – CAGCTCATCCTCAGTCATGTC – 3'; TDP-43 2: 5' – GATGGTGTGACTGCAAACTTC – 3' ; FL (Full Length) STMN2-Fwd: 5' – AGCTGTCCATGCTGTCACTG – 3'; FL-STMN2-Rev: 5' – GGTGGCTTCAAGATCAGCTC – 3'; Cryptic STMN2-Fwd: 5' – CTTTCTCTAGCACGGTCCCAC – 3' ; Cryptic STMN2-Rev: 5' – ATGCTCACACAGAGAGCCAAATTC – 3'.

Immunofluorescence and Imaging

All immunofluorescence presented in this chapter was confocal imaging captured by the Molecular Devices IXM. Cells were plated and stained in Perkin Elmer 96-well PhenoPlates.

General motor neuron images (Figure 3.1)

Neurons to be stained were fixed with 4% Paraformaldehyde for 20 minutes at room temperature or overnight at 4℃. Fixed cells were briefly washed with PBS and then coated with a

blocking and permeabilization buffer comprised of 0.1% (v/v) Triton X-100-PBS (Sigma Aldrich #T8787) and 10% Normal Donkey Serum (Jackson ImmunoResarch Laboratories #017-000-121) for one hour at room temperature. Primary antibodies were diluted in the stated blocking/permeabilization buffer and incubated overnight at 4°C. The following day, the plate was washed three times with PBS and the Alexa-Fluor conjugated secondary antibodies were added diluted 1:1000 in PBS for one hour in the dark. Two PBS washes were performed followed by incubation with 1µg/mL DAPI (Invitrogen #D3571) for 5 minutes in the dark. After two additional PBS washes, the plates were imaged or stored at 4°C until imaging. Primary antibodies used in the studies in this chapter were Rabbit anti-TDP43 (G400) at 1:100 dilution, Mouse anti-Tuj1/βIII-Tubulin at 1:100 dilution (R&D Systems #MAB1195) and/or Rabbit anti-NGN2 (Abcam #ab109236) at 1:100 dilution.

Oxidative stress application and stress granule imaging (Figure 3.4)

Oxidative stress was applied to neurons plated in a 96-well Perkin Elmer PhenoPlate by changing the media to fresh culture media additionally supplemented with 1mM Sodium Arsenite and returning the plate to the 37°C incubator for one hour. Following a PBS wash, neurons to be stained were fixed and permeabilized with ice-cold methanol and incubated on ice for 20 minutes. Methanol was then gently removed from the plate using a multi-channel pipette. Permeabilized neurons were blocked using 0.1% (w/v) BSA-PBS for 10 minutes at 4°C. Primary antibodies were diluted in 0.1% BSA-PBS, added to the neurons, and incubated overnight at 4°C. The following day, the plate was washed three times with PBS and the Alexa-Fluor conjugated secondary antibodies were added diluted 1:1000 in PBS for one hour in the dark. Two PBS washes were performed followed by incubation with 1µg/mL DAPI (Invitrogen #D3571) for 5 minutes in the dark. After two additional PBS washes the plates were imaged or stored at 4°C until imaging.

Primary antibodies used in the stress granule experiments were Mouse anti-TDP-43 at 1:150 dilution (Life Technologies #H00023435-M01) and Rabbit anti-G3BP1 at 1:300 dilution (Proteintech #13057-2-AP).

Imaging analysis was performed using a pipeline generated in the PerkinElmer Columbus™ image data storage and analysis system. Information from each channel was parsed in order to identify the nucleus, identify the region around each nucleus to define the approximate cell area, and then identify spots within this area that were classified as TDP-43 or G3BP1 aggregates based on the channel being visualized. Results by imaged field were exported into Excel and manually reviewed alongside the captured images. Fields where an analysis was performed on no viable cells (i.e., attempted to define cell boundaries despite no DAPI signal visible), were eliminated from the analysis.

Subcellular fractionation western blots

Subcellular protein fractionations were performed using the Subcellular Protein Fractionation Kit for Cultured Cells (Life Technologies #78840) according to manufacturer's instructions. Protein was quantified using the Pierce™ BCA Protein Assay Kit according to manufacturer's instructions (Thermo Scientific #23225). Absorbance of the quantification plate at 562nM was read using a Cytation3 plate reader. 10µg of protein from each sample was resuspended in Blue Loading buffer enriched with DTT as the reducing agent (Cell Signaling Technology #7722). Diluted samples were boiled for 5 minutes at 95°C before being loaded to Bio-Rad Mini-PROTEAN TGX 4 – 20% pre-cast gels (Bio-Rad #4561094). Precision Plus Protein Dual Color Standards (Bio-Rad #1610374) was used as the molecular weight ladder. Gels were run using Tris/Glycine/SDS Running Buffer (National Diagnostics #EC-870) at 200V for 40 minutes. Gels were transferred to a PVDF membrane using the iBlot 2 Dry Transfer system.

Membranes were cut to size and blocked for 1 hour in LI-COR Intercept® Blocking Buffer at room temperature (LI-COR #927-60001). Primary antibodies were then diluted as appropriate in 5% (w/v) BSA-TBS-T (Tris Buffered Saline with 0.1% (v/v) Tween 20) and added to the membranes to incubate at 4°C overnight. Primary antibodies used were Rabbit anti-TDP43 (G400) at 1:1000 dilution and Mouse anti-HistoneH3 (96C10) (Cell Signaling #3638).

The next day, membranes were washed with TBST, incubated with LI-COR anti-rabbit and anti-mouse IRDye secondary antibodies suspended in Blocking Buffer supplemented with 0.1% (v/v) Tween 20 and 0.01% (v/v) SDS for 1 hour and then washed again with TBST before being visualized on the LI-COR Odyssey Imager.

When needed for sequential blotting, I also used Restore Plus Western Blot Stripping Buffer (Thermo Scientific #46430) to gently remove the previous antibodies from the membrane. To complete this, the membrane was washed 3 times with PBS, coated with stripping buffer at room temperature with gentle shaking for 30 minutes, washed again 3 times with PBS, then re-blocked with Intercept Blocking Buffer before adding the primary antibody mix as previously described.

Cell Titer Glo Viability Assays for short-term differentiation

NGN2 infected iPSCs were plated on 96 well tissue culture plates at 10 – 20,000 cells per well per standard culture methods. LiMoNes motor neuron differentiation commenced 24 hours after plating until Day 6 of the procedure. Undifferentiated samples were exposed to the same differentiation media as the rest of the plate without Doxycycline, Puromycin, or EdU. On Day 6, the plate was assayed using Cell Titer Glo 2.0 reagent according to manufacturer's instructions. Luminescent readings were captured using a Cytation3 plate reader.

RNA sequencing

RNA was harvested from Day 12 (Day 5 post-differentiation) motor neurons as described in the qRT-PCR methods section. Neurons were not sorted prior to RNA harvest because ~80% of cultures in all assayed conditions were YFP+ as measured by flow cytometry (Supplementary Figure 3.2). Four biological replicates of RNA per neuron line were submitted for sequencing to The Bauer Core Facility at Harvard University. RNA integrity was verified using an Agilent TapeStation system. Sequencing libraries were generated using a Kapa mRNA HyperPrep Kit (Roche #KK8581). Sequencing was performed on an Illumina NovaSeq system.

Reads were aligned to the reference human genome build GRCh38 r109. Multidimensional scaling plots were generated from the top 1000 differentially expressed genes (Supplementary Figure 3.3). Differential gene expression (DGE) analysis was performed using edgeR with Benjamini-Hochberg FDR correction. Samples input to analysis were filtered to eliminate genes with less than one count per million in at least 8 samples. Heatmaps containing selected genes were derived from the DGE data. All differentially expressed genes with an FDR threshold of 0.05 were input into Over-enrichment analysis (ORA) to determine pathways enriched in the TDP-43ΔNLS:YFP compared to TDP-43:YFP condition.

Differentially expressed genes enriched each of the TDP-43ΔNLS:YFP compared to TDP-43:YFP conditions with a log2 fold change >±2 are listed in Supplementary Tables 3.1 and 3.2. Data is also available for comparisons to YFP expressing neurons and no transgene expressing (Empty Vector) neurons.

Additional Acknowledgements

Primer sequences for full length and cryptic *STMN2* were provided by Clotilde Lagier-Tourenne. Protocols for sodium arsenite stress and subsequent staining of stress granules were adapted from protocols provided by Clotilde Lagier-Tourenne and Rajesh Gunage. RNA sequencing analysis was performed in collaboration with Kris Holton.

Chapter 4: Validating and examining mechanisms of ATXN2 knockout-mediated neuroprotection on TDP-43 perturbed human motor neuron systems

Abstract

Transactive Response DNA-binding protein 43 (TDP-43) is a multifunctional nuclear protein ubiquitously expressed in all tissues. Although it is primarily nuclear, Amyotrophic Lateral Sclerosis (ALS) patients frequently present with cytoplasmic aggregates of TDP-43 in motor neurons on post-mortem examination. Although only about 5% of all ALS patients have a *TARDBP* mutation (Ghasemi and Brown 2018; Ingre et al. 2015), which is known to cause these insoluble cytoplasmic aggregates, 97% of ALS patients will develop cytoplasmic, insoluble TDP-43 aggregates regardless of whether they have a mutation in *TARDBP* or not (Ling et al. 2013). Overexpression of wild-type TDP-43 has previously been shown to be a valid model of inducing neurotoxicity as well as a limited amount of cytoplasmic re-localization and aggregation characteristic of ALS (Elden et al. 2010; Wils et al. 2010). In the search for modifiers of toxicity as conferred by TDP-43 overexpression in these models, knockout of *Ataxin-2* (ATXN2) was proposed as a protective intervention in the context of TDP-43 perturbation in non-human model systems (Elden et al. 2010, Becker et al. 2017). This promising finding had not previously been validated in a human motor neuron system, nor had a thorough investigation been conducted to determine the mechanism of neuroprotection that ATXN2 knockout employs to drive the therapeutic effect. In this chapter, I will present work on generating an ATXN2 knockout variant of my *in vitro* motor neuron model of inducible TDP-43 overexpression, validate the previous findings of viability protection from TDP-43 overexpression toxicity, and further employ the model to explore potential mechanisms of neurodegeneration that may be mitigated by ATXN2 knockout. I found that, among other perturbed cellular processes, ATXN2 knockout modifies nucleocytoplasmic transport of TDP-43, lessening the amount of TDP-43 that localizes to stress granules in response to stress conferred by high dose puromycin or sodium arsenite exposure.

Additionally, I used RNA sequencing to discover that in addition to significant pathway perturbations in nucleocytoplasmic transport processes, many other pathways, including apoptosis and stress response pathways, were modulated in such a way that may not be beneficial to neurons in the long term. This raises the notion that although ATXN2 knockout may correct some cell biological defects incurred by TDP-43 perturbation, ATXN2 knockout may not necessarily be a sustainable therapeutic intervention due to the other roles of ATXN2 and its effectors that may be modulated. This initial exploration establishes that this cell model is powered to discover and elucidate these mechanisms of ATXN2 knockout mediated processes which may be leverageable for continued therapeutic development, even if ATXN2 itself is not the best target.

Introduction

Transactive Response DNA-binding protein 43 (TDP-43) is a nucleic acid binding protein involved in several cellular processes including RNA splicing, nucleocytoplasmic transport of RNAs, and translational regulation (Birsa et al. 2020; Freibaum et al. 2010; Lee et al. 2021; Sephton et al. 2011). TDP-43 cytoplasmic localization and aggregation occurs in 97% of Amyotrophic Lateral Sclerosis (ALS) patients despite the fact that only about 5% of patients have a causal mutation in TDP-43 associated with driving aggregation (Ghasemi and Brown 2018; Ingre et al. 2015; Ling et al. 2013). As no long-term disease modifying therapy exists for ALS, research using models that represent TDP-43 mutation independent aggregation to elucidate mechanisms of neurodegeneration is important to continue to explore as findings with such models have the potential to be broadly efficacious in the ALS patient population.

Models of TDP-43 disruption via overexpression of an additional wild-type copy have been previously shown to recapitulate key features of TDP-43 proteinopathy such as toxicity, cytoplasmic re-localization, and aggregation (Elden et al. 2010). Naturally, several groups have

performed screens in the overexpression context and at baseline to find interactors of TDP-43 mRNA and protein and assess whether direct interactors of TDP-43 or the product of processes modulated by those interactors of TDP-43 could be leveraged for therapeutic benefit (Elden et al. 2010; Pintacuda et al. 2022; Sephton et al. 2011; Tollervey et al. 2011). One gene whose mRNA and protein have been shown to be a target and interactor with TDP-43 is *Ataxin-2* (ATXN2).

ATXN2 is also a multi-functional protein associated with metabolism via mTOR signaling (Bar et al. 2016; Lastres-Becker et al. 2008), mRNA stabilization (Yokoshi et al. 2014), miRNA mediated gene silencing (Su et al. 2011) and translation activation (Lee et al. 2017; Lim and Allada 2013). One of ATXN2's RNA binding targets is also TDP-43 mRNA (Yokoshi et al. 2014). Two aspects of ATXN2's functions and interactions with TDP-43 are particularly interesting to ALS-related neurodegeneration. First, knockout of ATXN2 was shown to be protective against TDP-43 overexpression mediated toxicity in non-human systems (Becker et al. 2017; Elden et al. 2010). This suggests that an ATXN2 centered therapy may be beneficial to patients with disease arising from TDP-43 proteinopathy that the overexpression model represents, including ALS. Secondly, ATXN2, similar to TDP-43, also localizes to stress granules upon activation of one of several stress response pathways including oxidative stress and heat shock (Nonhoff et al. 2007). These findings lend credence to the TDP-43 proteinopathy pathogenesis hypothesis that centers around stress granules as a driving force for negative cell health consequences (Dewey et al. 2012; Fang et al. 2019). If ATXN2 is known to interact with TDP-43 and could be modulated in a way that prevents TDP-43 localization to stress granules, this may prevent aggregates from forming and delay degeneration of neurons afflicted by TDP-43 dysregulation. Indeed, some have suggested that ATXN2 knockout does have the capacity to modulate nucleocytoplasmic transport (Becker et al. 2017), but this effect has yet to be shown in a motor neuron system. Furthermore, because of

ATXN2's diverse roles in several different cellular functions, it will be necessary to understand how a knockout affects these other processes as well, which little work has been done to understand in any *in vitro* system.

This chapter of the dissertation will showcase the development of an *in vitro* iPSC-derived motor neuron system that harbors an inducible TDP-43 overexpression system and a CRISPR knockout of ATXN2. I will verify that this model is representative of the context it aims to emulate by showing that, similar to non-human system studies, ATXN2 knockout is sufficient to confer protection against TDP-43 overexpression mediated toxicity. I will then take the next step in exploring several hypotheses as to why this protection may arise when ATXN2 is knocked out. I will explore the stress granule hypothesis using similar methods to the cytoplasmic TDP-43 studies in Chapter 3 to show that ATXN2 does indeed lead less TDP-43 to become localized to stress granules at baseline and in the context of puromycin and oxidative stress. Finally, I will use RNA sequencing to nominate additional hypotheses for consequences of ATXN2 knockout, such as modulation of certain factors associated with apoptosis and the oxidative stress response. As part of this inquiry, I will discuss why ATXN2 may not be the best therapeutic strategy to treat TDP-43 proteinopathy-associated conditions based on the detrimental change in cellular state that seems to occur when it is knocked out. Nevertheless, these discoveries shed light on what the next iteration of TDP-43 perturbation modifier model could be and the processes that have potential in being pharmacologically leveraged to lead to a more positive outcome for combating motor neuron degeneration.

Results

ATXN2 Knockout in iPSCs is achievable in combination with inducible TDP-43 overexpression and maintain the ability to differentiate into motor neurons

We began development of an ATXN2 knockout motor neuron model by CRISPR editing 11a iPSCs and selecting for successful knockout clones (Figure 4.1). We were able to identify two successfully edited knockout clones, labeled here initially as C8 and D2. We verified knockout of ATXN2 by western blot (Figure 4.1a), immunofluorescence (Figure 4.1b), and qRT-PCR (Figure 4.1c). We note that while the D2 clone had slightly more residual ATXN2 mRNA expression than the C8 clone, the clones gave similar results in all other assays, including the viability and phenotypic assays presented later in this chapter. We do not believe there is a substantial functional difference in most circumstances between these two clones beyond what could be expected from natural variation.

Using similar methods to those outlines in Chapters 2 and 3, I then transduced the verified ATXN2 knockout iPSCs with the AAVS1 inducible vector variants developed in Chapter 2 to generate ATXN2 -/- inducible TDP-43 iPSC clonal lines. I then transduced these lines with Neurogenin-2 (NGN2) to facilitate differentiation to motor neurons via the LiMoNes differentiation method (Limone et al. 2023). I observed successful expression of TDP-43:YFP upon assessment after 2µg/mL doxycycline treatment at the iPSC stage and after the completion of the LiMoNes motor neuron differentiation protocol by western blot (Figure 4.1d) and immunofluorescence (Figure 4.1e).

ATXN2 Knockout rescues toxicity conferred by TDP-43 overexpression in iPSCs and motor neurons

Taking advantage of the same assays used to establish that overexpression of TDP-43 was toxic to iPSCs and motor neurons in Chapter 2, I set out to validate my model of ATXN2 knockout by examining whether ATXN2 knockout was sufficient to mitigate the toxic effect of TDP-43

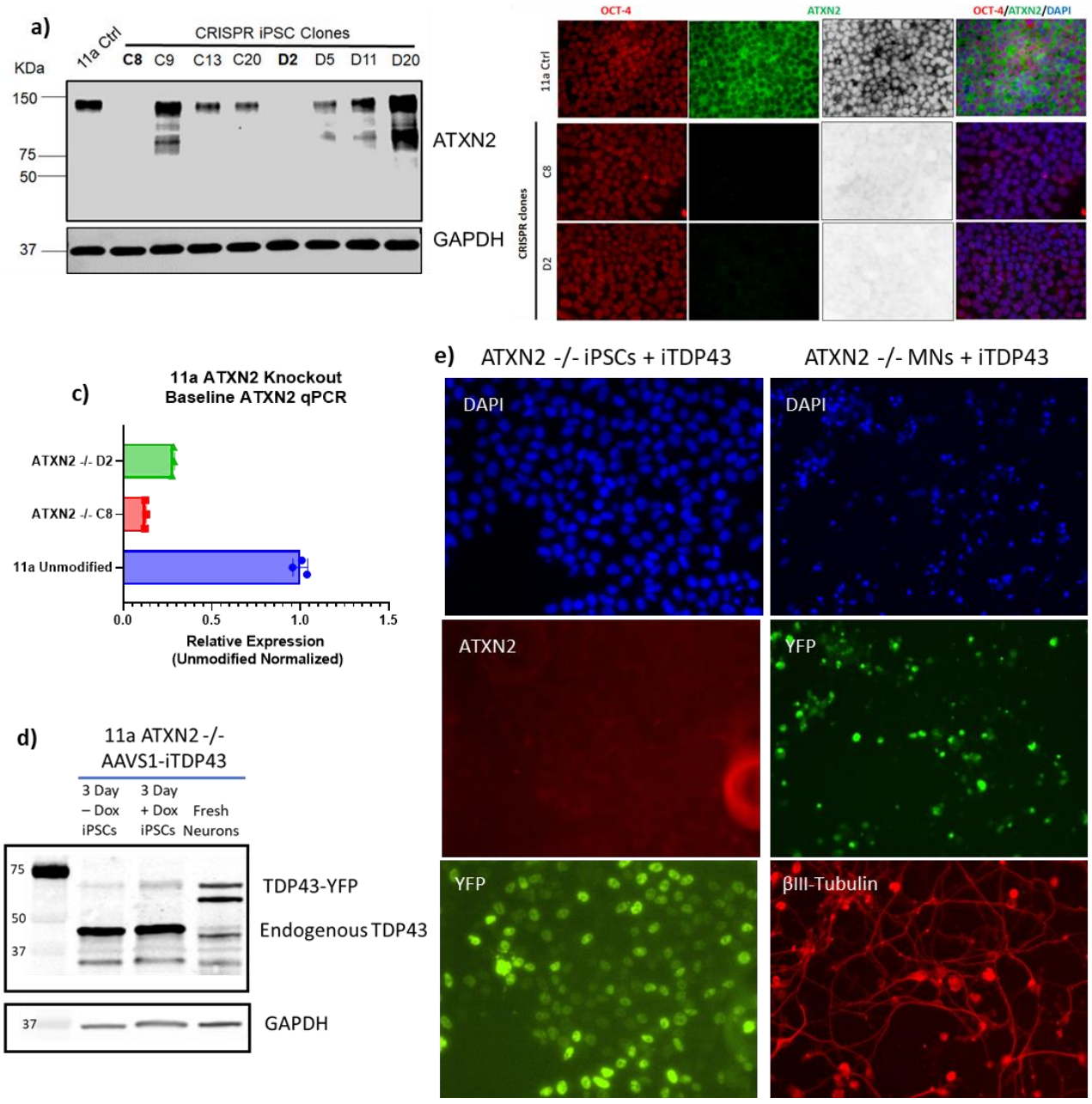

Figure 4.1: Generation of ATXN2 knockout iPSCs and motor neurons harboring inducible TDP-43:YFP (a) Western blot screening of single cell clones isolated from a culture of CRISPR edited 11a iPSCs. Two clones were successfully identified as ATXN2 knockout through this process **(b)** Immunofluorescence examination of ATXN2 knockout compared to control, unmodified iPSCs **(c)** qRT-PCR results of ATXN2 knockout clones using primers targeting ATXN2 (n = 3 technical replicates) **(d)** Whole cell western blot of iPSCs and neurons harboring the inducible TDP-43:YFP expression system. '+dox' iPSC samples were treated with 2µg/mL Doxycycline for 72 hours prior to protein harvest. Fresh neuron sample is LiMoNes motor neurons harvested immediately following the end of the 7-day differentiation protocol **(e)** Immunofluorescence of iPSCs and motor neurons expressing inducible TDP-43:YFP

overexpression as previously hypothesized in the non-human systems (Becker et al. 2017; Elden et al. 2010). I observed that ATXN2 knockout was indeed sufficient to reduce TDP-43 overexpression mediated toxicity by a colony formation assay of iPSCs at two different doses of doxycycline (Figure 4.2a; Supplementary Figure 4.1), short-term differentiation assay of

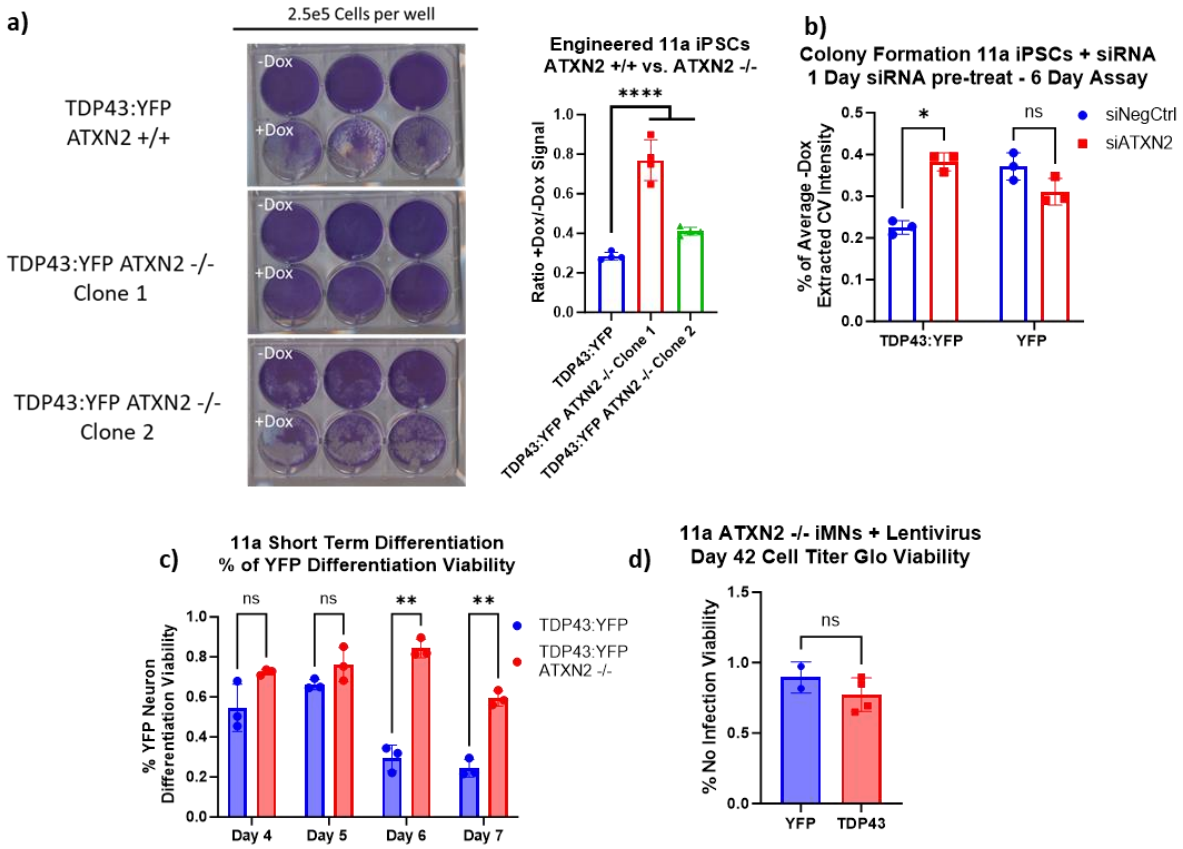

Figure 4.2: ATXN2 knockout confers protection from TDP-43 overexpression-mediated toxicity in iPSCs and motor neurons (a) Colony Formation Assay in iPSCs at 2µg/mL Doxycycline treatment for 6 days. Representative images of plates and quantification from Crystal Violet stain extraction by acetic acid. Significance calculated using t-tests compared to TDP-43:YFP (**** = $p < 0.0001$) (n = 3 biological replicates) **(b)** Quantification of colony formation assay plates in ATXN2 intact cells treated with siNegative Control or siATXN2 for one day prior to the 6-day assay start. Significance calculated using t-tests by condition pair (* = $p < 0.05$) (n = 3 biological replicates) **(c)** Cell Titer Glo viability assay results from short-term motor neuron differentiation assay of ATXN2 intact and knockout TDP-43 overexpressing iPSCs. Significance calculated using t-tests by condition pair per timepoint (** = $p < 0.01$) (n = 3 biological replicates) **(d)** Cell Titer Glo viability assay results from Day 42 motor neuron cultures infected at Day 14 with lentivirus containing TDP-43:YFP. Significance calculated by t-test (n = 3 biological replicates).

actively differentiating motor neurons (Figure 4.2c), and long-term neuronal culture where TDP-43 overexpression was conferred by lentivirus (Figure 4.2d). Additionally, I was able to establish that ATXN2 knockdown by siRNA in iPSCs was sufficient to achieve a rescue effect in the colony formation assay, albeit to a more modest degree than the CRISPR knockout (Figure 4.2b). Taken together, these findings validate the previous work that ATXN2 knockout has the power to be neuroprotective in a human motor neuron system.

ATXN2 knockout decreases TDP-43 nuclear efflux at baseline and in the context of puromycin-induced stress

Having established that ATXN2 knockout had the functional effect of neuroprotection as predicted, we sought to use these iPSC-derived motor neuron systems to investigate potential mechanisms as to why this neuroprotection occurs. For the preliminary experiments, we employed a high-dose puromycin stress model on motor neurons with and without ATXN2 knockout to examine if there were any changes in either TDP-43 nuclear efflux in response to stress (Figure 4.3a) or TDP-43 localization to stress granules in the same contexts (Figure 4.4). Puromycin at high doses is known to elicit a proteotoxic stress through its mechanism of binding to ribosomes and non-specifically inducing premature termination of translation (Aviner et al. 2020). Stress inflicted on cells in this way is sufficient to drive formation of stress granules (Fang et al. 2019). We observed that there was a significant difference in the DAPI/TDP-43 Pearson correlation coefficient between the stressed conditions of ATXN2 intact and knockout. Given that the correlation in the ATXN2 knockout condition between DAPI and TDP-43 was higher, this suggests that ATXN2 knockout was sufficient to decrease the amount of cytoplasmic TDP-43 localization upon exposure to a stress event that generally causes TDP-43 re-localization. We then proceeded to examine if differences in TDP-43 localization could be detected at baseline in the context of

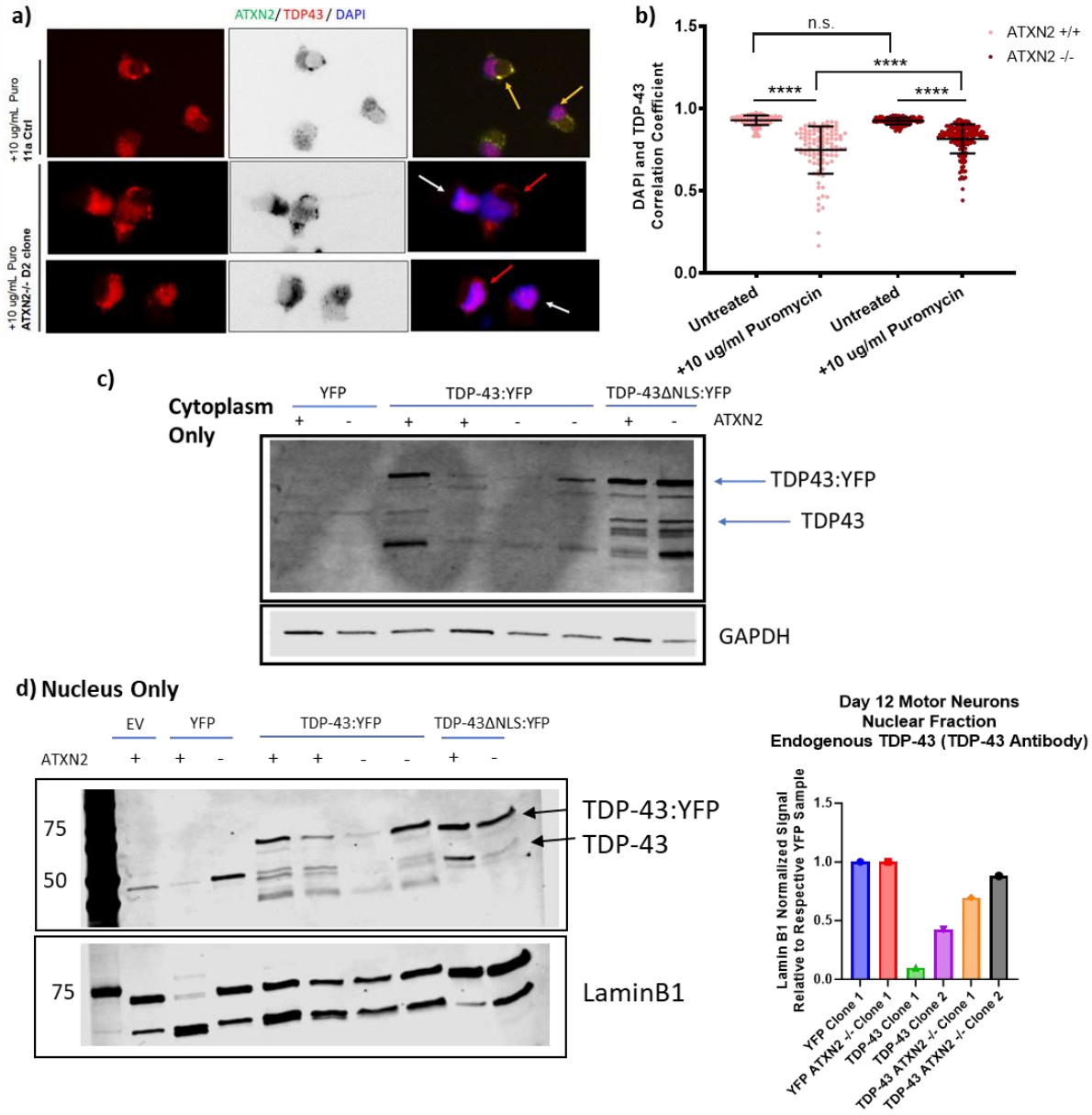

Figure 4.3: ATXN2 knockout is sufficient to lower cytoplasmic TDP-43 levels during puromycin stress and in the context of TDP-43 overexpression perturbation without stress **(a)** Representative images of motor neurons differentiated by 2D differentiation method with and without ATXN2 exposed to 10µg/mL Puromycin for 24 hours **(b)** Pearson's correlation coefficient between DAPI and TDP-43 signal calculated by image field in neuronal cultures with and without ATXN2, with and without exposure to puromycin stress. Significance calculated by ANOVA with Šídák's multiple comparisons test (**** = $p<0.001$) **(c)** Cytoplasmic fraction of subcellular fractionation western blot of Day 12 LiMoNes motor neurons harboring inducible TDP-43 with and without ATXN2 **(d)** Nuclear fraction of subcellular fraction western blot of Day 12 LiMoNes motor neurons harboring inducible TDP-43 with and without ATXN2, with accompanying quantification of endogenous TDP-43 levels normalized to the LaminB1 loading control signal.

TDP-43 overexpression perturbation. We used a subcellular fractionation western blot to observe that ATXN2 knockout was sufficient to reduce cytoplasmic localization of TDP-43 from the perspective of less TDP-43 detected in the cytoplasm in the ATXN2 knockout condition (Figure 4.3c) and more TDP-43 detectable in the nucleus in the ATXN2 knockout condition compared to the ATXN2 intact condition.

We then proceeded to examine whether the decrease in TDP-43 cytoplasmic localization would come in tandem with a decrease in TDP-43 localization to stress granules in the context of puromycin stress. We observed that this was true – when examining correlation of TDP-43 with G3BP1 after stress exposure, we noted a lower correlation of TDP-43 with G3BP1 when ATXN2 was knocked out than when ATXN2 was present (Figure 4.4). Taken together, these results as a package support the notion that ATXN2 knockout has a potentially neuroprotective effect of decreasing TDP-43 localization to the cytoplasm, possibly by preventing aggregation seeding and thus slowing the progression of TDP-43 proteinopathy.

ATXN2 Knockout moderately decreases TDP-43 localization to stress granules during oxidative stress events

To bolster confidence in our results from the puromycin proteotoxic stress condition, I evaluated an alternative stress condition, oxidative stress as conferred by acute exposure to 1mM sodium arsenite, to determine whether ATXN2 knockout also affected the localization of TDP-43 to stress granules and/or the total number of granules present (Figure 4.5). I observed that ATXN2 knockout increased the number of stress granules detected in motor neurons without TDP-43 perturbation (engineered to express the empty AAVS1-Neo-TRE-DEST-rtTA base destination vector only) in the context of oxidative stress (Figure 4.5a) as well as in lines with TDP-43

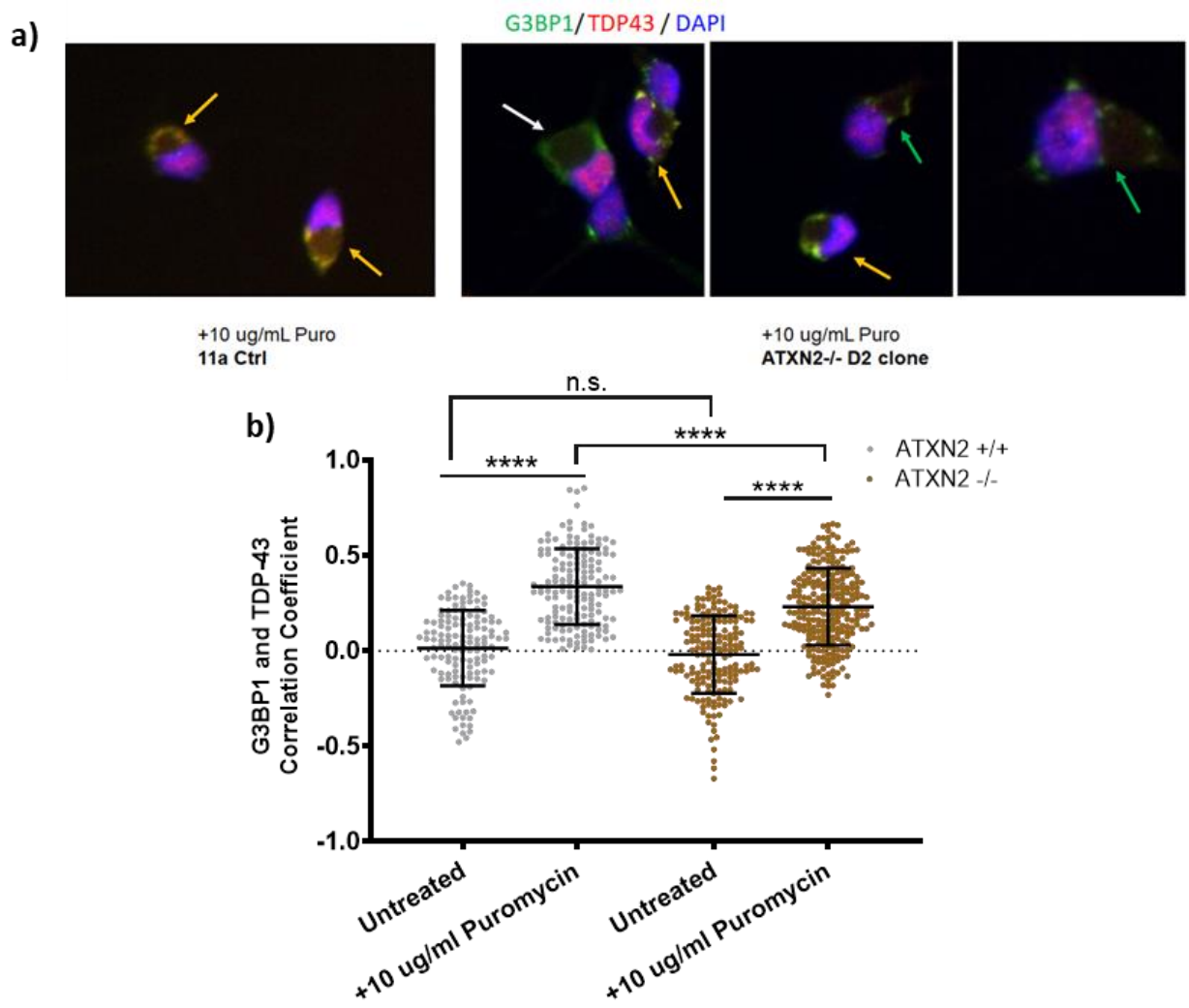

Figure 4.4: ATXN2 knockout decreases TDP-43 localization to stress granules during puromycin proteotoxic stress events (a) Representative images of 2D differentiation motor neurons stained for G3BP1 and TDP-43 in the context of 10µg/mL puromycin stress for 24 hours, with and without ATXN2 **(b)** Pearson's correlation coefficient between G3BP1 and TDP-43 signal calculated by image field in neuronal cultures with and without ATXN2, with and without exposure to puromycin stress. Significance calculated by ANOVA with Šídák's multiple comparisons test (**** = $p<0.001$)

overexpression (Figure 4.5b). This implies that ATXN2 knockout in the context of oxidative stress does not decrease burden of potential TDP-43 aggregates by lowering the total number of stress granules. Just the opposite, ATXN2 knockout seems to drive an increase in the total number of stress granules in motor neurons whether TDP-43 is perturbed or not. Looking at TDP-43 positive

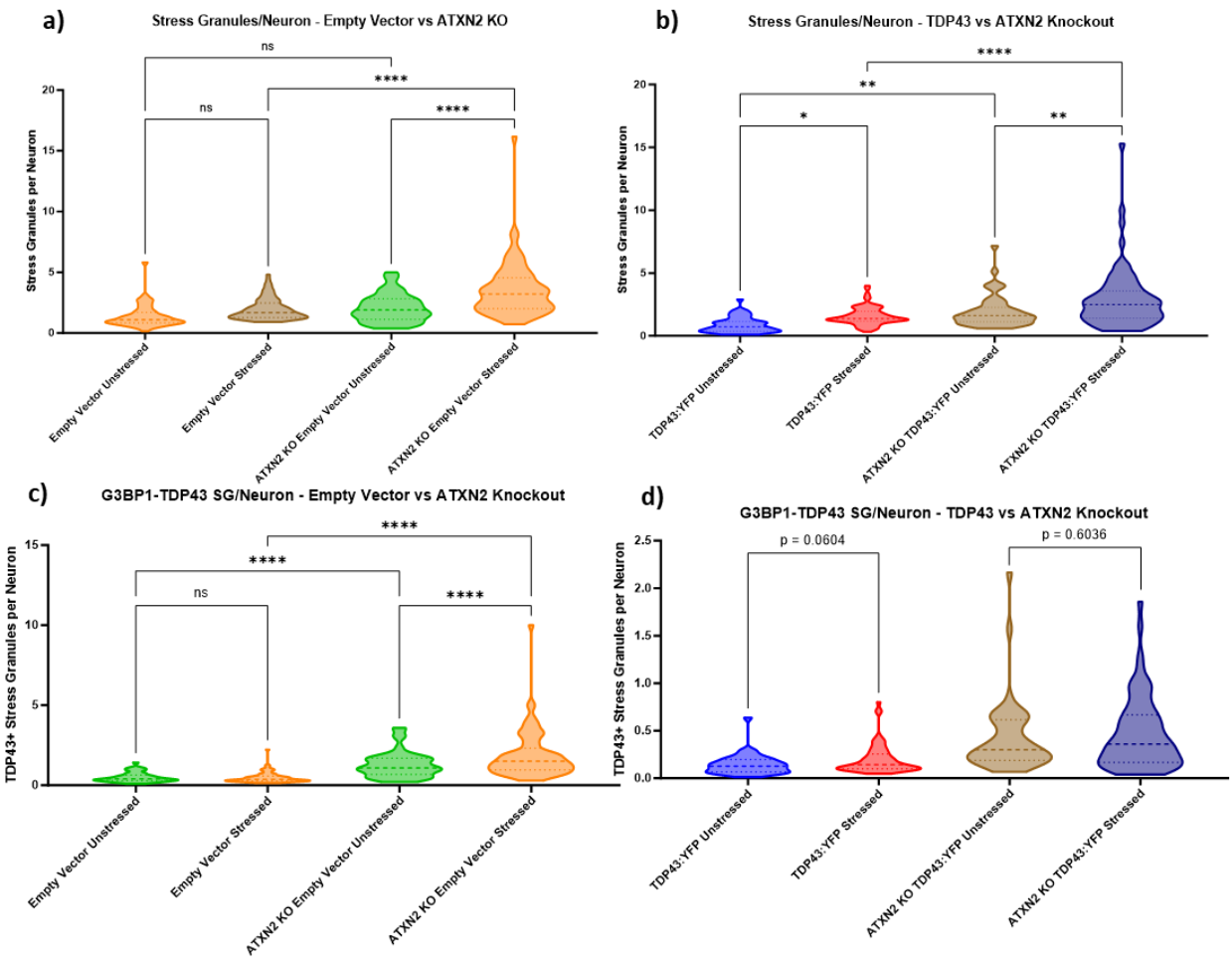

Figure 4.5: ATXN2 knockout modestly decreases TDP-43 localization to stress granules upon oxidative stress exposure in Day 12 LiMoNes motor neurons in the context of TDP-43 perturbation only, without affecting the total number of stress granules or the stress response when TDP-43 is unperturbed (a) Results of stress granules per neuron image analysis by captured field in stressed and unstressed motor neurons with and without ATXN2 expression, without TDP-43 perturbation. n = 44 ~ 80. Significance calculated using ANOVA with Šídák's multiple comparisons test (**** = $p<0.001$). Empty Vector = electroporated with the base, not subcloned inducible system plasmid. **(b)** Results of stress granules per neuron image analysis by captured field in stressed and unstressed motor neurons with and without ATXN2 expression, with TDP-43 perturbation Significance calculated using ANOVA with Šídák's multiple comparisons test (**** = $p<0.001$) **(c)** Results of TDP-43 positive stress granules per neuron image analysis by captured field in each neuron line in stressed and unstressed motor neurons with and without ATXN2 expression, without TDP-43 perturbation n = 44 ~ 80. Significance calculated using ANOVA with Šídák's multiple comparisons test (**** = $p<0.001$) **(d)** Results of TDP-43 positive stress granules per neuron image analysis by captured field in each neuron line with and without ATXN2 expression, with TDP-43 perturbation. n = 44 ~ 80. Pairwise significance calculated using t-tests.

stress granules, I observed that when TDP-43 is not overexpressed, ATXN2 knockout similarly increases the average amount of TDP-43 containing stress granules per well and increases the magnitude TDP-43 of localization response to stress; the difference between the number of TDP-43 positive stress granules in the stressed and unstressed conditions is larger when ATXN2 is knocked out than intact (Figure 4.5c). Interestingly, this relationship between ATXN2 and TDP-43 positive stress granules does not hold in the context of TDP-43 overexpression. In the context of TDP-43 overexpression with ATXN2 knockout, I did observe a slight (not statistically significant, but noticeable in magnitude) decrease in TDP-43 localization to stress granules in the ATXN2 knockout condition (Figure 4.5d). This observation implies two things. First, ATXN2 knockout may be able to mitigate neurotoxicity through decreasing TDP-43 localization to stress granules in the context of oxidative stress, preventing TDP-43 aggregates from being seeded. Second, the action and benefit of ATXN2 being able to do this is limited to the state where TDP-43 is already perturbed in some fashion. This context specific nature of the protective action of ATXN2 knockout confers merits additional study into the general effects of ATXN2 knockout. An increase of stress granules upon ATXN2 knockout when TDP-43 perturbation is not present and/or after the stress causing the perturbation is resolved is ostensibly not beneficial for neuronal health given the definition that stress granules are sites of translational stalling and potential aggregate seeds.

Transcriptomic analysis of TDP-43 overexpressing, ATXN2 knockout motor neurons reveals changes in pathways implicated in nucleocytoplasmic transport, apoptosis, and the cellular stress response

To begin to make inroads on understanding the global effects of ATXN2 knockout in the context of TDP-43 perturbation, I performed RNA sequencing on motor neurons expressing inducible TDP-43:YFP in both ATXN2 genetic contexts (Figure 4.6). 327 transcripts were called as significantly differentially expressed above a log2 fold change threshold of 2 in the ATXN2

knockout condition, including 146 transcripts that were not detected as being expressed at all in the ATXN2 intact condition (Figure 4.6a). 213 transcripts were significantly enriched in the TDP-43 overexpressed, ATXN2 intact condition. The over-enrichment analysis (ORA) called several pathways that were associated with ATXN2's known functions including mTORC1 signaling and glycolysis as differentially expressed between the two conditions, which was expected (Figure 4.6c). ORA also called pathways related to phosphatase and dephosphorylation activity which could potentially be neuroprotective given that TDP-43 aggregates are hyper phosphorylated (Hasegawa et al. 2008); apoptosis and p53 pathway modulators; response to multiple forms of stress including oxidative stress and hypoxia; inflammatory signaling via NF-κB;

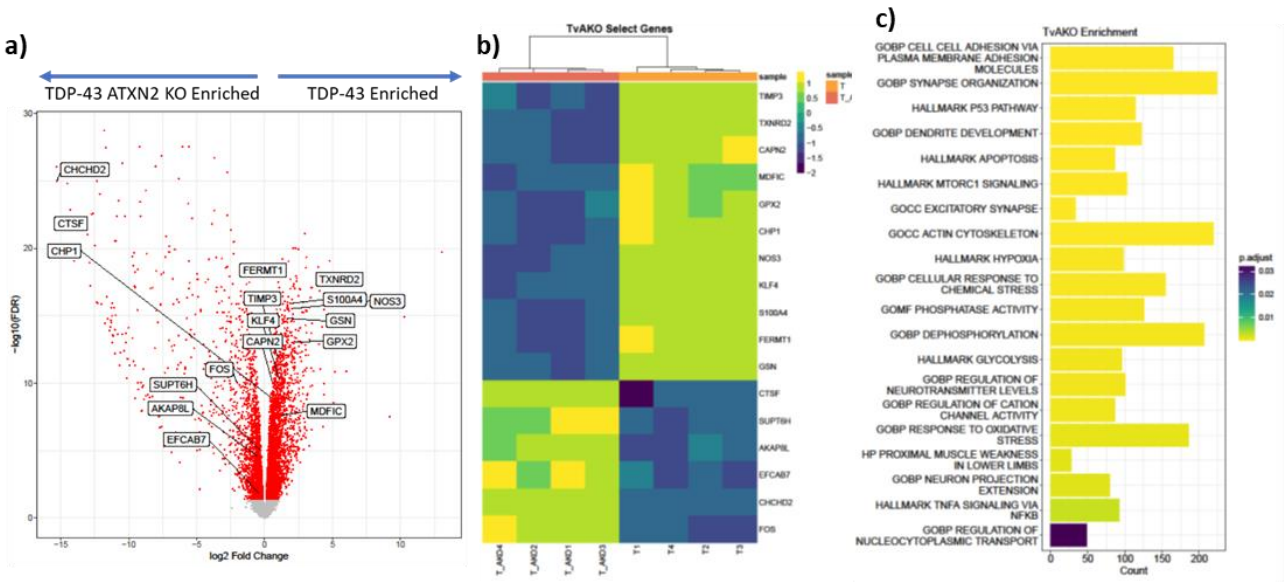

Figure 4.6: Transcriptomic effects of wild-type TDP-43 overexpression with ATXN2 knockout compared to the TDP-43 overexpressed, ATXN2 intact condition in motor neurons **(a)** Volcano plot of differentially expressed genes from RNA sequencing. Highlighted dots represent genes that pass an FDR < 0.05 significance threshold for discovery. **(b)** Heatmap of select genes related to nucleocytoplasmic transport, apoptosis, and the neuronal oxidative stress response discovered as significant in the RNAseq experiment. Each column represents a replicate sample submitted for sequencing. T = TDP-43 ATXN2 +/+; AKO = TDP-43 ATXN2 -/- **(c)** Pathway over-enrichment analysis results of differentially expressed genes in TDP-43 ATXN2 knockout motor neurons compared to TDP-43 ATXN2 intact motor neurons.

and nucleocytoplasmic transport. The effect of modulating two proteins like ATXN2 and TDP-43 that are broad in their functions and interactions is understandably varied – this dataset is a necessary first step in attempting to decode what the most consequential pathways are to modulate to elicit specific neuroprotective effects with the fewest negative side effects on long-term neuronal health.

Discussion

The goal of this chapter was to build, characterize, and demonstrate the utility of using the TDP-43 perturbation models I have previously generated to emulate and interrogate potential mechanisms underlying ATXN2 knockout-related neuroprotection. To facilitate this process, we generated an ATXN2 knockout iPSC knockout line that we combined with my inducible vector system with TDP-43 overexpression or lentivirus containing TDP-43 (Figure 4.1). ATXN2 knockout cells retained the capacity to differentiate into motor neurons in both the 2D (Klim et al. 2019) and LiMoNes differentiation modalities as well as continued to express engineered in TDP-43:YFP where applicable (Figure 4.1). Furthermore, I established that ATXN2 knockout was sufficient to reduce toxicity in the context of TDP-43 overexpression, which is in line with the previous results discovered in non-human systems (Figure 4.2; Becker et al. 2017; Elden et al. 2010). This observation was a vote of confidence that the model of ATXN2 knockout was behaving as predicted and may be used as a platform on which to examine more deeply what drives the neuroprotective features of ATXN2 knockout.

We then sought to move the field forward and make inroads on the mechanistic question – why is ATXN2 knockout neuroprotective? Much of the work done on the pathogenic mechanism of ATXN2 interrogates the effect of the PolyQ expansion tract (Damrath et al. 2012; Halbach et al. 2017; Hart and Gitler 2012). This is important work because of the association of PolyQ repeat

expansions with the onset of ALS and Spinal Cerebellar Ataxia Type 2, but the ATXN2 basal state in the neuronal models presented here and in the original discovery studies of ATXN2 as a modifier gene do not have a repeat expansion present. This implies that mechanisms driving ATXN2 pathogenesis in the repeat expansion context are likely to be independent from ATXN2's role as a TDP-43 toxicity modifier, which may occur regardless of the presence of said repeat expansion.

Given the consistent localization of both ATXN2 and TDP-43 to stress granules, looking at how modulation of both factors affected stress granule number and TDP-43 composition seemed like a natural first choice. We were surprised to note the difference in TDP-43 localization in both the puromycin and the oxidative stress paradigms that we saw, suggesting that ATXN2 knockout can have a profound effect on nucleocytoplasmic transport. One point to consider for further study is whether this effect is specific to ATXN2. I would hypothesize that this is not the case given that the number of stress granules in motor neurons seemed to go up when ATXN2 is knocked out and TDP-43 is unperturbed compared to when ATXN2 is intact (Figure 4.5a, b). That relationship tells me that although alleviation of the effects of TDP-43 transport may take precedence (i.e., TDP-43 mislocalization induced stress has the most profound short-term effect, so the result of modulating that is preferentially seen in these acute assays), there may be transport of other proteins and mRNAs that are modulated negatively by the loss of ATXN2. This could even lead to dysregulation of other factors and processes given the definition of stress granules as sites of translational stalling. More stress granules present, particularly at baseline, is not a positive sign of continuing long-term health of neurons.

The rationale for doing the RNA sequencing experiment was to attempt to observe and define the scope of processes affected by ATXN2 knockout in motor neurons. This is the first dataset of this type with samples that would allow for direct comparisons between isogenic cellular

states where the only thing differing was ATXN2 knockout status. Additionally, this data also includes information on TDP-43 perturbation via overexpression in the context of those ATXN2 expression states. Although RNA sequencing data for both TDP-43 and ATXN2 already exist (Sephton et al. 2011; Tollervey et al. 2011; Yokoshi et al. 2014), the point of this experiment was not necessarily to discover novel factors or processes associated with modulation of either protein; the main goal of this study was to meticulously define the scope and context in such a way that is ALS relevant to give us the best chance to discovering and validating features that are important to consider in the continued search for starting points for therapeutic development efforts. It was possible that we found nothing new, but even validating the previous findings through this unbiased survey is still of benefit to the field given that no one had looked in this specific context before. As stated in previous chapters, because ALS is a unique and specifically human condition, I believe that using a human-derived model is the best way to research the drivers of onset and progression of the condition.

In closely examining the RNA sequencing data, we observed an enrichment for genes with functions related to nucleocytoplasmic transport, as would be expected from the stress granule experiments (Figure 4.3, Figure 4.4, Figure 4.5). One annotated gene of this set, *CHP1*, is of particular interest due to its dual role as a vesicle trafficking protein (Di Sole et al. 2012) and interactor with the phosphatase calcineurin. TDP-43 is a target of calcineurin (Liachko et al. 2016), implying that upregulation of calcineurin may have a positive effect on TDP-43 aggregate formation as those aggregates tend to be hyper phosphorylated. *CHP1* has the capacity to negatively regulate calcineurin function (Di Sole et al. 2012). The gene level RNA sequencing data suggests that *CHP1* levels decrease when ATXN2 is knocked out. Should this relationship hold up to further scrutiny, this finding suggests that in addition to affecting transport processes that may

modulate TDP-43 trafficking, *CHP1* downregulation may be additionally beneficial in reducing TDP-43 aggregate burden by recruiting the endogenous phosphatase of TDP-43.

While mechanisms such as this can be nominated from this study, we must also acknowledge the other, potentially detrimental effects of ATXN2 knockout. For example, ORA nominated apoptosis and p53 pathway as enriched pathways in the ATXN2 intact versus knockout comparison. One gene that is highly upregulated in the ATXN2 knockout state is expression of *Cathepsin F (CTSF)*. CTSF is anti-apoptotic upon knockdown, effectively acting as a tumor suppressor gene in the context of cancer (Ji et al. 2018). The large upregulation of CTSF could be a sign that the neurons are assuming a more pro-apoptotic state when ATXN2 is knocked out. This observation, in concert with many of the top enriched genes in the ATXN2 knockout condition being other known apoptosis regulators, such as many members of the *PRAME* gene family (Xu et al. 2020b), raises the concern that ATXN2 knockout may do harm to neuronal health in the process of positively modulating TDP-43 function and localization. Additional assessment of how apoptotically primed ATXN2 knockout leaves neurons in both the context where TDP-43 is perturbed and not, will be important to understand the feasibility of establishing a therapeutic window for treatment via ATXN2.

At the end of the day, it is unlikely that ATXN2 knockout as a therapeutic treatment will not be without a host of biochemical side effects lending to its diverse set of endogenous functions. However, this motor neuron platform and sequencing data give hints for more targeted processes, particularly those involving nucleocytoplasmic transport and stress response, that can be modulated for therapeutic effect on TDP-43 associated toxicity and/or aggregation. Further iterations of this model with additional genetic perturbations relevant to those processes can use similar assays as presented in this chapter to investigate the mechanistic roles of those nominated

factors. Hopefully these data as presented here will be a good starting point for the next version of studies examining effects of ALS-associated neurodegeneration in a motor neuron specific context.

Materials and Methods

iPSC Cell Culture Conditions

The 11a iPSC line was derived from a biopsy from a 37-year-old healthy male patient as previously described in Boulting et al. 2011. iPSCs were maintained in mTESR1 or mTESR Plus (Stem Cell Technologies #85850, #100-0276) on Matrigel (Corning #354277) or Geltrex (Gibco #A1413201) coated tissue culture plates Matrigel coatings were prepared by diluting 600uL of concentrate (prepared according to the dilution factor on the certificate of analysis for that lot of reagent) diluted in 24mL of DMEM/F12. Geltrex coatings were prepared by diluting thawed Geltrex 1:100 in Minimal Essential Media (MEM – Gibco #11095080). Coated plates were cured at 37℃ for at least one hour and the coating media was aspirated immediately prior to cell addition. Media was changed every 1 – 2 days (mTESR1) or 2 – 3 days (mTESR plus) and cells were passaged using Accutase (Stem Cell Technologies #07920) as needed. On thaw and passage, media was also supplemented with 10uM Rock Inhibitor (Y-27632 – Stemgent #04-0012) to facilitate adherence and survival. Cells were maintained in a 37℃, 5% CO_2 incubator.

When needed, iPSCs were cryopreserved using CryoStor® CS10 Freeze Media (BioLife Solutions #210502) and stored in -80℃ or vapor phase liquid nitrogen.

Stable cell lines harboring the AAVS1 inducible expression plasmids in the context of ATXN2 knockout were generated using the same procedure outlined in Chapter 2. Resultant iPSC lines harboring the inducible vector system components (including empty vector control

transductants that contain rtTA but no additional transgene) were maintained in mTESR1 or mTESR Plus supplemented with 500µg/mL G-418 (Neomycin analog – Gibco #10131035).

CRISPR Knockout of ATXN2 in iPSCs

iPSCs were transiently transfected with sgRNAs targeting Exon 1 and Exon 3 of ATXN2 (Synthego) and TrueCut™ Cas9 Protein v2 (Invitrogen #A36496) using Lipofectamine™ RNAiMAX Transfection Reagent (Invitrogen #13778075) according to manufacturer's instructions. Single cell clones were generated by limiting dilution – similar to methods used to generate single cell clones of inducible plasmid transductants described in Chapter 2.

Motor Neuron Differentiations

LiMoNes Motor Neuron Differentiation

Adapted from Limone et al. 2023. Prior to all differentiations, iPSCs were infected with lentivirus containing TetO-NGN2-Puro at approximately 2 MOI in a 6 well tissue culture dish. Cells were expanded and cryopreserved prior to the first differentiation.

NGN2-infected iPSCs were plated in their desired format and grown until at least 80% confluent. Media changes each day were performed as follows. Day 1: N2 Media Base – DMEM/F12 Media (Gibco #11320033), 1X GlutaMAX (Gibco #35050061), 0.3% (v/v) Glucose (Sigma-Aldrich #G7021 – dissolved in PBS before addition), 1X N2 Supplement (Life Technologies #17502048) – supplemented with 4ug/mL Doxycycline (Sigma Aldrich #D9891 – dissolved in water), 200nM LDN-193189 (Stemgent #04-0074-02 – dissolved in DMSO), 10µM SB-431542 (Tocris #1614 – dissolved in DMSO), 2µM Retinoic Acid (Sigma Aldrich #R2625 – dissolved in DMSO), and 2µM Smoothened Agonist (SAG – Stem Cell Technologies #73412 – dissolved in DMSO). Day 2 and 3: N2 Media Base supplemented with 4µg/mL Doxycycline,

5µg/mL Puromycin (Gibco #A11138-03), 100nM LDN-193189, 10µM SB-431542, 1µM Retinoic Acid, 1µM SAG. Day 4: NBM/B27+ Media Base – Neurobasal Media (Gibco #21103049), 1X GlutaMAX, 1X MEM Non-Essential Amino Acids (NEAA – Gibco #11140050), 1X N2 Supplement, 1X B27 Plus Supplement (Gibco #A3582801) – supplemented with 4µg/mL Doxycycline, 5µg/mL Puromycin, 1µM Retinoic Acid, 1µM SAG, 10ng/mL recombinant Brain Derived Neurotrophic Factor (BDNF – R&D Systems #11166-BD – dissolved in 0.1% (w/v) BSA-PBS), 10ng/mL recombinant Ciliary Neurotrophic Factor (CNTF – R&D Systems #257-NT – dissolved in 0.1% (w/v) BSA-PBS), and 10ng/mL recombinant Glial Cell Line-derived Neurotrophic Factor (GDNF – R&D Systems #212-GD – dissolved in 0.1% (w/v) BSA-PBS). Day 5 and 6: NBM/B27+ Media Base supplemented with 4µg/mL Doxycycline, 5µg/mL Puromycin, 1µM Retinoic Acid, 1µM SAG, 10ng/mL BDNF, 10ng/mL CNTF, 10ng/mL GDNF, and 1µM EdU (Invitrogen #A10044 – dissolved in DMSO). Day 7: Freshly differentiated neurons were passaged using Accutase followed by resuspension in Day 5 differentiation media supplemented with 10uM Rock Inhibitor or cryopreserved in CryoStor CS10 as desired. Destination plates for passaged neurons were prepared as follows: plates were coated with Poly-D-Lysine (Gibco #A3890401) at 4°C overnight. Coated plates were then washed three times with PBS, coated with Natural Mouse Laminin (Gibco #23017015) diluted 1:200 in PBS and cured at 37°C for at least two hours. Plates were washed three times with PBS before neurons are seeded. Neurons thawed from frozen are plated using the same procedure as if they were freshly passaged Day 9+: Media was gently removed (i.e., without the use of a vacuum aspirator), and slowly replaced with NBM/B27+ Media Base supplemented with 4µg/mL Doxycycline if needed to maintain expression of inducible vector insert, 10ng/mL BDNF, 10ng/mL CNTF, 10ng/mL GDNF, and 1µM EdU. For maintenance of neuronal cultures, half-media changes were performed with the Day 9+ media every 2 – 3 days.

2D Differentiation

LiMoNes neurons are resistant to puromycin due to the puromycin resistance gene on the NGN2 expression vector. To test the effect of the high dose puromycin stress in ATXN2 intact compared to knockout lines, we used a non-NGN2 differentiation protocol adapted from Klim et al 2019. iPSCs were first plated using standard culture conditions and grown to 50~60% confluency. The differentiation base media used at all time points is composed as follows: 1:1 DMEM/F12:Neurobasal Media, 1X GlutaMAX, 1X MEM NEAA, 1X N2 Supplement, 1X B27 Supplement (Gibco #17504044) – hereafter referred to as N2/B27 Base. Media changes were performed daily. For Days 1 – 6 cells were cultured in the N2/B27 media base supplemented with 10μM SB-431542, 100nM LDN-193189, 1μM retinoic acid, and 1μM SAG. For Days 7 – 14 cells were cultured in N2/B27 media supplemented with 1μM retinoic acid, 1μM SAG, 5μM DAPT (Life Technologies #J65864.MA), and 4μM SU-5402 (Stem Cell Technologies #73914). On Day 15, the culture was dissociated with Accutase and resuspended in sorting buffer (PBS with 1mM EDTA, 15mM HEPES, 1% (w/v) BSA). Following harvest, neurons were incubated with conjugated antibodies targeting the neuron surface markers NCAM (Conjugated to Alexa 647 – Novus Biologicals #NBP2-52710AF647) and EpCAM (Conjugated to PE – BD Biosciences #347200). Motor neurons were purified by sorting for NCAM+, EpCAM- cells. Purified motor neurons were cultured on Poly-D-Lysine with Laminin coated plates prepared as described above. Neurons were maintained in N2/B27 media base with no additives. Neurons were incubated for 5 days after FACS sort before the puromycin stress experiments were conducted.

FACS and Flow Cytometry

Neuronal cultures were prepared for motor neuron enrichment sorting as described above. Support for FACS experiments was provided by the Department of Stem Cell and Regenerative

Biology Flow Cytometry Core. Live-cell sort experiments were conducted using a BD FACS Aria II+.

siRNA Transfection of iPSCs

Adapted from the procedure previously described in Klim et al. 2019. For each well of a 6-well plate of iPSCs transfected, 9µL Lipofectamine RNAiMAX Transfection Reagent (Invitrogen #13778075) was diluted in 150µL of OPTI-MEM (Gibco #31985062). Separately, Negative Control and ATXN2 targeting siRNAs were diluted in 150µL OPTI-MEM such that the final per well concentration of transfected siRNA was 60nM. These mixtures were combined and incubated at room temperature for 30 minutes. Following incubation, the combined mixture was added to iPSCs fed with fresh media immediately prior to transfection. iPSCs were then passaged and subjected to a colony formation assay 24 hours following siRNA transfection. The siRNAs used were the Invitrogen *Silencer*™ Select Negative Control No. 1 (Invitrogen #4390843) and siATXN2 acquired from the same *Silencer*™ Select collection (Invitrogen # 4392420-s12493).

RNA Extraction and qRT-PCR

RNA extractions from cultured cells were performed using the Qiagen RNEasy Plus Mini Kit (Qiagen #74134). QIAshredder columns (Qiagen #79656) were used for homogenization of harvested cultures prior to RNA purification. cDNA generation was performed using the iScript (Bio-Rad #1708890) or iScript Advanced (Bio-Rad #172037) cDNA Synthesis kits with 500ng RNA input. qRT-PCR was performed using the generated cDNA reactions diluted 1:5 and combined according to manufacturer's instructions with Fast SYBR Green Master Mix (Life Technologies #4385614). Samples were run as technical triplicates with an additional no template control. Reactions were run on an Applied Biosciences QuantStudio 6 in a 384-well format with

the following protocol: 1 step of 95°C 20s followed by 95°C 1s, 60°C 20s for 40 cycles. The following primers were used: GAPDH-Fwd: 5' – TTGTCAAGCTCATTTCCTGGTATG – 3; GAPDH-Rev: 5' – TTCTCTTGTGCTCTTGCTGG – 3'; ATXN2-Fwd: 5' – TAGTCCTGCATCGAACAGAGCTG – 3'; ATXN2-Rev: 5' – AGCTAGGTGATGTTTCATTGGG – 3'

Western Blots

Whole cell western blots

Protein was extracted from cultured cells using RIPA buffer (Thermo Scientific #89900) supplemented with 1X Halt™ Protease/Phosphatase Inhibitor Cocktail (Thermo Scientific #78440). Cells were incubated in a suspension of RIPA buffer on ice for 10 minutes before centrifugation at maximum speed for 20 minutes followed by collection of the protein containing supernatant. Protein was quantified using the Pierce™ BCA Protein Assay Kit according to manufacturer's instructions (Thermo Scientific #23225). Absorbance of the quantification plate at 562nM was read using a Cytation3 plate reader. 10µg of protein from each sample was resuspended in Blue Loading Buffer enriched with DTT as the reducing agent (Cell Signaling Technology #7722). Diluted samples were boiled for 5 minutes at 95°C before being loaded to Bio-Rad Mini-PROTEAN TGX 4 – 20% pre-cast gels (Bio-Rad #4561094). Precision Plus Protein Dual Color Standards (Bio-Rad #1610374) was used as the molecular weight ladder. Gels were run using Tris/Glycine/SDS Running Buffer (National Diagnostics #EC-870) at 200V for 40 minutes. Gels were transferred to a PVDF membrane using the iBlot 2 Dry Transfer system. Membranes were cut to size and blocked for 1 hour in LI-COR Intercept® Blocking Buffer at room temperature (LI-COR #927-60001). Primary antibodies were then diluted as appropriate in 5% (w/v) BSA-TBS-T (Tris Buffered Saline with 0.1% (v/v) Tween 20) and added to the

membranes to incubate at 4℃ overnight. Primary antibodies utilized were Rabbit anti-TDP43 (G400) (Cell Signaling #3448S) at 1:1000 dilution, Mouse anti-ATXN2 (BD Biosciences #611378), Rabbit anti-GAPDH (Cell Signaling Technology #2118) and Mouse anti-GAPDH (Millipore Sigma #MAB374) at 1:1000 dilution. The next day, membranes were washed with TBST, incubated with LI-COR anti-rabbit and anti-mouse IRDye secondary antibodies suspended in Blocking Buffer supplemented with 0.1% (v/v) Tween 20 and 0.01% (w/v) SDS for 1 hour and then washed again with TBST before being visualized on the LI-COR Odyssey Imager.

Cellular Fractionation Western Blots

Subcellular protein fractionations were performed using the Subcellular Protein Fractionation Kit for Cultured Cells (Life Technologies #78840) according to manufacturer's instructions. After the fractions were isolated, the same procedure was followed as the whole cell western blot for BCA quantification of the protein, running the gel, and analyzing the membrane. Primary antibodies used were Rabbit anti-TDP43 (G400) at 1:1000 dilution, Mouse anti-GAPDH at 1:1000 dilution, and Rabbit LaminB1 (ProteinTech #12987-1-AP) at 1:2000 dilution. When needed for sequential blotting, I also used Restore Plus Western Blot Stripping Buffer (Thermo Scientific #46430) to gently remove the previous antibodies from the membrane. To complete this, the membrane was washed 3 times with PBS, coated with stripping buffer at room temperature with gently shaking to 30 minutes, washed again 3 times with PBS, then re-blocked with Intercept Blocking Buffer before adding the primary antibody mix as previously described.

Immunofluorescence and Imaging

ATXN2 knockout validation images and puromycin stress granule imaging

Where applicable in neuronal cultures, proteotoxic stress was applied via exposure to standard culture media supplemented with 10µg/mL Puromycin for 24 hours. iPSCs or neurons to be stained were fixed with 4% Paraformaldehyde for 20 minutes at room temperature or overnight at 4°C. Fixed cells were briefly washed with PBS and then coated with a blocking and permeabilization buffer comprised of 0.1% (v/v) Triton X-100-PBS (Sigma Aldrich #T8787) and 10% Normal Donkey Serum (Jackson ImmunoResarch Laboratories #017-000-121) for one hour at room temperature. Primary antibodies were diluted in the stated blocking/permeabilization buffer and incubated overnight at 4°C. The following day, the plate was washed three times with PBS and the Alexa-Fluor conjugated secondary antibodies were added diluted 1:1000 in PBS for one hour in the dark. Two PBS washes were performed followed by incubation with 1µg/mL DAPI (Invitrogen #D3571) for 5 minutes in the dark. After two additional PBS washes, the plates were imaged or stored at 4°C until imaging. Primary antibodies used in the studies in this chapter were Rabbit anti-TDP43 at 1:100 dilution (ProteinTech #10782-2-AP), Mouse anti-G3BP1 (Millipore Sigma #05-1938) at 1:100 dilution, Mouse anti-ATXN2 at 1:100 dilution, and Goat anti-Oct-3/4 (R&D Systems #AF1759).

Images were captured using a Nikon Eclipse Ti microscope. Imaging analysis to generate the Pearson Correlation Coefficients by captured field of view was performed using the co-localization feature in Nikon Elements.

Sodium arsenite (Oxidative stress) stress granule imaging

Oxidative stress was applied to neurons plated in a 96-well Perkin Elmer PhenoPlate by changing the media to fresh culture media additionally supplemented with 1mM Sodium Arsenite and returning the plate to the 37°C incubator for one hour. Neurons to be stained were fixed and permeabilized with ice-cold methanol and incubated on ice for 20 minutes. Methanol was then

gently removed from the plate using a multi-channel pipette. Permeabilized neurons were blocked using 0.1% (w/v) BSA-PBS for 10 minutes at 4°C. Primary antibodies were diluted in 0.1% BSA-PBS, added to the neurons, and incubated overnight at 4°C. The following day, the plate was washed three times with PBS and the Alexa-Fluor conjugated secondary antibodies were added diluted 1:1000 in PBS for one hour in the dark. Two PBS washes were performed followed by incubation with 1µg/mL DAPI (Invitrogen #D3571) for 5 minutes in the dark. After two additional PBS washes the plates were imaged or stored at 4°C until imaging. Primary antibodies used in the stress granule experiments were Mouse anti-TDP-43 at 1:150 dilution (Life Technologies #H00023435-M01) and Rabbit anti-G3BP1 at 1:300 dilution (ProteinTech #13057-2-AP).

Images were captured using the Molecular Devices IXM automated confocal microscope. Imaging analysis was performed using a pipeline generated in the PerkinElmer Columbus™ image data storage and analysis system. Information from each channel was parsed in order to identify the nucleus, identify the region around each nucleus to define the approximate cell area, and then identify spots within this area that were classified as TDP-43 or G3BP1 aggregates based on the channel being visualized. Results by imaged field were exported into Excel and manually reviewed alongside the captured images. Fields where an analysis was performed on no viable cells (i.e., attempted to define cell boundaries despite no DAPI signal visible), were eliminated from the analysis.

Colony Formation Assays

iPSCs were plated at 250,000 cells per well in a 6 well tissue culture plate using standard methods. 24 hours after plating, media was supplemented with 2 (Figure 4.2) or 4µg/mL (Supplementary Figure 4.1) Doxycycline for half of the plate each. Cells were maintained in media with or without doxycycline on the regular feeding schedule for 6 additional days. On the final

day, cells were fixed with ice-cold methanol for 10 minutes on ice and stained with a 0.5% Crystal Violet solution comprised of water and 25% methanol (VWR #BT144750) with gentle shaking for at least 20 minutes at room temperature. Plates were scanned using a conventional flat screen paper scanner to capture images. Crystal Violet levels were quantified after imaging using 10% (v/v in water) Acetic Acid extraction by coating the wells with the solution, gently shaking for at least 30 minutes, and then measuring the absorbance of samples from each well at 570nM using a Cytation3 plate reader.

Cell Titer Glo Viability Assays

For the short-term differentiation assay, NGN2 infected iPSCs were plated on 96 well tissue culture plates at 10 – 20,000 cells per well per standard culture methods. LiMoNes motor neuron differentiation commenced 24 hours after plating until the captured timepoints listed. There was a separate 96 well plate for each time point. Undifferentiated samples were exposed to the same differentiation media as the rest of the plate without Doxycycline, Puromycin, or EdU. On each read day reported, one plate was assayed using Cell Titer Glo 2.0 reagent (Promega #G9243) according to manufacturer's instructions. Luminescent readings were captured using a Cytation3 plate reader.

For the long-term neurons with lentivirus viability assay, cells were plated on 96 well tissue culture plates at 30,000 cells per well per standard culture methods. Neurons were infected with a YFP or TDP-43:YFP lentivirus 7 days after plating. After 28 days, cells were assayed using Cell Titer Glo 2.0 reagent according to manufacturer's instructions Luminescent readings were captured using a Cytation3 plate reader.

RNA sequencing

RNA was harvested from Day 12 (Day 5 post-differentiation) motor neurons as described in the qRT-PCR methods section. Neurons were not sorted prior to RNA harvest because ~80% of cultures in all assayed conditions were YFP+ as measured by flow cytometry (Supplementary Figure 3.2). Four biological replicates of RNA per neuron line were submitted for sequencing to The Bauer Core Facility at Harvard University. RNA integrity was verified using an Agilent TapeStation system. Sequencing libraries were generated using a Kapa mRNA HyperPrep Kit (Roche #KK8581). Sequencing was performed on an Illumina NovaSeq system.

Reads were aligned to the reference human genome build GRCh38 r109. Multidimensional scaling plots were generated from the top 1000 differentially expressed genes (Supplementary Figure 3.3). Differential gene expression (DGE) analysis was performed using edgeR with Benjamini-Hochberg FDR correction. Samples input to analysis were filtered to eliminate genes with less than one count per million in at least 8 samples. Heatmaps containing selected genes were derived from the DGE data. All differentially expressed genes with an FDR threshold of 0.05 were input into Over-enrichment analysis (ORA) to determine pathways enriched in the TDP-43:YFP, ATXN2 -/- condition compared to the TDP-43:YFP, ATXN2 +/+ condition.

Differentially expressed genes enriched the TDP-43:YFP, ATXN2 intact compared to TDP-43:YFP, ATXN2 knockout conditions with a log2 fold change >±2 are listed in Supplementary Tables 4.1 and 4.2. Data is also available for comparisons to YFP expressing neurons and no transgene expressing (Empty Vector) neurons.

Data Availability

RNA sequencing data will be deposited to NCBI GEO by the end of February 2024. Please search for the dataset title “Transcriptomic characterization of in vitro human iPSC-derived motor

neuron systems for the exploration of cell autonomous mechanisms and modifiers of TDP-43 perturbation associated neurotoxicity" to locate and download.

Additional Acknowledgements

Irune Guerra performed the initial CRISPR modification to generate ATXN2 knockout 11a iPSCs as well as the preliminary puromycin-induced stress granule work presented in Figures 4.3 and 4.4. Protocols for sodium arsenite stress and subsequent staining of stress granules were adapted from protocols provided by Clotilde Lagier-Tourenne and Rajesh Gunage. RNA sequencing analysis was performed in collaboration with Kris Holton.

Chapter 5: Conclusions and Future Directions

Final Summary & Conclusions

This dissertation sought to establish, evaluate, and implement an *in vitro* human motor neuron model to study neurodegenerative mechanisms in ALS. In showcasing that the model was versatile enough to explore concrete mechanisms of neurodegeneration, I focused on two questions that remain unsolved in the ALS field. First, what is the pathogenic effect of persistent cytoplasmic TDP-43 localization in human motor neuron cultures? Second, what mechanisms does ATXN2 knockout engage to drive neuroprotection in the context of TDP-43 proteinopathy? Both lines of exploration represent aspects of motor neuron and TDP-43 biology that will benefit from additional research. My methods in model building are additionally uniquely suited to answer these questions because all work was conducted in human-derived systems. To take this a step further, the engineered lines I generated are an isogenic series derived from the same 11a parent line, which increases the confidence that results found in one context of TDP-43 or ATXN2 perturbation are due to the perturbation itself, not arising random variance that exists between two lines with different source backgrounds. To date, no other iPSC model has been published for the study of TDP-43 and its variants that has been designed in this fashion, specifically in motor neurons.

I began this work by engineering the 11a healthy control iPSC line to harbor inducible expression of TDP-43 or TDP-43ΔNLS. In characterizing the system that I developed, I showed that both engineered iPSCs and motor neurons derived from this method show loss of viability upon induction of wild-type TDP-43 perturbation, either during the differentiation via the inducible vector system or conferred by lentivirus after the differentiation is complete (Figure 2.5; Figure 2.6). Comparatively, I showed that in the short-term, TDP-43ΔNLS does not cause neural viability loss, which would be in line with acute localization of TDP-43 to the cytoplasm being a part of the adaptive cellular stress response as predicted by the literature (Figure 3.3). Additionally,

I was able to establish that over an intermediate length experiment (14 days after lentivirus infection) cytoplasmic TDP-43 begins to be toxic and has a preferentially profound negative effect on motor neurons over other neural cultures (Figure 2.6). Through the concordant behavior with what had been previously reported in non-human, non-neuronal models, these findings solidified that the *in vitro* model I developed was valid and applicable to the neurodegeneration context I wished to examine.

I continued the work by implementing the TDP-43ΔNLS variant cell model to tackle the first of my overarching questions: what is the pathogenic effect of persistent cytoplasmic TDP-43 localization? I observed that TDP-43ΔNLS expressing motor neurons showed high expression of cytoplasmic TDP-43 and had the propensity to spontaneously form cytoplasmic TDP-43 aggregates without exogenous stress application, which were all expected features of the model based on previous work in the field (Barmada et al. 2010; Winton et al. 2008a). In part to clarify whether the pathogenic effects I would discover would be more representative of early ALS progression or the end state of the disease, I evaluated whether I would be answering this question about cytoplasmic TDP-43 from the gain of function or loss of function perspective of TDP-43 disruption. I quickly determined that my model likely represents a gain of function TDP-43 perturbation model that exhibits partial nuclear clearance of endogenous TDP-43 as detected by immunofluorescence (Figure 3.1) but does not show signs of splicing deficits in *STMN2* that are associated with loss of TDP-43 function (Figure 3.2). This is also a point in favor for the uniqueness and versatility of this cellular model as many recent efforts in the field had centered around TDP-43 loss of function models rather than gain of function (Klim et al. 2019). I continued on to evaluate cytoplasmic TDP-43 expression as it relates to stress granule number in neurons to address the hypothesis that TDP-43 becomes pathogenic by becoming sequestered in stress

granules and forming as a seed for the aggregate to get progressively larger (Dewey et al. 2012; Fang et al. 2019). I observed that cytoplasmic TDP-43 expression seems to saturate the stress response; there is no increase in stress granules when an oxidative stress is applied, although there are more stress granules at baseline than in either the no transgene or wild-type TDP-43 expressing conditions. Additionally, perhaps owing to the protective nature in the short-term of TDP-43ΔNLS, TDP-43 localization to stress granules seems to initially go down after exposure to an oxidative stress conferred by an acute dose of sodium arsenite. These results indicate that cytoplasmic TDP-43 may be driving pathogenesis and neurodegeneration by putting the neuron in perpetual state of heightened stress, even when a stressor is not present. It would follow then that a potential therapeutic strategy for combating the gain of function effects of TDP-43 proteinopathy is to lower the cell's perceived amount of stress. Indeed, this pharmacology is part of the proposed mechanism of action of Relyvrio (Del Signore et al. 2008; Kusaczuk 2019). The fact that I was able to use the model to come to this stress modulating relationship of cytoplasmic TDP-43 independently further bolsters confidence that relationships and mechanisms discovered by this model are valid and representative of TDP-43 proteinopathy. This finding establishes that, at least at first, TDP-43 aggregate clearance may not be explicitly required to maintain neuronal health and function. Thinking further ahead, it may be possible to leverage a combination of a stress response modulating agent with a TDP-43 aggregate clearance drug for maximal therapeutic effect.

Inspired by the results from the initial phenotypic foray into characterizing the cellular effects of cytoplasmic TDP-43, we generated an RNA sequencing data set to get an unbiased view on the other processes that changed in the context of cytoplasmic TDP-43 expression compared to wild-type TDP-43 expression. This comparison was apt; this method allowed us to find factors that were specifically related to cytoplasmic TDP-43 defects, not a general scenario of TDP-43

perturbation. We affirmed the complexity of identifying a key driver for cytoplasmic TDP-43 toxicity as several pathways nominated prominent cellular pathways that could drive either neurotoxicity (e.g., supporting some excitotoxicity relevant properties by modulating synaptic structure) or support neuronal health (e.g., anti-apoptosis pathways, positively modulating the stress response) and even within those pathways there was not a strong consensus of the net effect of that pathway perturbation (Figure 3.5). A deeper analysis of each of these promising pathways in this cellular context is merited to make inroads at sorting out what cellular process may be most efficacious to modulate during the search for novel TDP-43 proteinopathy therapies. Further, although we did not deeply examine them in the course of these studies, this dataset also is powered to examine factors of TDP-43 overexpression compared to cytoplasmic TDP-43 expression and analyze what modulated factors are specific to nuclear TDP-43 overexpression toxicity. There is a rich vein of data here, never before generated in a human motor neuron context, that is worth continued examination.

Lastly in this dissertation, I employed a CRISPR-edited variant of my *in vitro* motor neuron models containing ATXN2 knockout to explore a question that has been neglected by the field since the discovery of ATXN2 as a genetic modifier of ALS-relevant cell biology – why does ATXN2 knockout provide the protective effect against TDP-43 perturbation toxicity that it does? To add to the work done by others to more precisely defining ATXN2's functions, which were not deeply understood at the time of the discovery of the ATXN2 – TDP-43 relationship, this dissertation is the first study to showcase multiple examples of how an *in vitro* model could be interrogated to learn more about both proteins in relation to each other. After establishing that the cell lines I generated were representative of the ATXN2 knockout, TDP-43 overexpression condition (Figure 4.1), I validated that ATXN2 knockout has a similar neuroprotective effect on

motor neurons in culture with TDP-43 perturbation, as would be suggested by the results from non-human model systems (Figure 4.2; Becker et al. 2017; Elden et al. 2010). To dive into the mechanism driving this neuroprotection not that the effect was established, we examined the effect of ATXN2 knockout on TDP-43 stress granule localization and observed that in both an oxidative stress and puromycin-induced stress context, ATXN2 knockout seemed to limit TDP-43 translocation to the cytoplasm and stress granules, suggesting that one of ATXN2's key neuroprotective mechanisms is modulating nucleocytoplasmic transport in a therapeutic fashion (Figure 4.3, Figure 4.4, Figure 4.5).

We then examined the global effects of ATXN2 knockout in the context of TDP-43 overexpression via RNA sequencing. This was in part motivated by a desire to see how nucleocytoplasmic transport compared in significance to other perturbed pathways. We observed, strikingly, that in addition to nucleocytoplasmic transport annotated factors being enriched in the ATXN2 intact versus knockout condition, there were also several pathways related to apoptosis and the stress response that were modulated as well. Unlike a more even-handed response in the functional distribution of gene effects in the enriched pathways that the TDP-43ΔNLS study showed, several of the top differentially expressed genes enriched in the ATXN2 knockout condition were associated with functions of these pathways that would be detrimental to cell health (e.g., *PRAME* family genes enriched in ATXN2 knockout condition, which is potentially pro-apoptotic) (Figure 4.6). This discovery raises the question of whether ATXN2 knockout itself will be a feasible therapeutic intervention in humans, despite the promise of the mouse data that showed increase in lifespan when ATXN2 is knocked out transgenically or by anti-sense oligonucleotide (Becker et al. 2017). Given the diverse set of ATXN2's endogenous functions, it seems understandable that the effects of knockdown needed to achieve therapeutic modulation of TDP-

43 may come at the cost of perturbing other cellular functions and/or sensitizing the cell to a non-TDP-43 stress which normally would have been surmounted. From the data I have generated, because of the additional perturbations in pathways detrimental to motor neuron health, I feel that it is unlikely for ATXN2 knockout to be the final therapy for TDP-43 disrupted ALS. Instead, I see examining features of ATXN2 knockout that were called as potential positive modulations, such as changing nucleocytoplasmic transport in a TDP-43 specific way (perhaps by developing a molecular binder to TDP-43 that encourages re-localization to the nucleus) as promising processes to explore in future therapeutic development initiatives.

In summary, this dissertation established a new human, *in* vitro, neuron-based cellular platform for the study of neurodegeneration in the context of TDP-43 disruption. The data presented here is a first step into deeper examinations of cell autonomous neurodegenerative mechanisms in a system that faithfully represents core features of a physiologically relevant disease context wherein we are powered to discover and interrogate processes that modulate the onset and/or progression of ALS.

Future Directions

Neurite length analysis to examine cytoskeletal specific phenotypes as an alternative phenotypic assay to assess neuronal cell state

One method that would have power to directly interrogate defects in cytoskeletal maintenance elements that arise from any genetic perturbation is to assay for changes in neurite growth with and/or without physical injury. It has previously been established that defects in motor neuron cytoskeletal elements may be a consequence of ALS-associated mutations. One prime example is the relationship of TDP-43 to STMN2. TDP-43 nuclear loss leads to inclusion of a

cryptic exon in STMN2 that truncates the mRNA, resulting in a non-functional protein (Klim et al. 2019). STMN2 is an axonal outgrowth and maintenance factor that is specifically expressed in neurons; additional studies of STMN2 knockout have found that loss of STMN2 was sufficient to induce motor neuropathy in mice (Guerra San Juan et al. 2022). In the discovery process of TDP-43 and STMN2's relationship, it was noted that there were defects in neuron outgrowth after axotomy that arose in the context of TDP-43 loss that could also be attributed to functional loss of STMN2 (Klim et al. 2019). Additionally, other cytoskeletal proteins such as TUB4A have been directly associated with ALS development upon mutation suggesting that this is a functional category worth exploring when examining mechanisms of ALS-relevant neurodegeneration (Brown and Al-Chalabi. 2017; Smith et al. 2014). Developing an assay to directly track the effect of genetic perturbation on the status of cytoskeletal regulation by tracking neurite growth rate at baseline or in the context of axon injury (Klim et al. 2019) would give additional information on this mechanism of neurodegeneration and allow for direct examination of whether modulating this process would be beneficial for ALS patients.

Deep validation and analysis of pathways nominated by the RNAseq dataset

The neurite outgrown or injury recovery assays described above could be one of a suite of additional phenotypic assays developed to assess the functional state of any neuronal process that could be associated with neurodegeneration. The RNA seq data presented in Chapter 3 and Chapter 4 nominated many different cellular processes and genes that deserve closer examination to determine their functional significance in driving or preventing neurodegeneration. To begin this process, it is necessary to functionally validate a subset of the enriched genes and pathways using qRT-PCR and western blot. This will confirm the functional differences that arise in the context of cytoplasmic TDP-43 presence or AXTN2 knockout. Following this, for pathways that are of

particular interest, it may be worthwhile to develop custom assays to track the phenotypic action of those pathways, similar to the neurite growth assay described above. For example, if glutamate-mediated excitotoxicity was proposed as a modulatory mechanism with proteins that validated as being significantly different between the two compared contexts, I could test the neurons' electrical and viability response to chronic exposure to moderate to high concentrations of glutamate in the media to try to stimulate that process. Such a test could provide mechanistic information for perturbations in pathways of interest in further exploration of neurodegenerative therapies.

Examining additional iPSC genetic backgrounds and/or TDP-43 perturbations

The AAVS1-directed inducible vector I built was designed with the intention of being a versatile system that could be deployed in any cell line and/or to overexpress any variant of *TARDBP* or any other gene that may be of interest to evaluate. An experiment that would be of interest to the field and further validate the model I have developed would be to compare the results I showed in this dissertation to results in similar assays using an ALS-patient derived line, with or without additional perturbation. One mutation that would particularly validate the TDP-43ΔNLS models would be to test that line in direct comparison to neurons from an ALS patient with an A90V mutation, which is an ALS-associated mutation that occurs in the Nuclear Localization Sequence (Winton et al. 2008b).

Also of potential interest to examine would be the effect of other functional, synthetic TDP-43 mutations that modulate other parts of its function. For example, there exists an RNA-binding deficient mutant, TDP-43 5F-L that can no longer perform the functions of TDP-43 associated with directly interacting with RNA (Elden et al. 2010). It would be curious to examine this variant in all the assays that I have developed to provide additional information on whether interactions that are associated with TDP-43 mediated toxicity, protective or destructive, are mediated via an

interaction with a particular or group of RNA. Combining these functional results with data from RNA seq, wherein differentially expressed transcript that could be affected by this lack of TDP-43 modulation have already been identified, has potential to be particularly insightful.

Compound screening using iPSC-derived motor neurons for modulators of the oxidative or proteotoxic stress response

One of the core obstacles to high throughput screening in iPSC-derived neuronal cultures was the problem of scale. Before development of the LiMoNes motor neuron protocol, it was largely infeasible to generate motor neurons at the scale needed to satisfyingly conduct a high-throughput screen. Now that I have shown the ability to reproducibly generate large amounts of neurons and use them repeatedly in my own studies, it should be possible to embark on any number of screening projects based on this differentiation modality, including those that take advantage of the engineered lines similar to or the same as the set that I made. One such screen could be an arrayed compound screen to identify molecules that modulate the amount of TDP-43 aggregation, total stress granule number, and/or TDP-43-containing stress granules in response to a proteotoxic or oxidative stress. This would use a similar protocol as established in Chapters 3 and 4. Lead compounds for future study discovered in these screens could act through a variety of mechanisms beneficial to neuronal health, such as positively modulating insoluble aggregate clearance; improving stress granule dynamics so that even if they do form, TDP-43 doesn't get sequestered there; or directly preventing TDP-43 from localizing to stress granules or aggregating at all; among other potential mechanisms.

Pooled genetic knockout or overexpression screen for additional neuroprotective factors that modulate short-term TDP-43 proteinopathy toxicity in the short-term differentiation assay

Following on the short-term differentiation assay design outlined in Chapter 2 and then tested in the context of ATXN2 knockout in Chapter 4, I could envision performing a pooled viability screen in an inducible TDP-43 expressing iPSC line using that assay as a readout to directly identify additional genes that when knocked out, provide a similar effect to ATXN2. This experiment could be conducted by culturing a large amount of inducible TDP-43 iPSCs, infecting them with a CRISPR (or overexpression construct) library, waiting a short while for the edit to take, and then performing the short-term differentiation assay in a large batch. The readout of the assay would be a sequencing readout similar to that in other pooled screening viability assays (Shalem et al. 2013). For a CRISPR based screen, the sgRNAs would be the barcodes to track via sequencing. This would be a positive selection screen. We would assess the distribution of barcodes immediately following infection with the sgRNA library and compare it to the distribution following 6 – 7 days of the motor neuron differentiation and determine which barcodes targeting which genes are still present to identify modifiers of TDP-43 toxicity upon knockout that behave similarly to ATXN2. In order to embark on this line of experimentation, we would need to perform additional assay development for the large-scale infections and assay procedures. It is also possible that this could potentially be cost prohibitive given the expense of iPSC reagents, however if expense was not a factor, I would have confidence that this would be a fruitful endeavor. The best-case scenario would be that other factors discovered which directly modulate TDP-43 toxicity share similar biological functions, which would give us a strong hint as to the dominant mechanism to target in future therapeutic development studies.

Appendix A: Supplementary Tables and Figures

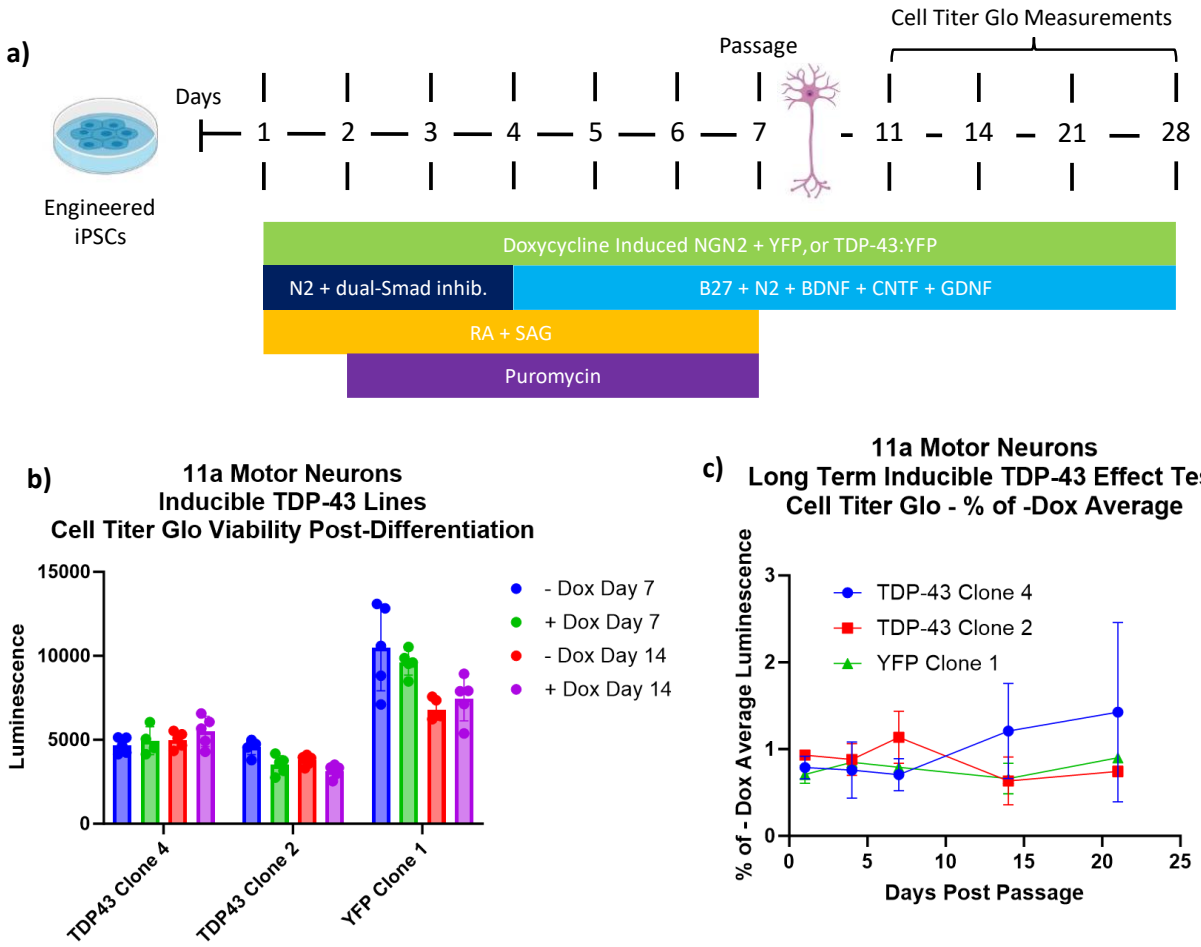

Supplementary Figure 2.1: Expression of inducible TDP-43 in motor neurons following LiMoNes differentiation does not indicate continued decrease in viability after passaging (a) Experimental Timeline **(b)** Luminescence data from Cell Titer Glo measurements at Day 7 post differentiation (Day 14 total) and Day 14 post differentiation (Day 21 total). While TDP-43:YFP expressing neurons do have lower viability compared to YFP only expressing neurons, this may be due to fewer cells that adhered or survived during the replating procedure. –Dox condition represents neurons where doxycycline was withdrawn after the passage and replating (removed at Day 2 Post differentiation, Day 9 total). Neurons in the +Dox condition were continually treated with 2µg/mL Doxycycline following the end of the core differentiation protocol (n = 5 biological replicates) **(c)** Alternative view of a similar cell titer glo assay to (b) with luminescence normalized to each condition's -Dox values at each timepoint. I observed that viability of TDP-43:YFP motor neurons does not decrease in the doxycycline treated condition compared to the doxycycline withdrawn condition over a span of 21 days post differentiation and passage (28 total days in culture) (n = 5 biological replicates).

a)

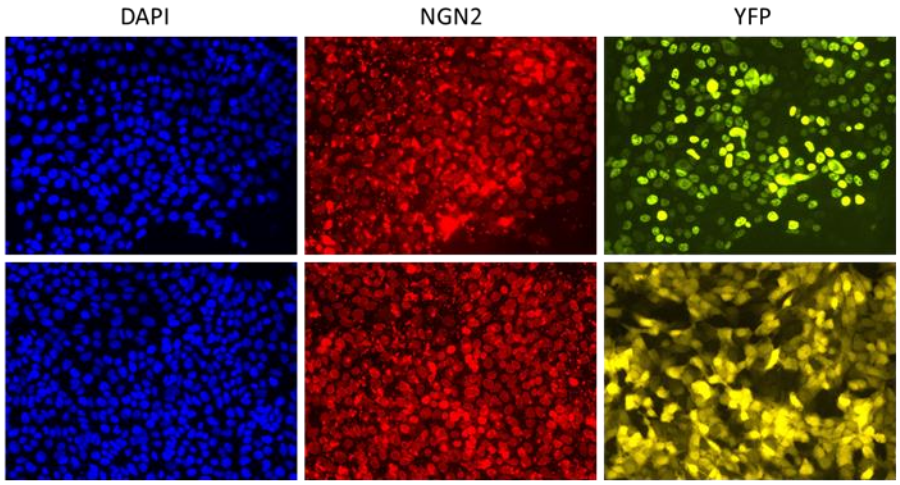

b)

Sample	Replicate	#DAPI+	#DAPI+, NGN2+	#DAPI+, NGN2+, YFP+	% Differentiable
TDP-43-YFP	1	332	299	247	74.4%
TDP-43-YFP	2	331	311	271	81.9%
TDP-43-YFP	3	366	343	277	75.7%
TDP-43-YFP	4	256	244	211	82.4%
				TDP-43-YFP Average	78.6%
YFP	1	464	436	266	57.3%
YFP	2	452	420	264	58.4%
YFP	3	476	451	270	56.7%
YFP	4	350	337	216	61.7%
				YFP Average	58.5%

Supplementary Figure 2.2: Analysis of differentiable cells in iPSC cultures transduced with NGN2 and inducible TDP-43:YFP or YFP shows that TDP-43 expressing cultures have similar, if not greater differentiation capacity than YFP cultures (a) Representative images of immunostained NGN2 infected iPSCs treated with 4µg/mL Doxycycline for 24 hours to activate inducible TDP-43:YFP or YFP and NGN2. **(b)** Hand-count analysis of select images tracking the total number of cells (DAPI), cells that co-stain positive for NGN2, and cells of that set that additionally express YFP from the inducible construct. Cells positive for both NGN2 and YFP were counted as differentiable. This preliminary analysis suggests that TDP-43:YFP iPSCs actually had higher propensity to differentiate than YFP only expressing iPSCs, cementing that the results of TDP-43 viability loss observed in the short-term differentiation assay are due to the biology, not a techical defect in transfection efficiency difference.

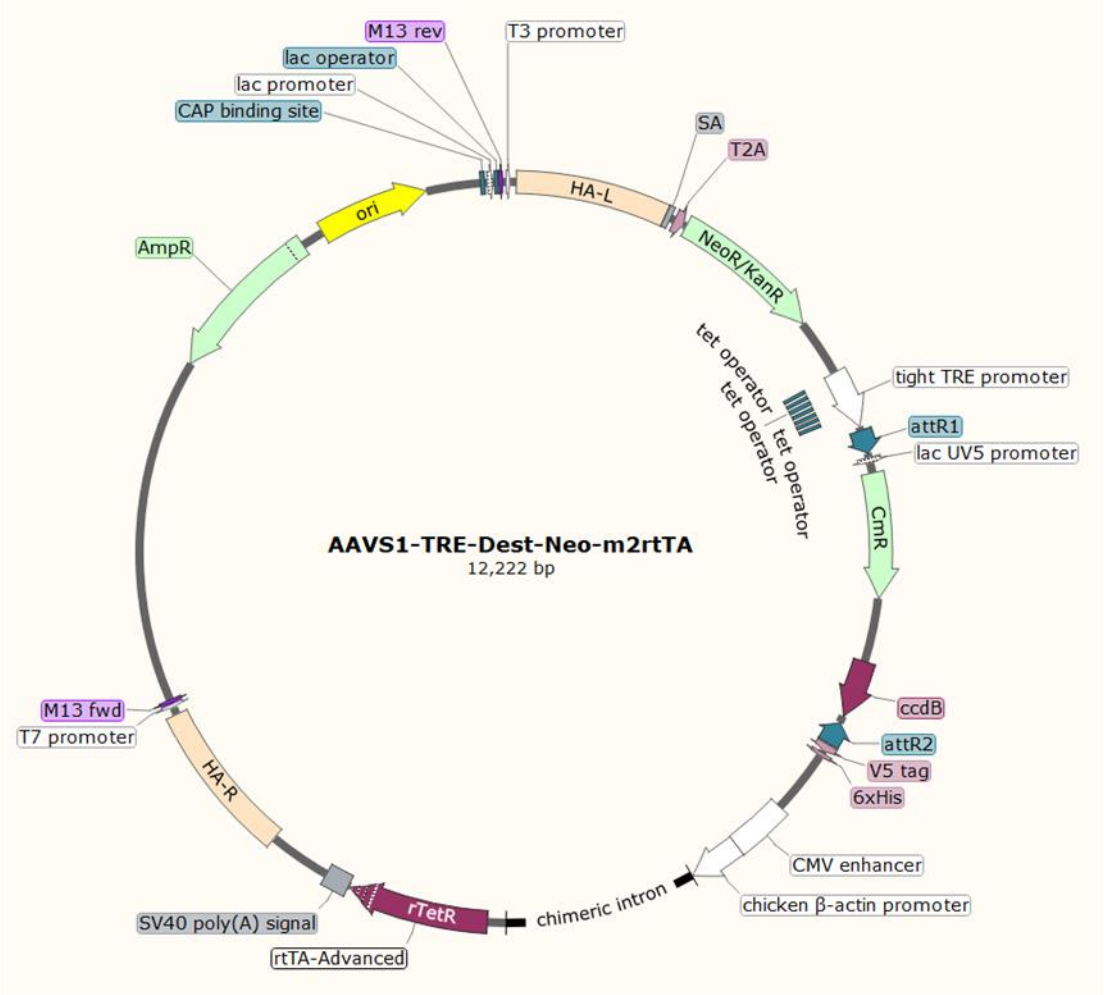

Supplementary Figure 2.3: AAVS1-TRE-Dest-Neo-m2rtTA Plasmid Vector Map. When applicable, YFP, TDP-43:YFP, or TDP-43ΔNLS:YFP were subcloned into the Gateway Cloning sites (between attR1/attR2). Samples marked as empty vector used this construct as presented here with no additional insert.

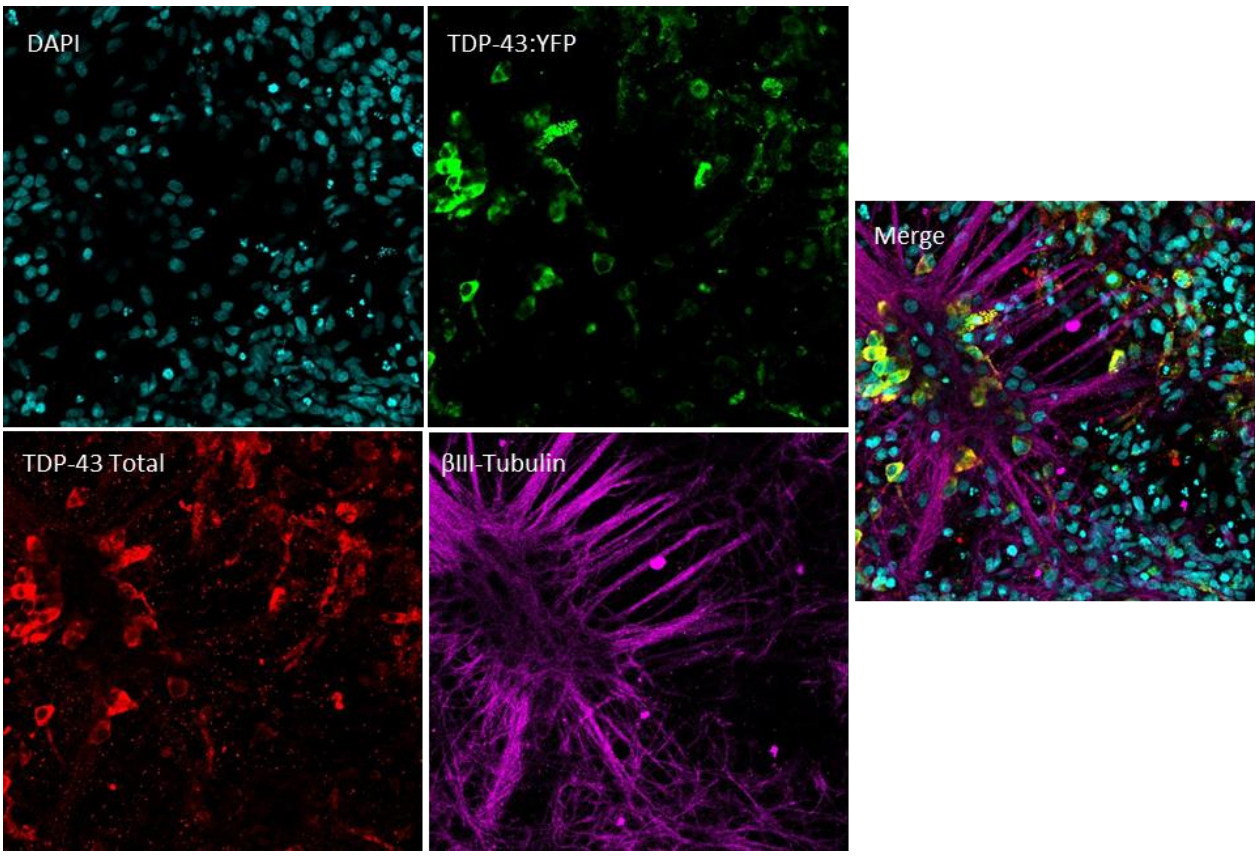

Supplementary Figure 2.4: Representative images of neurons infected with TDP-43ΔNLS lentivirus. Neurons were differentiated using the 'Dox' method outlined in Chapter 2.

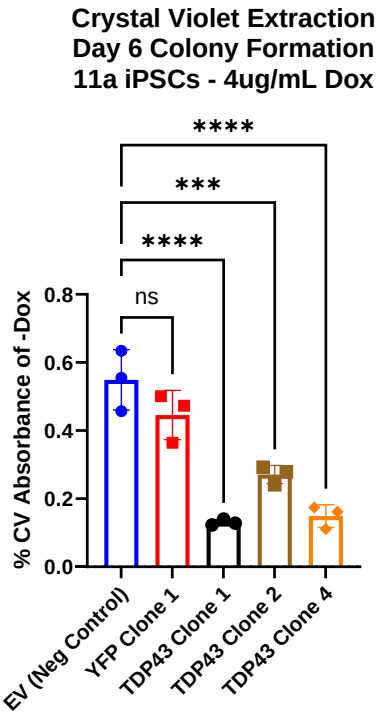

Supplementary Figure 2.5: Crystal Violent quantification of 6-day iPSC colony formation assay at 4µg/mL Doxycycline in lines harboring inducible TDP-43:YFP and YFP. Additional validation of TDP-43:YFP expression being sufficient to induce viability loss presented in Figure 2.2**.** Significance calculated using ANOVA with Dunnett's Multiple Comparisons test (*** = $p<0.001$; **** = $p<0.0001$) (n = 3 biological replicates)

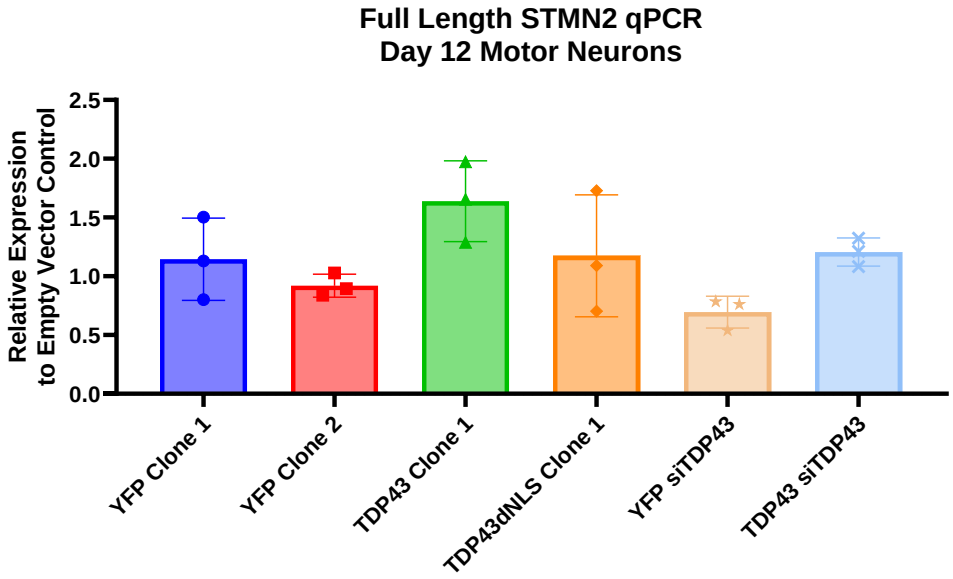

Supplementary Figure 3.1: Full length STMN2 expression does not change upon expression of TDP-43:YFP or TDP-43ΔNLS:YFP in motor neurons. Relative expression as measured by qRT-PCR compared to an Empty Vector (no transgene) control (n = 3 technical replicates).

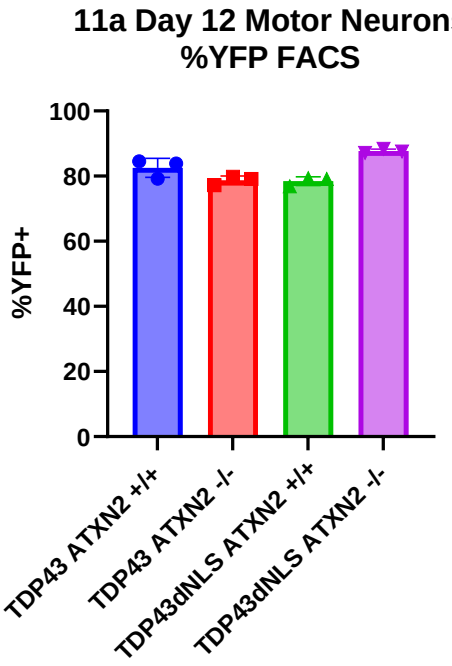

Supplementary Figure 3.2: Evaluation of YFP+ neuron levels by flow cytometry for RNAseq assay development shows cultures are 80% YFP+. As a result, neurons were not enriched for YFP+ cells before input into the RNAseq pipeline, which started with RNA harvest from neurons at this same timepoint (n = 3 biological replicates).

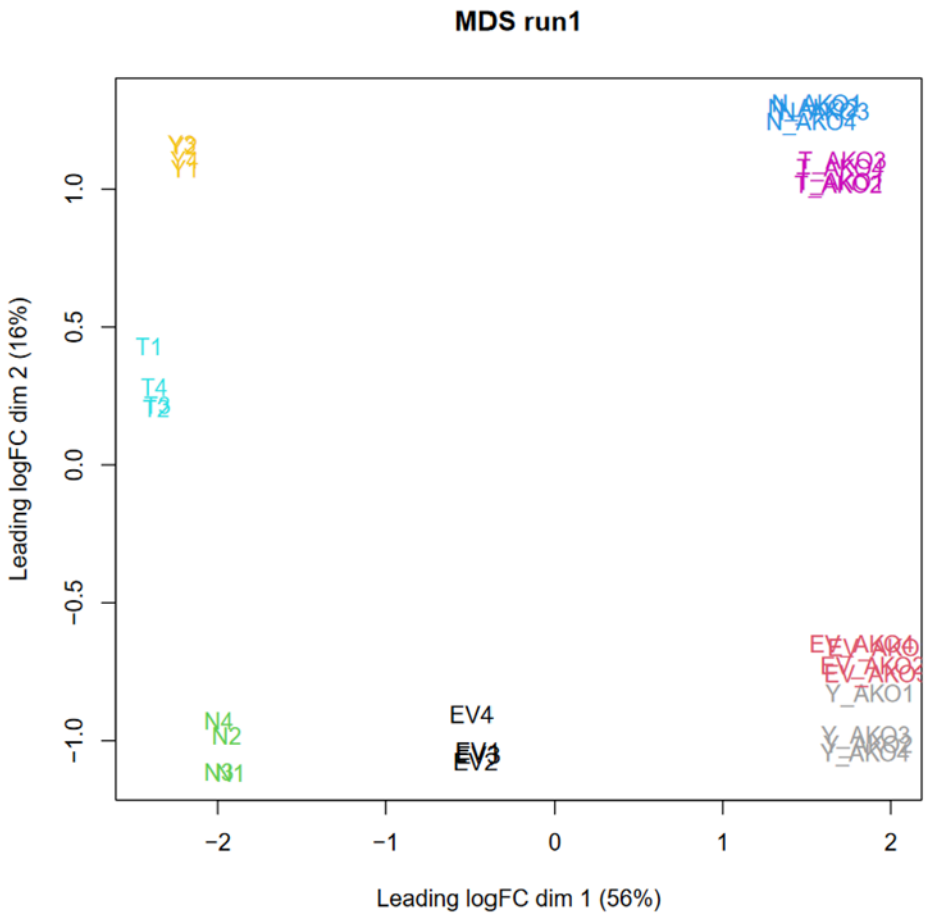

Supplementary Figure 3.3: Multidimensional scaling plot of RNA seq replicates shows good clustering of replicate samples. Generated using the top 1000 differentially expressed genes, which has been used as a standard in other sequencing papers (Klim et al. 2019). Replicate measures represent biological replicates — independent differentiations and independent RNA preps.

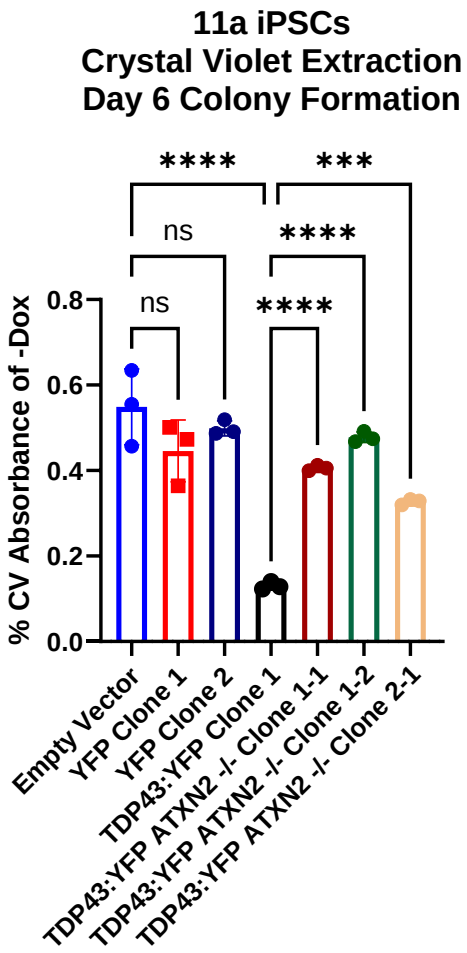

Supplementary Figure 4.1: Crystal Violent quantification of 6-day iPSC colony formation assay at 4µg/mL Doxycycline in lines harboring inducible TDP-43:YFP and YFP with ATXN2 knockout. Additional validation of TDP-43:YFP expression being sufficient to induce viability loss presented in Figure 2.2**.** Significance calculated using ANOVA with Dunnett's Multiple Comparisons test (*** = $p<0.001$; **** = $p<0.0001$) (n = 3 biological replicates).

Supplementary Table 3.1: TDP-43ΔNLS enriched transcripts in TDP-43 versus TDP-43ΔNLS comparison with Log2 Fold Change greater than 2. Because fold change is calculated as read counts of TDP-43 divided by TDP-43ΔNLS, TDP-43ΔNLS enriched transcripts have a negative fold change value.

Gene	Ensembl Transcript ID	Expression Fold Change
	ENSG00000290931	-7.06596675
PIWIL2	ENSG00000197181	-6.02402912
ZFP3	ENSG00000180787	-5.863808844
ZNF619	ENSG00000177873	-5.610268607
FAM66B	ENSG00000215374	-5.327304796
	ENSG00000286456	-4.669508787
H3P18	ENSG00000249620	-4.396041295
	ENSG00000289707	-4.090043775
ZNF572	ENSG00000180938	-4.048873287
BEX5	ENSG00000184515	-4.012485924
	ENSG00000286791	-3.975777112
C5orf63	ENSG00000164241	-3.905800634
MAGEA4	ENSG00000147381	-3.868469706
RBM46	ENSG00000151962	-3.855717357
TCEAL5	ENSG00000204065	-3.810043103
SSU72P4	ENSG00000283873	-3.719279936
	ENSG00000287460	-3.707696271
	ENSG00000278266	-3.609747388
ZNF300	ENSG00000145908	-3.416063716
	ENSG00000234710	-3.191852062
VSTM5	ENSG00000214376	-3.056435071
KCNE4	ENSG00000152049	-3.045060295
C2CD6	ENSG00000155754	-2.976733787
	ENSG00000240086	-2.962950752
	ENSG00000289217	-2.881245102
	ENSG00000213212	-2.84841129
TCHH	ENSG00000159450	-2.80688595
PWRN1	ENSG00000259905	-2.79252247
PWRN3	ENSG00000259905	-2.79252247
RGS11	ENSG00000076344	-2.776373872
	ENSG00000260848	-2.680950521
NAP1L6P	ENSG00000204118	-2.666547643
BCRP9	ENSG00000271287	-2.652658469
	ENSG00000290901	-2.651636523
NIPSNAP3B	ENSG00000165028	-2.602471811
	ENSG00000250467	-2.575250532
	ENSG00000284645	-2.558266026

Supplementary Table 3.1 (Continued)

SIM1	ENSG00000112246	-2.503034876
TF	ENSG00000091513	-2.483962454
FAM90A1	ENSG00000171847	-2.483952462
TLX1NB	ENSG00000236311	-2.483556876
PCDHGA8	ENSG00000253767	-2.460819434
WSCD2	ENSG00000075035	-2.387718733
DLEU1-AS1	ENSG00000186047	-2.385713667
DLEU7	ENSG00000186047	-2.385713667
SSU72P8	ENSG00000230268	-2.354516078
SYCE1	ENSG00000171772	-2.334333956
ZNF595	ENSG00000272602	-2.329336954
FOLH1	ENSG00000086205	-2.327384959
	ENSG00000259098	-2.324448355
LHFPL5	ENSG00000197753	-2.324381987
PRAMEF6	ENSG00000232423	-2.324373351
ANKRD26P3	ENSG00000237636	-2.32418442
DUXAP8	ENSG00000206195	-2.323592339
	ENSG00000254966	-2.312109157
GPRIN2	ENSG00000204175	-2.298178978
ARL9	ENSG00000196503	-2.298008943
	ENSG00000267784	-2.293626912
LOC100505715	ENSG00000267058	-2.249508922
KCNA3	ENSG00000177272	-2.246606733
	ENSG00000286123	-2.227036753
SLC26A8	ENSG00000112053	-2.21457446
KASH5	ENSG00000161609	-2.2121804
LINC00648	ENSG00000259129	-2.208651177
CCNP	ENSG00000105219	-2.200239901
SCN2B	ENSG00000149575	-2.193651652
CNGB1	ENSG00000070729	-2.192585133
	ENSG00000260918	-2.190846156
ZNF467	ENSG00000181444	-2.179104333
SCN1A	ENSG00000144285	-2.170525344
TCEAL2	ENSG00000184905	-2.165659609
SPDYE3	ENSG00000214300	-2.150975747
IPCEF1	ENSG00000074706	-2.146941467
LOC375196	ENSG00000269210	-2.139394049
	ENSG00000272734	-2.135675409
GLRA1	ENSG00000145888	-2.130746688
	ENSG00000262198	-2.12859979
KCNQ5	ENSG00000185760	-2.120787111
CHRNE	ENSG00000108556	-2.119897588

Supplementary Table 3.1 (Continued)

NAT16	ENSG00000167011	-2.118743812
MMEL1	ENSG00000142606	-2.118223172
C1QL4	ENSG00000186897	-2.102964904
	ENSG00000286613	-2.073168722
PCDHGB4	ENSG00000253953	-2.065667163
GPR139	ENSG00000180269	-2.062638354
LINC00682	ENSG00000245870	-2.061481672
CRH	ENSG00000147571	-2.061269514
HJV	ENSG00000168509	-2.058215959
TMEM229B	ENSG00000198133	-2.056829124
	ENSG00000283648	-2.048169341
LOC100420027	ENSG00000248185	-2.02278837
TRIM51BP	ENSG00000204455	-2.022651998
LOC105377177	ENSG00000286329	-2.019191273
GJB7	ENSG00000164411	-2.007585626
STYK1	ENSG00000060140	-2.003251101

Supplementary Table 3.2: TDP-43 enriched transcripts in TDP-43 versus TDP-43ΔNLS comparison with Log2 Fold Change greater than 2

Gene	Ensembl Transcript ID	Expression Fold Change
ZNF248	ENSG00000198105	10.23655513
ZNF879	ENSG00000234284	10.22421712
CHMP1B2P	ENSG00000278530	9.583132427
	ENSG00000249803	9.204300775
ZNF528-AS1	ENSG00000269834	8.092257787
CSAG3	ENSG00000268916	7.268253196
	ENSG00000232063	6.51697308
SLC6A13	ENSG00000010379	5.94937292
	ENSG00000290418	5.720047727
ZNF441	ENSG00000197044	5.597617742
NKAPL	ENSG00000189134	5.157121976
MIR4458HG	ENSG00000247516	4.964622573
FAR2P1	ENSG00000286058	4.943286343
KDM4F	ENSG00000255855	4.744383087
PCDHA2	ENSG00000204969	4.645404056
	ENSG00000242828	4.507214643
	ENSG00000258376	4.494004098
HNRNPCL3	ENSG00000277058	4.189192545
HAND1	ENSG00000113196	4.182924256
	ENSG00000279077	4.133886637
CLEC3B	ENSG00000163815	3.936055747
TRIM49C	ENSG00000204449	3.799424117
POTEF	ENSG00000196604	3.664707446
LINC01266	ENSG00000224957	3.63581661
C10orf71	ENSG00000177354	3.623616573
COL10A1	ENSG00000123500	3.622978262
ZNF354C	ENSG00000177932	3.603825969
NANOG	ENSG00000111704	3.594439932
BTLA	ENSG00000186265	3.510350543
C10orf99	ENSG00000188373	3.472509926
FAM151A	ENSG00000162391	3.464875547
PPIAP46	ENSG00000260266	3.40380936
	ENSG00000248663	3.38926957
GUCY2C	ENSG00000070019	3.375370052
	ENSG00000261226	3.333354999
ZNF439	ENSG00000171291	3.269048692
FAM90A27P	ENSG00000189348	3.265518022
PRAMEF12	ENSG00000116726	3.265160947
PRAMEF1	ENSG00000116721	3.265143379

Supplementary Table 3.2 (Continued)

TRIM53AP	ENSG00000225581	3.264492802
VWFP1	ENSG00000241717	3.262995513
	ENSG00000289508	3.11461282
THEMIS	ENSG00000172673	3.085673055
LOC101928475	ENSG00000232058	3.083258581
NLRP7	ENSG00000167634	3.04713812
SLPI	ENSG00000124107	3.046487348
ENG	ENSG00000106991	3.02763472
	ENSG00000283633	2.985562988
TBXT	ENSG00000164458	2.971567934
	ENSG00000279208	2.94677821
	ENSG00000289262	2.879114193
XKRX	ENSG00000182489	2.876783483
FGR	ENSG00000000938	2.87053204
LIM2	ENSG00000105370	2.868676081
ATP12A	ENSG00000075673	2.860503492
LYZ	ENSG00000090382	2.847581025
IFITM1	ENSG00000185885	2.830076123
VENTXP2	ENSG00000215037	2.797782046
WFDC21P	ENSG00000261040	2.789489761
MLKL	ENSG00000168404	2.789259875
PRB2	ENSG00000121335	2.77935356
TDGF1	ENSG00000241186	2.773522856
TFCP2L1	ENSG00000115112	2.772394658
F13A1	ENSG00000124491	2.767901052
DAPP1	ENSG00000070190	2.762794146
PRB4	ENSG00000230657	2.753232719
RAET1L	ENSG00000155918	2.737907862
	ENSG00000273416	2.734274703
	ENSG00000279718	2.721636695
ACTL8	ENSG00000117148	2.710797057
SIX2	ENSG00000170577	2.71026176
TAC3	ENSG00000166863	2.708474167
XIRP1	ENSG00000168334	2.681343607
ALOX15	ENSG00000161905	2.674074027
GPAT3	ENSG00000138678	2.6616356
PVALB	ENSG00000100362	2.639511853
	ENSG00000290397	2.628823466
TNFRSF8	ENSG00000120949	2.618705316
LINC01833	ENSG00000259439	2.612147167
ITGAM	ENSG00000169896	2.602263957
CEACAM5	ENSG00000105388	2.599642147

Supplementary Table 3.2 (Continued)

ACTG1P15	ENSG00000259904	2.598835304
TACSTD2	ENSG00000184292	2.594314189
MUC16	ENSG00000181143	2.587193746
GRHL2	ENSG00000083307	2.570597557
NMBR	ENSG00000135577	2.56574272
OLAH	ENSG00000152463	2.56121161
CP	ENSG00000047457	2.55467302
CD177	ENSG00000204936	2.551003499
GBP3	ENSG00000117226	2.547437562
PRB1	ENSG00000251655	2.534889835
PRB2	ENSG00000251655	2.534889835
C2orf66	ENSG00000187944	2.529647404
	ENSG00000249661	2.525021886
	ENSG00000287059	2.523793
LOC101927551	ENSG00000230922	2.51673399
FOLR1	ENSG00000110195	2.499041409
PRR15	ENSG00000176532	2.492454932
	ENSG00000289308	2.490471277
FAM107A	ENSG00000168309	2.484037345
FOSB	ENSG00000125740	2.481231558
	ENSG00000291309	2.468510193
LINC01036	ENSG00000230426	2.466192842
BACE2	ENSG00000182240	2.463838024
PAX9	ENSG00000198807	2.462242229
TRH	ENSG00000170893	2.46222724
	ENSG00000276791	2.458315884
ABHD12B	ENSG00000131969	2.457627595
APOL1	ENSG00000100342	2.453427027
RCSD1	ENSG00000198771	2.450473056
ZNF563	ENSG00000188868	2.444185933
UCP1	ENSG00000109424	2.437803929
PIK3R5	ENSG00000141506	2.435409188
SIX3	ENSG00000138083	2.433525117
SCGB3A2	ENSG00000164265	2.425618813
PMP22	ENSG00000109099	2.42558215
SLC7A11	ENSG00000151012	2.422429225
ZNF37A	ENSG00000075407	2.421423675
TRIM64B	ENSG00000189253	2.420342786
STARD8	ENSG00000130052	2.414721844
	ENSG00000285876	2.414479716
C3	ENSG00000125730	2.413088935
CD34	ENSG00000174059	2.413034251

Supplementary Table 3.2 (Continued)

LINC00839	ENSG00000185904	2.409959594
APLNR	ENSG00000134817	2.409299108
	ENSG00000250658	2.408551715
	ENSG00000248583	2.408164555
TRIM49B	ENSG00000182053	2.407777436
	ENSG00000249156	2.407406553
LOC101927815	ENSG00000254319	2.407120242
	ENSG00000250782	2.407092543
PRAMEF2	ENSG00000120952	2.407067066
CD52	ENSG00000169442	2.405151772
	ENSG00000286182	2.391796054
VAMP8	ENSG00000118640	2.390504841
STING1	ENSG00000184584	2.376047147
CYBRD1	ENSG00000071967	2.371368704
APOD	ENSG00000189058	2.370810847
LINC00624	ENSG00000278811	2.367902292
COL6A3	ENSG00000163359	2.364518966
	ENSG00000271984	2.359458698
ZNF442	ENSG00000198342	2.359247036
PLAC8	ENSG00000145287	2.358519884
TCF21	ENSG00000118526	2.355705481
TMPRSS4	ENSG00000137648	2.355437646
GSN	ENSG00000148180	2.354939909
IGFBP6	ENSG00000167779	2.348601719
FOXE1	ENSG00000178919	2.347533537
RAB38	ENSG00000123892	2.34739601
	ENSG00000254339	2.343923006
OLFML3	ENSG00000116774	2.343619109
TMEM37	ENSG00000171227	2.34269447
ROBO4	ENSG00000154133	2.33762119
TENT5B	ENSG00000158246	2.337054174
TRIM43	ENSG00000144015	2.335222179
RPS6KA2-IT1	ENSG00000232082	2.328326347
LOC105375166	ENSG00000237070	2.325559825
	ENSG00000272068	2.3241998
SLC51B	ENSG00000186198	2.31906
ZIC1	ENSG00000152977	2.312274324
SPINK1	ENSG00000164266	2.303929764
TEX14	ENSG00000121101	2.30319186
FRG2C	ENSG00000172969	2.295110617
KLK13	ENSG00000167759	2.294543635
HAL	ENSG00000084110	2.287969282

Supplementary Table 3.2 (Continued)

FLVCR2-AS1	ENSG00000224721	2.282880529
	ENSG00000276975	2.28106237
FBP1	ENSG00000165140	2.280699485
PLLP	ENSG00000102934	2.269997529
CSF1R	ENSG00000182578	2.26973055
FLI1	ENSG00000151702	2.269477184
IL23A	ENSG00000110944	2.259345625
KLRG2	ENSG00000188883	2.257557183
PCDHA3	ENSG00000255408	2.252655091
GJB1	ENSG00000169562	2.250953262
F3	ENSG00000117525	2.250706425
POF1B	ENSG00000124429	2.245915216
IGKC	ENSG00000211592	2.240155614
PCED1B	ENSG00000179715	2.235707524
PCDHB5	ENSG00000113209	2.229354539
CD109	ENSG00000156535	2.221325013
NT5E	ENSG00000135318	2.213426869
MYCT1	ENSG00000120279	2.213179844
COL15A1	ENSG00000204291	2.211548592
LINC00678	ENSG00000254934	2.211004057
	ENSG00000289122	2.209846108
HMOX1	ENSG00000100292	2.207702719
PDGFRL	ENSG00000104213	2.207069756
S1PR1	ENSG00000170989	2.203558793
RRAD	ENSG00000166592	2.202858082
PROSER2	ENSG00000148426	2.202564199
FLNB	ENSG00000136068	2.19463768
RASL12	ENSG00000103710	2.193898741
CA6	ENSG00000131686	2.192829783
PTPRB	ENSG00000127329	2.191358898
GCNT3	ENSG00000140297	2.190766854
CLIC5	ENSG00000112782	2.188225008
NMB	ENSG00000197696	2.182341906
	ENSG00000250284	2.181050876
C1QL2	ENSG00000144119	2.180794549
LOC391711	ENSG00000236941	2.178619976
CDX1	ENSG00000113722	2.174352407
MEOX1	ENSG00000005102	2.173162732
H3P21	ENSG00000250386	2.1673242
H3Y1	ENSG00000269466	2.165252291
GDPD2	ENSG00000130055	2.165040658
ATP10A	ENSG00000206190	2.158142225

Supplementary Table 3.2 (Continued)

DLX3	ENSG00000064195	2.155420228
	ENSG00000260364	2.150534681
RASSF6	ENSG00000169435	2.149070791
DUXB	ENSG00000282757	2.136447784
EXOC3L2	ENSG00000283632	2.133762629
EMP1	ENSG00000134531	2.133611268
CEACAM6	ENSG00000086548	2.130760731
TGM2	ENSG00000198959	2.130485003
LAMC2	ENSG00000058085	2.129930792
WFDC1	ENSG00000103175	2.122967738
ADCY4	ENSG00000129467	2.12275952
ABCG2	ENSG00000118777	2.122705089
MUC22	ENSG00000261272	2.121799265
DLK1	ENSG00000185559	2.11969022
LINC00520	ENSG00000258791	2.118215139
ADAP2	ENSG00000184060	2.112824168
MYO1G	ENSG00000136286	2.112138624
SLC37A2	ENSG00000134955	2.108378803
	ENSG00000289168	2.106712899
KLK10	ENSG00000129451	2.104808942
SPHK1	ENSG00000176170	2.101913
C10orf105	ENSG00000214688	2.101302904
NID2	ENSG00000087303	2.094100904
	ENSG00000231764	2.093805533
DSG1	ENSG00000134760	2.087268859
METTL7A	ENSG00000185432	2.079792579
LINC02582	ENSG00000261780	2.076818412
CTSV	ENSG00000136943	2.075378377
CTSH	ENSG00000103811	2.07319653
ADGRE5	ENSG00000123146	2.073154961
SDC4	ENSG00000124145	2.068277266
AFP	ENSG00000081051	2.066317483
TFAP2C	ENSG00000087510	2.065796903
TESC	ENSG00000088992	2.059387008
BDKRB2	ENSG00000168398	2.058038097
HLA-G	ENSG00000204632	2.055825103
PLAUR	ENSG00000011422	2.055320444
SNTB1	ENSG00000172164	2.054487008
CXCR1	ENSG00000163464	2.053109735
NIBAN1	ENSG00000135842	2.05024756
C2CD4A	ENSG00000198535	2.04648056
CHMP4C	ENSG00000164695	2.045319193

Supplementary Table 3.2 (Continued)

LBX2	ENSG00000179528	2.043922134
PTHLH	ENSG00000087494	2.043791684
CAPN6	ENSG00000077274	2.040015008
GALNT6	ENSG00000139629	2.038554974
C1S	ENSG00000182326	2.038362481
MT1E	ENSG00000169715	2.03771932
TMEM154	ENSG00000170006	2.035003676
CCDC69	ENSG00000198624	2.031677367
SLC7A4	ENSG00000099960	2.030827791
FIBCD1	ENSG00000130720	2.028806192
SH2D3A	ENSG00000125731	2.027950128
MED4-AS1	ENSG00000229111	2.021718415
CD9	ENSG00000010278	2.021125816
MT2A	ENSG00000125148	2.017847486
EXPH5	ENSG00000110723	2.009308354
S100A4	ENSG00000196154	2.008908344
SLC38A5	ENSG00000017483	2.005137538
TNFSF9	ENSG00000125657	2.004109756
PRDM1	ENSG00000057657	2.002947925
ANPEP	ENSG00000166825	2.002309337
GALNT5	ENSG00000136542	2.001737454
BNC1	ENSG00000169594	2.000723736
MMP9	ENSG00000100985	2.00037507

Supplementary Table 4.1: TDP-43, ATXN2 knockout enriched transcripts in TDP-43 overexpression ATXN2 intact versus knockout comparison with Log2 Fold Change greater than 2. Because fold change is calculated as read counts of ATXN2 intact divided by ATXN2 knockout, ATXN2 enriched transcripts have a negative fold change value.

Gene	Ensembl Transcript ID	Expression Fold Change
PEG3	ENSG00000198300	-15.3388254
CHCHD2	ENSG00000106153	-15.28961054
H3P18	ENSG00000249620	-14.53445105
H3Y2	ENSG00000268799	-14.30870528
TRIM53CP	ENSG00000254764	-14.02109493
	ENSG00000283776	-13.0293569
PRAMEF14	ENSG00000204481	-12.86992215
LEUTX	ENSG00000213921	-12.80794948
CTSF	ENSG00000174080	-12.73309029
ZNF595	ENSG00000272602	-12.60998524
FOLH1	ENSG00000086205	-12.48097193
RFPL4A	ENSG00000223638	-12.35067969
	ENSG00000249156	-12.34517621
PRAMEF8	ENSG00000182330	-12.28800988
TRIM49B	ENSG00000182053	-12.12514845
TRIM48	ENSG00000150244	-12.03696057
H3Y1	ENSG00000269466	-11.80049967
PRAMEF13	ENSG00000279169	-11.7607567
	ENSG00000257951	-11.70999556
	ENSG00000219061	-11.59324242
PRAMEF15	ENSG00000204501	-11.52254068
MBD3L3	ENSG00000182315	-11.41035677
MBD3L2	ENSG00000230522	-11.36518252
PRAMEF27	ENSG00000274764	-11.32019622
PRAMEF28P	ENSG00000274178	-11.28617402
ZNF662	ENSG00000182983	-11.27776693
PRAMEF9	ENSG00000204505	-11.22827545
	ENSG00000258732	-11.20915822
MBD3L2B	ENSG00000196589	-11.20092186
RFPL4AL1	ENSG00000229292	-11.17822504
	ENSG00000284484	-11.1604116
PRAMEF4	ENSG00000243073	-11.07585401
	ENSG00000256779	-10.99351389
UBTFL7	ENSG00000229361	-10.98750995
PRAMEF2	ENSG00000120952	-10.98064359
PRAMEF20	ENSG00000204478	-10.97556521
	ENSG00000250782	-10.86693761

Supplementary Table 4.1 (Continued)

HNRNPCL2	ENSG00000275774	-10.80804557
PRAMEF12	ENSG00000116726	-10.74565377
PRAMEF7	ENSG00000204510	-10.69991764
	ENSG00000247765	-10.63837579
ZSCAN1	ENSG00000152467	-10.49327243
H3P21	ENSG00000250386	-10.46669339
PRAMEF6	ENSG00000232423	-10.31438329
TRIM49	ENSG00000168930	-10.28934488
DDX43	ENSG00000080007	-10.23230633
ZSCAN5DP	ENSG00000267908	-10.21599774
PRAMEF11	ENSG00000239810	-10.14432043
	ENSG00000255366	-10.02457421
SSU72P4	ENSG00000283873	-9.966095047
PRAMEF1	ENSG00000116721	-9.726682892
PNPLA4	ENSG00000006757	-9.709164827
RFPL4B	ENSG00000251258	-9.664523741
PRAMEF33	ENSG00000237700	-9.660354638
FAM90A27P	ENSG00000189348	-9.586322537
TRIM53AP	ENSG00000225581	-9.57078831
TRIM51CP	ENSG00000249910	-9.554853956
	ENSG00000166013	-9.549974472
TRIM49C	ENSG00000204449	-9.53817886
LINC02027	ENSG00000243694	-9.527610369
	ENSG00000257230	-9.356410018
RBM46	ENSG00000151962	-9.341617086
TRIM51	ENSG00000124900	-9.321117299
CSNKA2IP	ENSG00000283434	-9.305358193
SLC34A2	ENSG00000157765	-9.215156997
	ENSG00000283740	-9.164272701
ZFP3	ENSG00000180787	-9.15577545
PRAMEF10	ENSG00000187545	-9.104132417
	ENSG00000260409	-9.084576451
DUXA	ENSG00000258873	-9.020930844
	ENSG00000230080	-8.995546438
ANKRD26P3	ENSG00000237636	-8.927654694
ZNF835	ENSG00000127903	-8.908111751
PRAMEF5	ENSG00000270601	-8.892373719
ZSCAN4	ENSG00000180532	-8.758251834
FOXO1B	ENSG00000214295	-8.749794713
	ENSG00000144188	-8.679768118
SYCE1	ENSG00000171772	-8.613812583
LINC02899	ENSG00000248874	-8.4526871

Supplementary Table 4.1 (Continued)

SSU72P8	ENSG00000230268	-8.412308902
LINC02050	ENSG00000242781	-8.267730106
ZNF439	ENSG00000171291	-8.238665189
	ENSG00000289361	-8.202310101
BHMT2	ENSG00000132840	-8.182463645
ZNF705A	ENSG00000196946	-8.086413311
TRIM43B	ENSG00000144010	-8.028083547
TPRX1	ENSG00000178928	-7.970664573
LINC00839	ENSG00000185904	-7.963178835
	ENSG00000269118	-7.861422125
	ENSG00000290588	-7.78336248
	ENSG00000291126	-7.72290549
	ENSG00000254348	-7.720995168
TRIM64B	ENSG00000189253	-7.670605665
KDM4F	ENSG00000255855	-7.652898085
ZXDA	ENSG00000198205	-7.604016238
TRIM43	ENSG00000144015	-7.581580036
	ENSG00000272913	-7.564020228
KLF18	ENSG00000283039	-7.439234746
	ENSG00000234710	-7.388861441
MAGEA3	ENSG00000221867	-7.35760191
SSU72P3	ENSG00000284546	-7.345581607
CYP2E1	ENSG00000130649	-7.301837542
	ENSG00000290418	-7.25816363
	ENSG00000272983	-7.126700277
SSU72P2	ENSG00000284306	-7.033709308
	ENSG00000283633	-7.020580669
ZNF441	ENSG00000197044	-7.017563757
LINC01111	ENSG00000254300	-7.00039187
	ENSG00000289707	-6.846864653
	ENSG00000250658	-6.820784814
TC2N	ENSG00000165929	-6.773609221
RFPL1	ENSG00000128250	-6.761340198
LINC02714	ENSG00000251226	-6.722813526
SSU72P7	ENSG00000284438	-6.624516867
ZNF578	ENSG00000258405	-6.614798539
	ENSG00000261127	-6.540060837
SSU72P5	ENSG00000284018	-6.457280084
FRG2C	ENSG00000172969	-6.443997968
CPHXL	ENSG00000283755	-6.362523697
ZNF560	ENSG00000198028	-6.336955234
	ENSG00000290376	-6.333209324

Supplementary Table 4.1 (Continued)

CCNA1	ENSG00000133101	-6.297537661
	ENSG00000261200	-6.237005505
	ENSG00000286791	-6.181113357
	ENSG00000287352	-6.158483998
ZNF37A	ENSG00000075407	-6.069508027
	ENSG00000290461	-6.009573774
LOC391711	ENSG00000236941	-5.905154828
HNRNPCL3	ENSG00000277058	-5.84344567
TRIM51BP	ENSG00000204455	-5.815089831
ZSCAN5C	ENSG00000204532	-5.747461109
FAM90A1	ENSG00000171847	-5.720707572
C5orf63	ENSG00000164241	-5.689994905
KDM4E	ENSG00000235268	-5.617311608
PIWIL2	ENSG00000197181	-5.563309731
	ENSG00000285876	-5.563124963
	ENSG00000237194	-5.549560985
RFPL2	ENSG00000128253	-5.531416269
VWFP1	ENSG00000241717	-5.50227262
ZNF572	ENSG00000180938	-5.50150599
NKAPL	ENSG00000189134	-5.438825053
HNRNPCL1	ENSG00000179172	-5.405485439
SCIN	ENSG00000006747	-5.358838533
	ENSG00000291264	-5.345295551
ZNF528-AS1	ENSG00000269834	-5.33836759
ZNF619	ENSG00000177873	-5.328633776
LOC105377177	ENSG00000286329	-5.196367334
MIR4458HG	ENSG00000247516	-5.149549046
LOC101927815	ENSG00000254319	-5.126176943
	ENSG00000291101	-5.082745381
ALPG	ENSG00000163286	-4.970847361
	ENSG00000287592	-4.941820177
TBX1	ENSG00000184058	-4.934175332
	ENSG00000278266	-4.902900799
PCDHA1	ENSG00000204970	-4.85872189
BCRP9	ENSG00000271287	-4.78511829
LOC102723655	ENSG00000205456	-4.772667193
LOC102723713	ENSG00000205456	-4.772667193
TP53TG3D	ENSG00000205456	-4.772667193
TP53TG3E	ENSG00000205456	-4.772667193
TP53TG3F	ENSG00000205456	-4.772667193
HJV	ENSG00000168509	-4.767371041
DPPA3	ENSG00000187569	-4.72789058

Supplementary Table 4.1 (Continued)

	ENSG00000290414	-4.710846898
FAM66B	ENSG00000215374	-4.695792201
PCDHA3	ENSG00000255408	-4.684092765
LINC02466	ENSG00000246876	-4.607416671
LOC375196	ENSG00000269210	-4.578897169
	ENSG00000287460	-4.509342262
ALPP	ENSG00000163283	-4.506981385
TCHH	ENSG00000159450	-4.495582159
	ENSG00000290931	-4.404828554
	ENSG00000233058	-4.336132498
PCDHGA11	ENSG00000253873	-4.16458784
	ENSG00000287996	-4.119188668
PCDHGA3	ENSG00000254245	-4.071047079
	ENSG00000242828	-4.069991254
C2CD6	ENSG00000155754	-4.047932717
URB1-AS1	ENSG00000256073	-4.013757107
SLC30A8	ENSG00000164756	-4.012605355
	ENSG00000250874	-3.980219321
PITX1	ENSG00000069011	-3.952399536
	ENSG00000258376	-3.946062146
CHRNE	ENSG00000108556	-3.923278211
	ENSG00000291242	-3.907477759
	ENSG00000290895	-3.892262764
COX4I2	ENSG00000131055	-3.882643884
TLX1	ENSG00000107807	-3.870623937
	ENSG00000198555	-3.793289242
	ENSG00000283648	-3.777005638
SLC39A12	ENSG00000148482	-3.766964142
FLG	ENSG00000143631	-3.748710565
TYW3	ENSG00000162623	-3.740790498
TLX1NB	ENSG00000236311	-3.727382549
LINC00648	ENSG00000259129	-3.709571936
HSPA2	ENSG00000126803	-3.709137645
	ENSG00000289217	-3.622206426
	ENSG00000286123	-3.579344259
ZNF300	ENSG00000145908	-3.564890427
PCDHGA6	ENSG00000253731	-3.558678549
	ENSG00000290894	-3.545709913
	ENSG00000260302	-3.54163388
	ENSG00000288856	-3.531007127
ZNF491	ENSG00000177599	-3.526617629
PCDHGB5	ENSG00000276547	-3.480281492

Supplementary Table 4.1 (Continued)

	ENSG00000237161	-3.477608955
NLRP11	ENSG00000179873	-3.431808435
CIDEB	ENSG00000136305	-3.396403265
PCDHA2	ENSG00000204969	-3.348739635
	ENSG00000282906	-3.346134462
CCL28	ENSG00000151882	-3.343940733
MAGEA4	ENSG00000147381	-3.273876405
	ENSG00000282995	-3.259397777
	ENSG00000233928	-3.257438256
	ENSG00000276975	-3.196112773
ZNF528	ENSG00000167555	-3.185299658
ITGBL1	ENSG00000198542	-3.166180743
	ENSG00000253706	-3.137939343
ZNF440	ENSG00000171295	-3.129643165
PCDHA5	ENSG00000204965	-3.095769514
HOXC6	ENSG00000197757	-3.095519375
	ENSG00000226816	-3.084323385
	ENSG00000270112	-3.070336634
FLG-AS1	ENSG00000237975	-3.068791729
POU4F3	ENSG00000091010	-3.067237005
LINC01602	ENSG00000205293	-3.030948135
KL	ENSG00000133116	-3.028222008
ZIC3	ENSG00000156925	-2.991000986
ZNF354C	ENSG00000177932	-2.989374204
ZBED6CL	ENSG00000188707	-2.964895552
ZIM2-AS1	ENSG00000286125	-2.959048895
DUXB	ENSG00000282757	-2.947084869
	ENSG00000254044	-2.931530387
LINC01748	ENSG00000226476	-2.890496684
	ENSG00000253853	-2.866274362
MT1F	ENSG00000198417	-2.860123268
ATP2B3	ENSG00000067842	-2.848593244
C1QL4	ENSG00000186897	-2.829950169
ZNF442	ENSG00000198342	-2.829942924
LINC01619	ENSG00000257242	-2.829080361
SRPK3	ENSG00000184343	-2.810402301
	ENSG00000227012	-2.774952696
	ENSG00000290555	-2.774820079
CSF1R	ENSG00000182578	-2.766265815
CACNG5	ENSG00000075429	-2.762489345
REC8	ENSG00000100918	-2.747359083
PCDHB5	ENSG00000113209	-2.727971743

Supplementary Table 4.1 (Continued)

STYK1	ENSG00000060140	-2.717631462
LINC01630	ENSG00000227115	-2.714539264
	ENSG00000287630	-2.650105742
HMX1	ENSG00000215612	-2.640727956
	ENSG00000284645	-2.635783513
	ENSG00000250131	-2.610291891
BEX5	ENSG00000184515	-2.607080326
LINC01807	ENSG00000232023	-2.604653754
	ENSG00000287069	-2.600003681
ZNF506	ENSG00000081665	-2.586441197
	ENSG00000213212	-2.58350103
LRRC61	ENSG00000127399	-2.582600393
SNAI1	ENSG00000124216	-2.556361198
ZNF69	ENSG00000198429	-2.547489003
TEX41	ENSG00000226674	-2.545536084
	ENSG00000290901	-2.54440901
PAX8-AS1	ENSG00000189223	-2.529647627
TAF7L	ENSG00000102387	-2.523236853
	ENSG00000248663	-2.51510892
	ENSG00000267481	-2.508808255
IRX4	ENSG00000113430	-2.508167995
GRIN1	ENSG00000176884	-2.497051984
	ENSG00000249413	-2.483009757
KIAA0319	ENSG00000137261	-2.479662269
	ENSG00000290319	-2.475346561
PNP	ENSG00000198805	-2.471947404
GATA5	ENSG00000130700	-2.47043708
TMEM273	ENSG00000204161	-2.454263111
	ENSG00000290114	-2.45354269
	ENSG00000280776	-2.441251558
PALM3	ENSG00000187867	-2.433548875
DUXAP8	ENSG00000206195	-2.430690664
COX7A1	ENSG00000161281	-2.403460462
LOC728485	ENSG00000267260	-2.401155748
ZNF467	ENSG00000181444	-2.397189346
PCDHA13	ENSG00000239389	-2.396998114
ZNF296	ENSG00000170684	-2.379424212
INHBE	ENSG00000139269	-2.373471018
ZNF763	ENSG00000197054	-2.370386145
	ENSG00000250790	-2.339231212
	ENSG00000258998	-2.339020451
FEV	ENSG00000163497	-2.336822122

Supplementary Table 4.1 (Continued)

ZNF563	ENSG00000188868	-2.317126652
BCYRN1	ENSG00000236824	-2.310593807
TPBGL	ENSG00000261594	-2.305392861
SIX1	ENSG00000126778	-2.283823049
UGT3A1	ENSG00000145626	-2.26628961
ZNF44	ENSG00000197857	-2.251947457
KCNA1	ENSG00000111262	-2.244586129
ZNF799	ENSG00000196466	-2.242561008
	ENSG00000279511	-2.239199989
FOXF2	ENSG00000137273	-2.234695824
	ENSG00000260848	-2.2219794
PRDM16-DT	ENSG00000177133	-2.214417095
	ENSG00000228158	-2.198104177
	ENSG00000228709	-2.179565764
REM1	ENSG00000088320	-2.165523323
LOC112267871	ENSG00000228549	-2.158115106
	ENSG00000255136	-2.150531788
RCN3	ENSG00000142552	-2.149725353
PCDHGA1	ENSG00000204956	-2.148917831
PCDHGA7	ENSG00000253537	-2.14657013
FAM24B	ENSG00000213185	-2.135091578
ZNF433-AS1	ENSG00000219665	-2.123134728
BCL11B	ENSG00000127152	-2.089056318
AGPAT2	ENSG00000169692	-2.085914902
CLDN5	ENSG00000184113	-2.084514604
	ENSG00000267336	-2.083440424
LINC01694	ENSG00000233922	-2.071277402
GADD45B	ENSG00000099860	-2.06924692
C17orf107	ENSG00000205710	-2.068277461
EN2	ENSG00000164778	-2.068216293
	ENSG00000237713	-2.044335932
FOS	ENSG00000170345	-2.038344355
RUBCNL	ENSG00000102445	-2.038006572
PDZD7	ENSG00000186862	-2.023971736
	ENSG00000226070	-2.01833553
TUBB8B	ENSG00000173213	-2.014774511
	ENSG00000228334	-2.00333266

Supplementary Table 4.2: TDP-43, ATXN2 intact enriched transcripts in TDP-43 overexpression ATXN2 intact versus knockout comparison with Log2 Fold Change greater than 2.

Gene	Ensembl Transcript ID	Expression Fold Change
RPS4Y1	ENSG00000129824	13.06062531
MTLN	ENSG00000175701	10.27083389
	ENSG00000249803	9.204300775
NKX6-2	ENSG00000148826	6.013948243
LOC101928475	ENSG00000232058	5.184789426
	ENSG00000281961	5.072836521
VSX2	ENSG00000119614	4.792190528
OTX2	ENSG00000165588	4.389235656
CSAG3	ENSG00000268916	4.365959051
TFAP2D	ENSG00000008197	4.343497014
GALP	ENSG00000197487	4.274540401
BTLA	ENSG00000186265	4.234032317
LINC02577	ENSG00000228742	4.093037566
TXNRD2	ENSG00000184470	4.042705597
PAX3	ENSG00000135903	3.997892915
COMT	ENSG00000093010	3.940442679
ACTL8	ENSG00000117148	3.734846054
CXCR1	ENSG00000163464	3.592926162
C10orf99	ENSG00000188373	3.504064718
NPSR1	ENSG00000187258	3.481435659
LHX9	ENSG00000143355	3.47671466
CYP26C1	ENSG00000187553	3.460133736
GCNT3	ENSG00000140297	3.452493009
FBP1	ENSG00000165140	3.448035663
CXCL13	ENSG00000156234	3.432372429
ADIPOQ	ENSG00000181092	3.392419007
NALCN-AS1	ENSG00000233009	3.338258969
ITGAM	ENSG00000169896	3.316717196
PARVG	ENSG00000138964	3.280462427
KCNJ10	ENSG00000177807	3.271639098
ARGFX	ENSG00000186103	3.199094548
CLEC4E	ENSG00000166523	3.179610558
	ENSG00000289308	3.123054343
ATP12A	ENSG00000075673	3.093164993
RSPO3	ENSG00000146374	3.08539729
FUT3	ENSG00000171124	3.075430585
APELA	ENSG00000248329	3.075044159
LINC01992	ENSG00000260019	3.065955758

Supplementary Table 4.2 (Continued)

KCNE5	ENSG00000176076	3.064105836
SLC22A2	ENSG00000112499	3.044876722
ALDH1A2	ENSG00000128918	3.042165848
F13A1	ENSG00000124491	3.021219022
CTXND1	ENSG00000259417	3.013729307
PRLR	ENSG00000113494	3.00722757
SMIM43	ENSG00000164112	3.006853177
	ENSG00000250027	2.997101393
HLA-DQB1	ENSG00000179344	2.993530903
VCAM1	ENSG00000162692	2.961633442
RPS2P32	ENSG00000232818	2.957198022
	ENSG00000255860	2.957005336
LINC00545	ENSG00000236094	2.940887368
OTP	ENSG00000171540	2.939480148
NANOG	ENSG00000111704	2.931011447
PRND	ENSG00000171864	2.882666024
GUCY2C	ENSG00000070019	2.881736246
LOC100420587	ENSG00000283403	2.875633402
LINC00678	ENSG00000254934	2.868325811
FLVCR2-AS1	ENSG00000224721	2.860242704
LOC284930	ENSG00000224271	2.859167582
	ENSG00000291309	2.8479055
CMKLR2	ENSG00000183671	2.830021371
POU2F3	ENSG00000137709	2.827271394
LIM2	ENSG00000105370	2.821039581
NMBR	ENSG00000135577	2.807141841
NOS2	ENSG00000007171	2.806639317
FAM107A	ENSG00000168309	2.796925188
NLRP7	ENSG00000167634	2.765069106
PIK3R5	ENSG00000141506	2.763954262
MYH6	ENSG00000197616	2.733934848
DMRTA2	ENSG00000142700	2.724246793
TFAP2B	ENSG00000008196	2.713624354
B4GALNT2	ENSG00000167080	2.683159894
MUC16	ENSG00000181143	2.671942013
LRTM1	ENSG00000144771	2.649185399
MBNL3	ENSG00000076770	2.643752387
	ENSG00000289894	2.641168536
RNASE1	ENSG00000129538	2.632337975
FOXN4	ENSG00000139445	2.630771996
CA6	ENSG00000131686	2.626823222
HTR1D	ENSG00000179546	2.603324245

Supplementary Table 4.2 (Continued)

ITLN1	ENSG00000179914	2.602137497
CLC	ENSG00000105205	2.597139962
LGALS9	ENSG00000168961	2.593069491
PDE7B	ENSG00000171408	2.590033599
PVALB	ENSG00000100362	2.580419493
ZDBF2	ENSG00000204186	2.576504592
LCK	ENSG00000182866	2.549082416
CNTNAP4	ENSG00000152910	2.543268521
MIR4432HG	ENSG00000228590	2.534818512
FGFBP1	ENSG00000137440	2.53393516
	ENSG00000250284	2.530098753
	ENSG00000228863	2.527471762
TRPC7	ENSG00000069018	2.520377402
CDX1	ENSG00000113722	2.519479637
DLEC1	ENSG00000008226	2.510777835
PLA2G2A	ENSG00000188257	2.499012736
PLP1	ENSG00000123560	2.496275458
	ENSG00000289508	2.490989379
CILP2	ENSG00000160161	2.487456808
EFCC1	ENSG00000114654	2.484796576
C3	ENSG00000125730	2.475583353
SPN	ENSG00000197471	2.472549205
LINC01559	ENSG00000180861	2.470745715
	ENSG00000285939	2.451842897
HCAR2	ENSG00000182782	2.44845236
TACR3	ENSG00000169836	2.447160931
LINC01374	ENSG00000280560	2.446638369
TRIM10	ENSG00000204613	2.443704843
GPR160	ENSG00000173890	2.438034538
MED4-AS1	ENSG00000229111	2.415889102
LGR6	ENSG00000133067	2.412081033
HLA-F	ENSG00000204642	2.409429081
TRIM61	ENSG00000183439	2.4053441
GDPD2	ENSG00000130055	2.400925997
	ENSG00000289850	2.398970597
	ENSG00000230836	2.387970964
VENTXP2	ENSG00000215037	2.384998907
LYZ	ENSG00000090382	2.380623588
APOL4	ENSG00000100336	2.373361718
IL12B	ENSG00000113302	2.366451094
DSG1	ENSG00000134760	2.359005361
PRB4	ENSG00000230657	2.354596921

Supplementary Table 4.2 (Continued)

CLDN19	ENSG00000164007	2.346727437
APLNR	ENSG00000134817	2.33607704
	ENSG00000229271	2.331841879
	ENSG00000229060	2.330257765
KLRG2	ENSG00000188883	2.329061554
CHI3L2	ENSG00000064886	2.324692435
TTYH1	ENSG00000167614	2.32320098
PRKCB	ENSG00000166501	2.318659077
	ENSG00000229108	2.297307731
DAZL	ENSG00000092345	2.294973425
	ENSG00000260364	2.294821323
SLITRK2	ENSG00000185985	2.290556412
RNF128	ENSG00000133135	2.290249312
GAU1	ENSG00000255474	2.286376394
	ENSG00000287059	2.269776946
ARHGEF15	ENSG00000198844	2.268417752
	ENSG00000227838	2.265312512
INSYN2B	ENSG00000204767	2.261578032
PIK3AP1	ENSG00000155629	2.257170471
TFCP2L1	ENSG00000115112	2.254690825
TRPC5	ENSG00000072315	2.252696881
L1TD1	ENSG00000240563	2.245094307
PLAC8	ENSG00000145287	2.243929959
HNRNPA1P21	ENSG00000228168	2.243290544
GPX2	ENSG00000176153	2.233816478
EREG	ENSG00000124882	2.229541831
LOC105375166	ENSG00000237070	2.224754317
HAL	ENSG00000084110	2.224488609
HSPA12B	ENSG00000132622	2.222603797
COL23A1	ENSG00000050767	2.21824819
CD177	ENSG00000204936	2.218206887
HLA-DRB5	ENSG00000198502	2.216919298
WDR11-DT	ENSG00000227165	2.212464231
SLC52A3	ENSG00000101276	2.212102385
HVCN1	ENSG00000122986	2.201565993
ABI3	ENSG00000108798	2.199000436
ADAMTS4	ENSG00000158859	2.196338196
CNMD	ENSG00000136110	2.193294946
NXPH2	ENSG00000144227	2.187105296
CCR8	ENSG00000179934	2.18036262
NOL4	ENSG00000101746	2.179691404
UCP1	ENSG00000109424	2.176236599

Supplementary Table 4.2 (Continued)

SLC6A20	ENSG00000163817	2.170939421
C2orf16	ENSG00000221843	2.166770576
LPAR4	ENSG00000147145	2.153534727
CDX4	ENSG00000131264	2.153223538
GJB1	ENSG00000169562	2.152806484
DBX1	ENSG00000109851	2.152240113
SLC13A5	ENSG00000141485	2.151985548
CTNNA3	ENSG00000183230	2.15072035
FAM20A	ENSG00000108950	2.147537122
LINC00624	ENSG00000278811	2.147163237
CRB1	ENSG00000134376	2.143692174
TDGF1	ENSG00000241186	2.143395179
GLP1R	ENSG00000112164	2.130567315
	ENSG00000287355	2.126334622
MX1	ENSG00000157601	2.122936612
SCGB3A2	ENSG00000164265	2.119229952
INSM2	ENSG00000168348	2.105641272
SLC6A5	ENSG00000165970	2.105176819
LINC02192	ENSG00000261325	2.105039328
	ENSG00000233290	2.103758003
XKRX	ENSG00000182489	2.099481037
PPP1R3G	ENSG00000219607	2.095469533
	ENSG00000234261	2.089942489
TEK	ENSG00000120156	2.088848125
TM4SF19	ENSG00000145107	2.084851903
NID2	ENSG00000087303	2.084097692
THEMIS	ENSG00000172673	2.079176475
	ENSG00000287784	2.076098295
CRYBG1	ENSG00000112297	2.074532484
B3GALT5	ENSG00000183778	2.067054874
SLFN13	ENSG00000154760	2.061436644
	ENSG00000248588	2.050183935
TRPC6	ENSG00000137672	2.049900435
KLF8	ENSG00000102349	2.047595544
BEST2	ENSG00000039987	2.03762996
SCARA5	ENSG00000168079	2.035759927
BDKRB2	ENSG00000168398	2.033704888
	ENSG00000249790	2.03046698
SLC7A4	ENSG00000099960	2.03044204
	ENSG00000244650	2.027127654
PKD1L1	ENSG00000158683	2.02644532
LUZP2	ENSG00000187398	2.025806842

Supplementary Table 4.2 (Continued)

PRB1	ENSG00000251655	2.022457716
PRB2	ENSG00000251655	2.022457716
	ENSG00000250796	2.020903143
LINC00534	ENSG00000253394	2.01536253
NOS3	ENSG00000164867	2.015254919
ABO	ENSG00000175164	2.002715968
PRB2	ENSG00000121335	2.00133844

References

Abe, Koji, Masashi Aoki, Shoji Tsuji, Yasuto Itoyama, Gen Sobue, Masanori Togo, Chikuma Hamada, et al. “Safety and Efficacy of Edaravone in Well Defined Patients with Amyotrophic Lateral Sclerosis: A Randomised, Double-Blind, Placebo-Controlled Trial.” The Lancet Neurology 16, no. 7 (July 1, 2017):505–12. https://doi.org/10.1016/S1474-4422(17)30115-1.

Abel, Olubunmi, John F Powell, Peter M. Andersen, and Ammar Al-Chalabi. “ALSoD: A User-Friendly Online Bioinformatics Tool for Amyotrophic Lateral Sclerosis Genetics.” Human Mutation 33, no. 9 (2012): 1345–51. https://doi.org/10.1002/humu.22157.

Aggad, Dina, Julie Vérièpe, Arnaud Tauffenberger, and J. Alex Parker. “TDP-43 Toxicity Proceeds via Calcium Dysregulation and Necrosis in Aging Caenorhabditis Elegans Motor Neurons.” The Journal of Neuroscience 34, no. 36 (September 3, 2014): 12093–103. https://doi.org/10.1523/JNEUROSCI.2495-13.2014.

Alami, Nael H., Rebecca B. Smith, Monica A. Carrasco, Luis A. Williams, Christina S. Winborn, Steve S. W. Han, Evangelos Kiskinis, et al. “Axonal Transport of TDP-43 mRNA Granules Is Impaired by ALS- Causing Mutations.” Neuron 81, no. 3 (February 5, 2014): 536–43. https://doi.org/10.1016/j.neuron.2013.12.018.

Amoroso, Mackenzie W., Gist F. Croft, Damian J. Williams, Sean O’Keeffe, Monica A. Carrasco, Anne R. Davis, Laurent Roybon, et al. “Accelerated High-Yield Generation of Limb-Innervating Motor Neurons from Human Stem Cells.” Journal of Neuroscience 33, no. 2 (January 9, 2013): 574–86. https://doi.org/10.1523/JNEUROSCI.0906-12.2013.

Aviner, Ranen. “The Science of Puromycin: From Studies of Ribosome Function to Applications in Biotechnology.” Computational and Structural Biotechnology Journal 18 (April 24, 2020): 1074–83. https://doi.org/10.1016/j.csbj.2020.04.014.

Babinchak, W. Michael, Raza Haider, Benjamin K. Dumm, Prottusha Sarkar, Krystyna Surewicz, Jin-Kyu Choi, and Witold K. Surewicz. “The Role of Liquid–Liquid Phase Separation in Aggregation of the TDP-43 Low-Complexity Domain.” Journal of Biological Chemistry 294, no. 16 (April 19, 2019):6306–17. https://doi.org/10.1074/jbc.RA118.007222.

Bar, Daniel Z., Chayki Charar, Jehudith Dorfman, Tam Yadid, Lionel Tafforeau, Denis L. J. Lafontaine, and Yosef Gruenbaum. “Cell Size and Fat Content of Dietary-Restricted Caenorhabditis Elegans Are Regulated by ATX-2, an mTOR Repressor.” Proceedings of the National Academy of Sciences 113, no. 32 (August 9, 2016): E4620–29. https://doi.org/10.1073/pnas.1512156113.

Barmada, Sami J., Gaia Skibinski, Erica Korb, Elizabeth J. Rao, Jane Y. Wu, and Steven Finkbeiner. “Cytoplasmic Mislocalization of TDP-43 Is Toxic to Neurons and Enhanced by a Mutation Associated with Familial Amyotrophic Lateral Sclerosis.” The Journal of Neuroscience: The Official Journal of the Society for Neuroscience 30, no. 2 (January 13, 2010): 639–49. https://doi.org/10.1523/JNEUROSCI.4988-09.2010.

Baxi, Emily G., Terri Thompson, Jonathan Li, Julia A. Kaye, Ryan G. Lim, Jie Wu, Divya Ramamoorthy, et al. “Answer ALS, a Large-Scale Resource for Sporadic and Familial ALS Combining Clinical and Multi-Omics Data from Induced Pluripotent Cell Lines.” Nature Neuroscience 25, no. 2 (February 2022): 226–37. https://doi.org/10.1038/s41593-021-01006-0.

Becker, Lindsay A., Brenda Huang, Gregor Bieri, Rosanna Ma, David A. Knowles, Paymaan Jafar-Nejad, James Messing, et al. “Therapeutic Reduction of Ataxin 2 Extends Lifespan and Reduces Pathology in TDP-43 Mice.” Nature 544, no. 7650 (April 20, 2017): 367–71. https://doi.org/10.1038/nature22038.

Bensimon, G., L. Lacomblez, and V. Meininger. “A Controlled Trial of Riluzole in Amyotrophic Lateral Sclerosis.” New England Journal of Medicine 330, no. 9 (March 3, 1994): 585–91. https://doi.org/10.1056/NEJM199403033300901.

Berdyński, Mariusz, Przemysław Miszta, Krzysztof Safranow, Peter M. Andersen, Mitsuya Morita, Sławomir Filipek, Cezary Żekanowski, and Magdalena Kuźma-Kozakiewicz. “SOD1 Mutations Associated with Amyotrophic Lateral Sclerosis Analysis of Variant Severity.” Scientific Reports 12 (January 7, 2022):103. https://doi.org/10.1038/s41598-021-03891-8.

Bilican, Bilada, Andrea Serio, Sami J. Barmada, Agnes Lumi Nishimura, Gareth J. Sullivan, Monica Carrasco, Hemali P. Phatnani, et al. “Mutant Induced Pluripotent Stem Cell Lines Recapitulate Aspects of TDP-43 Proteinopathies and Reveal Cell-Specific Vulnerability.” Proceedings of the National Academy of Sciences 109, no. 15 (April 10, 2012): 5803–8. https://doi.org/10.1073/pnas.1202922109.

Birsa, Nicol, Matthew Peter Bentham, and Pietro Fratta. “Cytoplasmic Functions of TDP-43 and FUS and Their Role in ALS.” Seminars in Cell & Developmental Biology, SI: Protein-protein interactions in health and disease, 99 (March 1, 2020): 193–201. https://doi.org/10.1016/j.semcdb.2019.05.023.

Blair, Hannah A. “Tofersen: First Approval.” Drugs 83, no. 11 (July 1, 2023): 1039–43. https://doi.org/10.1007/s40265-023-01904-6.

Boda, Bernadett, Stefano Alberi, Irina Nikonenko, Roxanne Node-Langlois, Pascal Jourdain, Marlyse Moosmayer, Lorena Parisi-Jourdain, and Dominique Muller. “The Mental Retardation Protein PAK3 Contributes to Synapse Formation and Plasticity in Hippocampus.” The Journal of Neuroscience 24, no. 48 (December 1, 2004): 10816–25. https://doi.org/10.1523/JNEUROSCI.2931-04.2004.

Bossolasco, Patrizia, Francesca Sassone, Valentina Gumina, Silvia Peverelli, Maria Garzo, and Vincenzo Silani. “Motor Neuron Differentiation of iPSCs Obtained from Peripheral Blood of a Mutant TARDBP ALS Patient.” Stem Cell Research 30 (July 1, 2018): 61–68. https://doi.org/10.1016/j.scr.2018.05.009.

Boulting, Gabriella L., Evangelos Kiskinis, Gist F. Croft, Mackenzie W. Amoroso, Derek H. Oakley, Brian J. Wainger, Damian J. Williams, et al. “A Functionally Characterized Test Set of Human Induced Pluripotent Stem Cells.” Nature Biotechnology 29, no. 3 (March 2011): 279–86. https://doi.org/10.1038/nbt.1783.

Brooks, B. R., R. A. Thisted, S. H. Appel, W. G. Bradley, R. K. Olney, J. E. Berg, L. E. Pope, and R. A. Smith. “Treatment of Pseudobulbar Affect in ALS with Dextromethorphan/Quinidine: A Randomized Trial.” Neurology 63, no. 8 (October 26, 2004): 1364–70. https://doi.org/10.1212/01.WNL.0000142042.50528.2F.

Brown, Robert H., and Ammar Al-Chalabi. “Amyotrophic Lateral Sclerosis.” New England Journal of Medicine 377, no. 2 (July 13, 2017): 162–72. https://doi.org/10.1056/NEJMra1603471.

Buratti, Emanuele. “Chapter One - Functional Significance of TDP-43 Mutations in Disease.” In Advances in Genetics, edited by Theodore Friedmann, Jay C. Dunlap, and Stephen F. Goodwin, 91:1–53. Academic Press, 2015. https://doi.org/10.1016/bs.adgen.2015.07.001.

Buratti, Emanuele, and Francisco E. Baralle. “TDP-43: Gumming up Neurons through Protein–Protein and Protein–RNA Interactions.” Trends in Biochemical Sciences 37, no. 6 (June 1, 2012): 237–47. https://doi.org/10.1016/j.tibs.2012.03.003.

Burkhardt, Matthew F., Fernando J. Martinez, Sarah Wright, Carla Ramos, Dmitri Volfson, Michael Mason, Jeff Garnes, et al. “A Cellular Model for Sporadic ALS Using Patient-Derived Induced Pluripotent Stem Cells.” Molecular and Cellular Neuroscience, RNA and splicing regulation in neurodegeneration, 56 (September 1, 2013): 355–64. https://doi.org/10.1016/j.mcn.2013.07.007.

Chambers, Stuart M., Christopher A. Fasano, Eirini P. Papapetrou, Mark Tomishima, Michel Sadelain, and Lorenz Studer. “Highly Efficient Neural Conversion of Human ES and iPS Cells by Dual Inhibition of SMAD Signaling.” Nature Biotechnology 27, no. 3 (March 2009): 275–80. https://doi.org/10.1038/nbt.1529.

Chittenden, Thomas, Elizabeth A. Harrington, Rosemary O’Connor, Cathy Remington, Robert J. Lutz, Gerard I. Evan, and Braydon C. Guild. “Induction of Apoptosis by the Bcl-2 Homologue Bak.” Nature 374, no. 6524 (April 1995): 733–36. https://doi.org/10.1038/374733a0.

Chou, Ching-Chieh, Yi Zhang, Mfon E. Umoh, Spencer W. Vaughan, Ileana Lorenzini, Feilin Liu, Melissa Sayegh, et al. “TDP-43 Pathology Disrupts Nuclear Pore Complexes and Nucleocytoplasmic Transport in ALS/FTD.” Nature Neuroscience 21, no. 2 (February 2018): 228–39. https://doi.org/10.1038/s41593-017-0047-3.

Cruz, Martin Paspe. “Edaravone (Radicava).” Pharmacy and Therapeutics 43, no. 1 (January 2018): 25–28. Dafinca, Ruxandra, Paola Barbagallo, Lucy Farrimond, Ana Candalija, Jakub Scaber, Nida’a A. Ababneh,
Chaitra Sathyaprakash, Jane Vowles, Sally A. Cowley, and Kevin Talbot. “Impairment of Mitochondrial Calcium Buffering Links Mutations in C9ORF72 and TARDBP in iPS-Derived

Motor Neurons from Patients with ALS/FTD." Stem Cell Reports 14, no. 5 (May 12, 2020): 892–908. https://doi.org/10.1016/j.stemcr.2020.03.023.

Dafinca, Ruxandra, Paola Barbagallo, and Kevin Talbot. "The Role of Mitochondrial Dysfunction and ER Stress in TDP-43 and C9ORF72 ALS." Frontiers in Cellular Neuroscience 15 (2021). https://www.frontiersin.org/articles/10.3389/fncel.2021.653688.

Damrath, Ewa, Melanie V. Heck, Suzana Gispert, Mekhman Azizov, Joachim Nowock, Carola Seifried, Udo Rüb, Michael Walter, and Georg Auburger. "ATXN2-CAG42 Sequesters PABPC1 into Insolubility and Induces FBXW8 in Cerebellum of Old Ataxic Knock-In Mice." PLOS Genetics 8, no. 8 (August 30, 2012): e1002920. https://doi.org/10.1371/journal.pgen.1002920.

Das, Atze T., Liliane Tenenbaum, and Ben Berkhout. "Tet-On Systems For Doxycycline-Inducible Gene Expression." Current Gene Therapy 16, no. 3 (June 2016): 156–67. https://doi.org/10.2174/1566523216666160524144041.

Del Signore, Steven J., Daniel J. Amante, Jinho Kim, Edward C. Stack, Sarah Goodrich, Kerry Cormier, Karen Smith, Merit E. Cudkowicz, and Robert J. Ferrante. "Combined Riluzole and Sodium Phenylbutyrate Therapy in Transgenic Amyotrophic Lateral Sclerosis Mice." Amyotrophic Lateral Sclerosis 10, no. 2 (January 1, 2009): 85–94. https://doi.org/10.1080/17482960802226148.

Dewey, Colleen M., Basar Cenik, Chantelle F. Sephton, Brett A. Johnson, Joachim Herz, and Gang Yu. "TDP-43 Aggregation In Neurodegeneration: Are Stress Granules The Key?" Brain Research 1462 (June 26, 2012): 16–25. https://doi.org/10.1016/j.brainres.2012.02.032.

Di Sole, Francesca, Komal Vadnagara, Orson W. Moe, and Victor Babich. "Calcineurin Homologous Protein: A Multifunctional Ca2+-Binding Protein Family." American Journal of Physiology - Renal Physiology 303, no. 2 (July 15, 2012): F165–79. https://doi.org/10.1152/ajprenal.00628.2011.

Ding, Qiao, Justin Chaplin, Matthew J. Morris, Massimo A. Hilliard, Ernst Wolvetang, Dominic C. H. Ng, and Peter G. Noakes. "TDP-43 Mutation Affects Stress Granule Dynamics in Differentiated NSC-34 Motoneuron-Like Cells." Frontiers in Cell and Developmental Biology 9 (2021): 611601. https://doi.org/10.3389/fcell.2021.611601.

Doble, A. "The Pharmacology and Mechanism of Action of Riluzole." Neurology 47, no. Issue 6, Supplement 4 (December 1, 1996): 233S-241S. https://doi.org/10.1212/WNL.47.6_Suppl_4.233S.

Duarte, Kévin, Solveig Heide, Sandrine Poëa-Guyon, Véronique Rousseau, Christel Depienne, Agnès Rastetter, Caroline Nava, et al. "PAK3 Mutations Responsible for Severe Intellectual Disability and Callosal Agenesis Inhibit Cell Migration." Neurobiology of Disease 136 (March 1, 2020): 104709. https://doi.org/10.1016/j.nbd.2019.104709.

Eck, Randall J., Brian C. Kraemer, and Nicole F. Liachko. “Regulation of TDP-43 Phosphorylation in Aging and Disease.” GeroScience 43, no. 4 (May 25, 2021): 1605–14. https://doi.org/10.1007/s11357-021-00383-5.

Egawa, Naohiro, Shiho Kitaoka, Kayoko Tsukita, Motoko Naitoh, Kazutoshi Takahashi, Takuya Yamamoto, Fumihiko Adachi, et al. “Drug Screening for ALS Using Patient-Specific Induced Pluripotent Stem Cells.” Science Translational Medicine 4, no. 145 (August 2012): 145ra104-145ra104. https://doi.org/10.1126/scitranslmed.3004052.

Elden, Andrew C., Hyung-Jun Kim, Michael P. Hart, Alice S. Chen-Plotkin, Brian S. Johnson, Xiaodong Fang, Maria Armakola, et al. “Ataxin-2 Intermediate-Length Polyglutamine Expansions Are Associated with Increased Risk for ALS.” Nature 466, no. 7310 (August 26, 2010): 1069–75. https://doi.org/10.1038/nature09320.

Fang, Mark Y., Sebastian Markmiller, Anthony Q. Vu, Ashkan Javaherian, William E. Dowdle, Philippe Jolivet, Paul J. Bushway, et al. “Small Molecule Modulation of TDP-43 Recruitment to Stress Granules Prevents Persistent TDP-43 Accumulation in ALS/FTD.” Neuron 103, no. 5 (September 4, 2019): 802-819.e11. https://doi.org/10.1016/j.neuron.2019.05.048.

Fang, Ton, Felix Jozsa, and Ammar Al-Chalabi. “Chapter Fifty-One - Nonmotor Symptoms in Amyotrophic Lateral Sclerosis: A Systematic Review.” In International Review of Neurobiology, edited by K. Ray Chaudhuri and Nataliya Titova, 134:1409–41. Nonmotor Parkinson’s: The Hidden Face. Academic Press, 2017. https://doi.org/10.1016/bs.irn.2017.04.009.

Fecto, Faisal, Jianhua Yan, S. Pavan Vemula, Erdong Liu, Yi Yang, Wenjie Chen, Jian Guo Zheng, et al. “SQSTM1 Mutations in Familial and Sporadic Amyotrophic Lateral Sclerosis.” Archives of Neurology 68, no. 11 (November 1, 2011): 1440–46. https://doi.org/10.1001/archneurol.2011.250.

Feiler, Marisa S., Benjamin Strobel, Axel Freischmidt, Anika M. Helferich, Julia Kappel, Bryson M. Brewer, Deyu Li, et al. “TDP-43 Is Intercellularly Transmitted across Axon Terminals.” Journal of Cell Biology 211, no. 4 (November 23, 2015): 897–911. https://doi.org/10.1083/jcb.201504057.

Finelli, Mattéa J., Luis Sanchez-Pulido, Kevin X. Liu, Kay E. Davies, and Peter L. Oliver. “The Evolutionarily Conserved Tre2/Bub2/Cdc16 (TBC), Lysin Motif (LysM), Domain Catalytic (TLDc) Domain Is Neuroprotective against Oxidative Stress.” The Journal of Biological Chemistry 291, no. 6 (February 5, 2016): 2751–63. https://doi.org/10.1074/jbc.M115.685222.

Fisher, Elizabeth M.C., Linda Greensmith, Andrea Malaspina, Pietro Fratta, Michael G. Hanna, Giampietro Schiavo, Adrian M. Isaacs, Richard W. Orrell, Thomas J. Cunningham, and Abraham Acevedo Arozena. “Opinion: More Mouse Models and More Translation Needed for ALS.” Molecular Neurodegeneration 18, no. 1 (May 4, 2023): 30. https://doi.org/10.1186/s13024-023-00619-2.

Freibaum, Brian D., Raghu Chitta, Anthony A. High, and J. Paul Taylor. “Global Analysis of TDP-43 Interacting Proteins Reveals Strong Association with RNA Splicing and Translation Machinery.”

Journal of Proteome Research 9, no. 2 (February 5, 2010): 1104–20. https://doi.org/10.1021/pr901076y.

Ghasemi, Mehdi, and Robert H. Brown. “Genetics of Amyotrophic Lateral Sclerosis.” Cold Spring Harbor Perspectives in Medicine 8, no. 5 (May 2018): a024125. https://doi.org/10.1101/cshperspect.a024125.

Giacomelli, Elisa, Björn F. Vahsen, Elizabeth L. Calder, Yinyan Xu, Jakub Scaber, Elizabeth Gray, Ruxandra Dafinca, Kevin Talbot, and Lorenz Studer. “Human Stem Cell Models of Neurodegeneration: From Basic Science of Amyotrophic Lateral Sclerosis to Clinical Translation.” Cell Stem Cell 29, no. 1 (January 6, 2022): 11–35. https://doi.org/10.1016/j.stem.2021.12.008.

Giannini, Marta, Aleix Bayona-Feliu, Daisy Sproviero, Sonia I. Barroso, Cristina Cereda, and Andrés Aguilera. “TDP-43 Mutations Link Amyotrophic Lateral Sclerosis with R-Loop Homeostasis and RLoop-Mediated DNA Damage.” PLOS Genetics 16, no. 12 (December 10, 2020): e1009260. https://doi.org/10.1371/journal.pgen.1009260.

Green, Jordan R., Kristen M. Allison, Claire Cordella, Brian D. Richburg, Gary L. Pattee, James D. Berry, Eric A. Macklin, Erik P. Pioro, and Richard A. Smith. “Additional Evidence for a Therapeutic Effect of Dextromethorphan/Quinidine on Bulbar Motor Function in Patients with Amyotrophic Lateral Sclerosis: A Quantitative Speech Analysis.” British Journal of Clinical Pharmacology 84, no. 12 (2018): 2849–56. https://doi.org/10.1111/bcp.13745.

Guerra San Juan, Irune, Leslie A. Nash, Kevin S. Smith, Marcel F. Leyton-Jaimes, Menglu Qian, Joseph R. Klim, Francesco Limone, et al. “Loss of Mouse Stmn2 Function Causes Motor Neuropathy.” Neuron 110, no. 10 (May 18, 2022): 1671-1688.e6. https://doi.org/10.1016/j.neuron.2022.02.011.

Halbach, Melanie Vanessa, Suzana Gispert, Tanja Stehning, Ewa Damrath, Michael Walter, and Georg Auburger. “Atxn2 Knockout and CAG42-Knock-in Cerebellum Shows Similarly Dysregulated Expression in Calcium Homeostasis Pathway.” The Cerebellum 16, no. 1 (February 1, 2017): 68–81. https://doi.org/10.1007/s12311-016-0762-4.

Hans, Friederike, Fabienne C. Fiesel, Jennifer C. Strong, Sandra Jäckel, Tobias M. Rasse, Sven Geisler, Wolfdieter Springer, Jörg B. Schulz, Aaron Voigt, and Philipp J. Kahle. “UBE2E Ubiquitin-Conjugating Enzymes and Ubiquitin Isopeptidase Y Regulate TDP-43 Protein Ubiquitination *.” Journal of Biological Chemistry 289, no. 27 (July 1, 2014): 19164–79. https://doi.org/10.1074/jbc.M114.561704.

Hao, Wenrui, and Avner Friedman. “Mathematical Model on Alzheimer’s Disease.” BMC Systems Biology 10, no. 1 (November 18, 2016): 108. https://doi.org/10.1186/s12918-016-0348-2.

Hardiman, Orla, Ammar Al-Chalabi, Adriano Chio, Emma M. Corr, Giancarlo Logroscino, Wim Robberecht, Pamela J. Shaw, Zachary Simmons, and Leonard H. van den Berg. “Amyotrophic Lateral Sclerosis.” Nature Reviews Disease Primers 3, no. 1 (October 5, 2017): 1–19. https://doi.org/10.1038/nrdp.2017.71.

Hasegawa, Masato, Tetsuaki Arai, Takashi Nonaka, Fuyuki Kametani, Mari Yoshida, Yoshio Hashizume, Thomas G. Beach, et al. “Phosphorylated TDP-43 in Frontotemporal Lobar Degeneration and Amyotrophic Lateral Sclerosis.” Annals of Neurology 64, no. 1 (2008): 60–70. https://doi.org/10.1002/ana.21425.

Hockemeyer, Dirk, Frank Soldner, Caroline Beard, Qing Gao, Maisam Mitalipova, Russell C. DeKelver, George E. Katibah, et al. “Highly Efficient Gene Targeting of Expressed and Silent Genes in Human ESCs and iPSCs Using Zinc Finger Nucleases.” Nature Biotechnology 27, no. 9 (September 2009): 851–57. https://doi.org/10.1038/nbt.1562.

Hong, Kun, Yi Li, Weisong Duan, Yansu Guo, Hong Jiang, Wenju Li, and Chunyan Li. “Full-Length TDP-43 and Its C-Terminal Fragments Activate Mitophagy in NSC34 Cell Line.” Neuroscience Letters 530, no. 2 (November 21, 2012): 144–49. https://doi.org/10.1016/j.neulet.2012.10.003.

Ingre, Caroline, Per M Roos, Fredrik Piehl, Freya Kamel, and Fang Fang. “Risk Factors for Amyotrophic Lateral Sclerosis.” Clinical Epidemiology 7 (February 12, 2015): 181–93. https://doi.org/10.2147/CLEP.S37505.

Ittner, Lars M., Glenda M. Halliday, Jillian J. Kril, Jürgen Götz, John R. Hodges, and Matthew C. Kiernan. “FTD and ALS--Translating Mouse Studies into Clinical Trials.” Nature Reviews. Neurology 11, no. 6 (June 2015): 360–66. https://doi.org/10.1038/nrneurol.2015.65.

Ji, Ce, Ying Zhao, You-Wei Kou, Hua Shao, Lin Guo, Chen-Hui Bao, Ben-Chun Jiang, et al. “Cathepsin F Knockdown Induces Proliferation and Inhibits Apoptosis in Gastric Cancer Cells.” Oncology Research 26, no. 1 (January 19, 2018): 83–93. https://doi.org/10.3727/096504017X14928634401204.

Jiang, Ganggang, Xue Liang, Yiqiao Huang, Ziquan Lan, Zhiming Zhang, Zhengming Su, Zhiyuan Fang, et al. “P62 Promotes Proliferation, Apoptosis-Resistance and Invasion of Prostate Cancer Cells through the Keap1/Nrf2/ARE Axis.” Oncology Reports 43, no. 5 (May 2020): 1547–57. https://doi.org/10.3892/or.2020.7527.

Johnson, Brian S., J. Michael McCaffery, Susan Lindquist, and Aaron D. Gitler. “A Yeast TDP-43 Proteinopathy Model: Exploring the Molecular Determinants of TDP-43 Aggregation and Cellular Toxicity.” Proceedings of the National Academy of Sciences of the United States of America 105, no. 17 (April 29, 2008): 6439–44. https://doi.org/10.1073/pnas.0802082105.

Johnson, Stephen A., Ton Fang, Fabiola De Marchi, Dylan Neel, Donatienne Van Weehaeghe, James D. Berry, and Sabrina Paganoni. “Pharmacotherapy for Amyotrophic Lateral Sclerosis: A Review of Approved and Upcoming Agents.” Drugs 82, no. 13 (September 1, 2022): 1367–88. https://doi.org/10.1007/s40265-022-01769-1.

Kedersha, N., and P. Anderson. “Stress Granules: Sites of mRNA Triage That Regulate mRNA Stability and Translatability.” Biochemical Society Transactions 30, no. 6 (November 1, 2002): 963–69. https://doi.org/10.1042/bst0300963.

Kiernan, Matthew C., Steve Vucic, Benjamin C. Cheah, Martin R. Turner, Andrew Eisen, Orla Hardiman, James R. Burrell, and Margaret C. Zoing. “Amyotrophic Lateral Sclerosis.” The Lancet 377, no. 9769 (March 12, 2011): 942–55. https://doi.org/10.1016/S0140-6736(10)61156-7.

Klaassen, Remco V., Jasper Stroeder, Françoise Coussen, Anne-Sophie Hafner, Jennifer D. Petersen, Cedric Renancio, Leanne J. M. Schmitz, et al. “Shisa6 Traps AMPA Receptors at Postsynaptic Sites and Prevents Their Desensitization during Synaptic Activity.” Nature Communications 7 (March 2, 2016): 10682. https://doi.org/10.1038/ncomms10682.

Klim, Joseph R., Luis A. Williams, Francesco Limone, Irune Guerra San Juan, Brandi N. Davis-Dusenbery, Daniel A. Mordes, Aaron Burberry, et al. “ALS-Implicated Protein TDP-43 Sustains Levels of STMN2, a Mediator of Motor Neuron Growth and Repair.” Nature Neuroscience 22, no. 2 (February 2019): 167–79. https://doi.org/10.1038/s41593-018-0300-4.

Kraemer, Brian C., Theresa Schuck, Jeanna M. Wheeler, Linda C. Robinson, John Q. Trojanowski, Virginia M. Y. Lee, and Gerard D. Schellenberg. “Loss of Murine TDP-43 Disrupts Motor Function and Plays an Essential Role in Embryogenesis.” Acta Neuropathologica 119, no. 4 (April 2010): 409–19. https://doi.org/10.1007/s00401-010-0659-0.

Krus, Kelsey L., Amy Strickland, Yurie Yamada, Laura Devault, Robert E. Schmidt, A. Joseph Bloom, Jeffrey Milbrandt, and Aaron DiAntonio. “Loss of Stathmin-2, a Hallmark of TDP-43-Associated ALS, Causes Motor Neuropathy.” Cell Reports 39, no. 13 (June 28, 2022): 111001. https://doi.org/10.1016/j.celrep.2022.111001.

Kusaczuk, Magdalena. “Tauroursodeoxycholate—Bile Acid with Chaperoning Activity: Molecular and Cellular Effects and Therapeutic Perspectives.” Cells 8, no. 12 (December 2019): 1471. https://doi.org/10.3390/cells8121471.

Laferriere, Florent, and Magdalini Polymenidou. “Advances and Challenges in Understanding the Multifaceted Pathogenesis of Amyotrophic Lateral Sclerosis.” Swiss Medical Weekly 145, no. 0506 (January 25, 2015): w14054–w14054. https://doi.org/10.4414/smw.2015.14054.

Lamptey, Richard N. L., Bivek Chaulagain, Riddhi Trivedi, Avinash Gothwal, Buddhadev Layek, and Jagdish Singh. “A Review of the Common Neurodegenerative Disorders: Current Therapeutic Approaches and the Potential Role of Nanotherapeutics.” International Journal of Molecular Sciences 23, no. 3 (February 6, 2022): 1851. https://doi.org/10.3390/ijms23031851.

Lastres-Becker, Isabel, Susanne Brodesser, Dieter Lütjohann, Mekhman Azizov, Jana Buchmann, Edith Hintermann, Konrad Sandhoff, Annette Schürmann, Joachim Nowock, and Georg Auburger. “Insulin Receptor and Lipid Metabolism Pathology in Ataxin-2 Knock-out Mice.” Human Molecular Genetics 17, no. 10 (May 15, 2008): 1465–81. https://doi.org/10.1093/hmg/ddn035.

Lee, Jongbo, Minjong Kim, Taichi Q. Itoh, and Chunghun Lim. “Ataxin-2: A Versatile Posttranscriptional Regulator and Its Implication in Neural Function.” WIREs RNA 9, no. 6 (2018): e1488. https://doi.org/10.1002/wrna.1488.

Lee, Jongbo, Eunseok Yoo, Hoyeon Lee, Keunhee Park, Jin-Hoe Hur, and Chunghun Lim. “LSM12 and ME31B/DDX6 Define Distinct Modes of Posttranscriptional Regulation by ATAXIN-2 Protein Complex in Drosophila Circadian Pacemaker Neurons.” Molecular Cell 66, no. 1 (April 6, 2017): 129-140.e7. https://doi.org/10.1016/j.molcel.2017.03.004.

Lee, Youn-Bok, Emma L Scotter, Do-Young Lee, Claire Troakes, Jacqueline Mitchell, Boris Rogelj, Jean- Marc Gallo, and Christopher E Shaw. “Cytoplasmic TDP-43 Is Involved in Cell Fate during Stress Recovery.” Human Molecular Genetics 31, no. 2 (August 10, 2021): 166–75. https://doi.org/10.1093/hmg/ddab227.

Leigh, P N. “The Management of Motor Neurone Disease.” Journal of Neurology, Neurosurgery & Psychiatry 74, no. 90004 (December 1, 2003): 32iv–3247. https://doi.org/10.1136/jnnp.74.suppl_4.iv32.

Lesnick, Timothy G., Eric J. Sorenson, J. Eric Ahlskog, John R. Henley, Lina Shehadeh, Spiridon Papapetropoulos, and Demetrius M. Maraganore. “Beyond Parkinson Disease: Amyotrophic Lateral Sclerosis and the Axon Guidance Pathway.” PLOS ONE 3, no. 1 (January 16, 2008): e1449. https://doi.org/10.1371/journal.pone.0001449.

Liachko, Nicole F., Aleen D. Saxton, Pamela J. McMillan, Timothy J. Strovas, Heather N. Currey, Laura M. Taylor, Jeanna M. Wheeler, et al. “The Phosphatase Calcineurin Regulates Pathological TDP-43 Phosphorylation.” Acta Neuropathologica 132, no. 4 (October 1, 2016): 545–61. https://doi.org/10.1007/s00401-016-1600-y.

Lim, Chunghun, and Ravi Allada. “ATAXIN-2 Activates PERIOD Translation to Sustain Circadian Rhythms in Drosophila.” Science (New York, N.Y.) 340, no. 6134 (May 17, 2013): 875–79. https://doi.org/10.1126/science.1234785.

Limone, Francesco, Irune Guerra San Juan, Jana M. Mitchell, Janell L.M. Smith, Kavya Raghunathan, Daniel Meyer, Sulagna Dia Ghosh, et al. “Efficient Generation of Lower Induced Motor Neurons by Coupling Ngn2 Expression with Developmental Cues.” Cell Reports 42, no. 1 (January 31, 2023): 111896. https://doi.org/10.1016/j.celrep.2022.111896.

Ling, Shuo-Chien, Magdalini Polymenidou, and Don W. Cleveland. “Converging Mechanisms in ALS and FTD: Disrupted RNA and Protein Homeostasis.” Neuron 79, no. 3 (August 7, 2013): 416–38. https://doi.org/10.1016/j.neuron.2013.07.033.

Liu-Yesucevitz, Liqun, Aylin Bilgutay, Yong-Jie Zhang, Tara Vanderweyde, Allison Citro, Tapan Mehta, Nava Zaarur, et al. “Tar DNA Binding Protein-43 (TDP-43) Associates with Stress Granules: Analysis of Cultured Cells and Pathological Brain Tissue.” PloS One 5, no. 10 (October 11, 2010): e13250. https://doi.org/10.1371/journal.pone.0013250.

LIYANG, Gao, Syahril ABDULLAH, Rozita ROSLI, and Norshariza NORDIN. “Neural Commitment of Embryonic Stem Cells through the Formation of Embryoid Bodies (EBs).” The Malaysian Journal of Medical Sciences : MJMS 21, no. 5 (2014): 8–16.

Lombardo, Angelo, Daniela Cesana, Pietro Genovese, Bruno Di Stefano, Elena Provasi, Daniele F. Colombo, Margherita Neri, et al. “Site-Specific Integration and Tailoring of Cassette Design for Sustainable Gene Transfer.” Nature Methods 8, no. 10 (October 2011): 861–69. https://doi.org/10.1038/nmeth.1674.

Ma, X. Rosa, Mercedes Prudencio, Yuka Koike, Sarat C. Vatsavayai, Garam Kim, Fred Harbinski, Adam Briner, et al. “TDP-43 Represses Cryptic Exon Inclusion in the FTD–ALS Gene UNC13A.” Nature 603, no. 7899 (March 2022): 124–30. https://doi.org/10.1038/s41586-022-04424-7.

Malik, Nasir, and Mahendra S. Rao. “A Review of the Methods for Human iPSC Derivation.” In Pluripotent Stem Cells: Methods and Protocols, edited by Uma Lakshmipathy and Mohan C Vemuri, 23–33. Methods in Molecular Biology. Totowa, NJ: Humana Press, 2013. https://doi.org/10.1007/978-1-62703-348-0_3.

Mann, Jacob R., Amanda M. Gleixner, Jocelyn C. Mauna, Edward Gomes, Michael R. DeChellis-Marks, Patrick G. Needham, Katie E. Copley, et al. “RNA Binding Antagonizes Neurotoxic Phase Transitions of TDP-43.” Neuron 102, no. 2 (April 17, 2019): 321-338.e8. https://doi.org/10.1016/j.neuron.2019.01.048.

Markmiller, Sebastian, Sahar Soltanieh, Kari L. Server, Raymond Mak, Wenhao Jin, Mark Y. Fang, En-Ching Luo, et al. “Context-Dependent and Disease-Specific Diversity in Protein Interactions within Stress Granules.” Cell 172, no. 3 (January 25, 2018): 590-604.e13. https://doi.org/10.1016/j.cell.2017.12.032.

McClelland III, Shearwood, Francois A. Bethoux, Nicholas M. Boulis, Matthew H. Sutliff, Darlene K. Stough, Kathleen M. Schwetz, Danuta M. Gogol, Michelle Harrison, and Erik P. Pioro. “Intrathecal Baclofen for Spasticity-Related Pain in Amyotrophic Lateral Sclerosis: Efficacy and Factors Associated with Pain Relief.” Muscle & Nerve 37, no. 3 (2008): 396–98. https://doi.org/10.1002/mus.20900.

Mehta, Paul, Jaime Raymond, Reshma Punjani, Moon Han, Theodore Larson, Wendy Kaye, Lorene M. Nelson, et al. “Prevalence of Amyotrophic Lateral Sclerosis in the United States Using Established and Novel Methodologies, 2017.” Amyotrophic Lateral Sclerosis and Frontotemporal Degeneration 24, no. 1–2 (January 2, 2023): 108–16. https://doi.org/10.1080/21678421.2022.2059380.

Mehta, Paul, Jaime Raymond, Reshma Punjani, Theodore Larson, Frank Bove, Wendy Kaye, Lorene M. Nelson, et al. “Prevalence of Amyotrophic Lateral Sclerosis (ALS), United States, 2016.” Amyotrophic Lateral Sclerosis and Frontotemporal Degeneration 23, no. 3–4 (April 3, 2022): 220–25. https://doi.org/10.1080/21678421.2021.1949021.

Melamed, Ze'ev, Jone López-Erauskin, Michael W. Baughn, Ouyang Zhang, Kevin Drenner, Ying Sun, Fernande Freyermuth, et al. "Premature Polyadenylation-Mediated Loss of Stathmin-2 Is a Hallmark of TDP-43-Dependent Neurodegeneration." Nature Neuroscience 22, no. 2 (February 2019): 180–90. https://doi.org/10.1038/s41593-018-0293-z.

Mennini, Tiziana, Massimiliano De Paola, Paolo Bigini, Cristina Mastrotto, Elena Fumagalli, Sara Barbera, Manuela Mengozzi, et al. "Nonhematopoietic Erythropoietin Derivatives Prevent Motoneuron Degeneration In Vitro and In Vivo." Molecular Medicine 12, no. 7 (July 2006): 153–60. https://doi.org/10.2119/2006-00045.Mennini.

Mercadante, Sebastiano, and Lou'i Al-Husinat. "Palliative Care in Amyotrophic Lateral Sclerosis." Journal of Pain and Symptom Management 66, no. 4 (October 1, 2023): e485–99. https://doi.org/10.1016/j.jpainsymman.2023.06.029.

Miller, Kathleen L., Lewis J. Fermaglich, and Janet Maynard. "Using Four Decades of FDA Orphan Drug Designations to Describe Trends in Rare Disease Drug Development: Substantial Growth Seen in Development of Drugs for Rare Oncologic, Neurologic, and Pediatric-Onset Diseases." Orphanet Journal of Rare Diseases 16, no. 1 (June 9, 2021): 265. https://doi.org/10.1186/s13023-021-01901-6.

Miller, Robert G, J D Mitchell, and Dan H Moore. "Riluzole for Amyotrophic Lateral Sclerosis (ALS)/Motor Neuron Disease (MND)." The Cochrane Database of Systematic Reviews 2012, no. 3 (March 14, 2012): CD001447. https://doi.org/10.1002/14651858.CD001447.pub3.

Nehme, Ralda, Emanuela Zuccaro, Sulagna Dia Ghosh, Chenchen Li, John L. Sherwood, Olli Pietilainen, Lindy E. Barrett, et al. "Combining NGN2 Programming with Developmental Patterning Generates Human Excitatory Neurons with NMDAR-Mediated Synaptic Transmission." Cell Reports 23, no. 8 (May 22, 2018): 2509–23. https://doi.org/10.1016/j.celrep.2018.04.066.

Neumann, Manuela, Deepak M. Sampathu, Linda K. Kwong, Adam C. Truax, Matthew C. Micsenyi, Thomas T. Chou, Jennifer Bruce, et al. "Ubiquitinated TDP-43 in Frontotemporal Lobar Degeneration and Amyotrophic Lateral Sclerosis." Science 314, no. 5796 (October 6, 2006): 130–33. https://doi.org/10.1126/science.1134108.

Nilaver, Benjamin I., and Henryk F. Urbanski. "Mechanisms Underlying TDP-43 Pathology and Neurodegeneration: An Updated Mini-Review." Frontiers in Aging Neuroscience 15 (2023). https://www.frontiersin.org/articles/10.3389/fnagi.2023.1142617.

Nonaka, Takashi, Tetsuaki Arai, Emanuele Buratti, Francisco E. Baralle, Haruhiko Akiyama, and Masato Hasegawa. "Phosphorylated and Ubiquitinated TDP-43 Pathological Inclusions in ALS and FTLD-U Are Recapitulated in SH-SY5Y Cells." FEBS Letters 583, no. 2 (2009): 394–400. https://doi.org/10.1016/j.febslet.2008.12.031.

Nonaka, Takashi, Fuyuki Kametani, Tetsuaki Arai, Haruhiko Akiyama, and Masato Hasegawa. "Truncation and Pathogenic Mutations Facilitate the Formation of Intracellular Aggregates of

TDP-43." Human Molecular Genetics 18, no. 18 (September 15, 2009): 3353–64. https://doi.org/10.1093/hmg/ddp275.

Nonaka, Takashi, Genjiro Suzuki, Yoshinori Tanaka, Fuyuki Kametani, Shinobu Hirai, Haruo Okado, Tomoyuki Miyashita, et al. "Phosphorylation of TAR DNA-Binding Protein of 43 kDa (TDP-43) by Truncated Casein Kinase 1δ Triggers Mislocalization and Accumulation of TDP-43 *." Journal of Biological Chemistry 291, no. 11 (March 11, 2016): 5473–83. https://doi.org/10.1074/jbc.M115.695379.

Ormeño, Fernando, Juan Hormazabal, José Moreno, Felipe Riquelme, Javiera Rios, Alfredo Criollo, Amelina Albornoz, Iván E. Alfaro, and Mauricio Budini. "Chaperone Mediated Autophagy Degrades TDP-43 Protein and Is Affected by TDP-43 Aggregation." Frontiers in Molecular Neuroscience 13 (2020). https://www.frontiersin.org/articles/10.3389/fnmol.2020.00019.

Ou, S. H., F. Wu, D. Harrich, L. F. García-Martínez, and R. B. Gaynor. "Cloning and Characterization of a Novel Cellular Protein, TDP-43, That Binds to Human Immunodeficiency Virus Type 1 TAR DNA Sequence Motifs." Journal of Virology 69, no. 6 (June 1995): 3584–96. https://doi.org/10.1128/JVI.69.6.3584-3596.1995.

Paganoni, Sabrina, Suzanne Hendrix, Samuel P. Dickson, Newman Knowlton, Eric A. Macklin, James D. Berry, Michael A. Elliott, et al. "Long-Term Survival of Participants in the CENTAUR Trial of Sodium Phenylbutyrate-Taurursodiol in Amyotrophic Lateral Sclerosis." Muscle & Nerve 63, no. 1 (2021): 31–39. https://doi.org/10.1002/mus.27091. (a)

Paganoni, Sabrina, Eric A. Macklin, Suzanne Hendrix, James D. Berry, Michael A. Elliott, Samuel Maiser, Chafic Karam, et al. "Trial of Sodium Phenylbutyrate–Taurursodiol for Amyotrophic Lateral Sclerosis." New England Journal of Medicine 383, no. 10 (September 3, 2020): 919–30. https://doi.org/10.1056/NEJMoa1916945. (b)

Philips, Thomas, and Jeffrey D. Rothstein. "Rodent Models of Amyotrophic Lateral Sclerosis." Current Protocols in Pharmacology / Editorial Board, S.J. Enna (Editor-in-Chief) ... [et Al.] 69 (June 1, 2015): 5.67.1-5.67.21. https://doi.org/10.1002/0471141755.ph0567s69.

Pintacuda, Greta, Frederik H. Lassen, Yu-Han H. Hsu, April Kim, Jacqueline M. Martín, Edyta Malolepsza, Justin K. Lim, Nadine Fornelos, Kevin C. Eggan, and Kasper Lage. "Genoppi Is an Open-Source Software for Robust and Standardized Integration of Proteomic and Genetic Data." Nature Communications 12, no. 1 (May 10, 2021): 2580. https://doi.org/10.1038/s41467-021-22648-5.

Ragagnin, Audrey M. G., Sina Shadfar, Marta Vidal, Md Shafi Jamali, and Julie D. Atkin. "Motor Neuron Susceptibility in ALS/FTD." Frontiers in Neuroscience 13 (2019). https://www.frontiersin.org/articles/10.3389/fnins.2019.00532.

Renton, Alan E., Elisa Majounie, Adrian Waite, Javier Simón-Sánchez, Sara Rollinson, J. Raphael Gibbs, Jennifer C. Schymick, et al. "A Hexanucleotide Repeat Expansion in C9ORF72 Is the

Cause of Chromosome 9p21-Linked ALS-FTD." Neuron 72, no. 2 (October 20, 2011): 257–68. https://doi.org/10.1016/j.neuron.2011.09.010.

Riemenschneider, Henrick, Qiang Guo, Jakob Bader, Frédéric Frottin, Daniel Farny, Gernot Kleinberger, Christian Haass, et al. "Gel-like Inclusions of C-Terminal Fragments of TDP-43 Sequester Stalled Proteasomes in Neurons." EMBO Reports 23, no. 6 (June 7, 2022): e53890. https://doi.org/10.15252/embr.202153890.

Ringholz, G. M., S. H. Appel, M. Bradshaw, N. A. Cooke, D. M. Mosnik, and P. E. Schulz. "Prevalence and Patterns of Cognitive Impairment in Sporadic ALS." Neurology 65, no. 4 (August 23, 2005): 586–90. https://doi.org/10.1212/01.wnl.0000172911.39167.b6.

Rothstein, Jeffrey D. "Therapeutic Horizons for Amyotrophic Lateral Sclerosis." Current Opinion in Neurobiology 6, no. 5 (October 1, 1996): 679–87. https://doi.org/10.1016/S0959-4388(96)80103-6.

Sato, T., S. Takeuchi, A. Saito, W. Ding, H. Bamba, H. Matsuura, Y. Hisa, I. Tooyama, and M. Urushitani. "Axonal Ligation Induces Transient Redistribution of TDP-43 in Brainstem Motor Neurons." Neuroscience 164, no. 4 (December 29, 2009): 1565–78. https://doi.org/10.1016/j.neuroscience.2009.09.050.

Sephton, Chantelle F., Can Cenik, Alper Kucukural, Eric B. Dammer, Basar Cenik, YuHong Han, Colleen M. Dewey, et al. "Identification of Neuronal RNA Targets of TDP-43-Containing Ribonucleoprotein Complexes *♦." Journal of Biological Chemistry 286, no. 2 (January 14, 2011): 1204–15. https://doi.org/10.1074/jbc.M110.190884.

Shalem, Ophir, Neville E. Sanjana, Ella Hartenian, Xi Shi, David A. Scott, Tarjei S. Mikkelsen, Dirk Heckl, et al. "Genome-Scale CRISPR-Cas9 Knockout Screening in Human Cells." Science 343, no. 6166 (January 3, 2014): 84–87. https://doi.org/10.1126/science.1247005.

Smith, Bradley N., Nicola Ticozzi, Claudia Fallini, Athina Soragia Gkazi, Simon Topp, Kevin P. Kenna, Emma L. Scotter, et al. "Exome-Wide Rare Variant Analysis Identifies TUBA4A Mutations Associated with Familial ALS." Neuron 84, no. 2 (October 22, 2014): 324–31. https://doi.org/10.1016/j.neuron.2014.09.027.

Smith, Joseph R., Sean Maguire, Lesley A. Davis, Morgan Alexander, Fentang Yang, Siddharthan Chandran, Charles ffrench-Constant, and Roger A. Pedersen. "Robust, Persistent Transgene Expression in Human Embryonic Stem Cells Is Achieved with AAVS1-Targeted Integration." Stem Cells 26, no. 2 (February 1, 2008): 496–504. https://doi.org/10.1634/stemcells.2007-0039.

Smith, Richard A., Timothy M. Miller, Koji Yamanaka, Brett P. Monia, Thomas P. Condon, Gene Hung, Christian S. Lobsiger, et al. "Antisense Oligonucleotide Therapy for Neurodegenerative Disease." The Journal of Clinical Investigation 116, no. 8 (August 1, 2006): 2290–96. https://doi.org/10.1172/JCI25424.

Su, Hong, Shuxia Meng, Yanyan Lu, Melanie I. Trombly, Jian Chen, Chengyi Lin, Anita Turk, and Xiaozhong Wang. “Mammalian Hyperplastic Discs Homolog EDD Regulates microRNA-Mediated Gene Silencing.” Molecular Cell 43, no. 1 (July 8, 2011): 97–109. https://doi.org/10.1016/j.molcel.2011.06.013.

Suk, Terry R., and Maxime W. C. Rousseaux. “The Role of TDP-43 Mislocalization in Amyotrophic Lateral Sclerosis.” Molecular Neurodegeneration 15, no. 1 (August 15, 2020): 45. https://doi.org/10.1186/s13024-020-00397-1.

Suzuki, Hiroaki, Kikyo Lee, and Masaaki Matsuoka. “TDP-43-Induced Death Is Associated with Altered Regulation of BIM and Bcl-xL and Attenuated by Caspase-Mediated TDP-43 Cleavage *.” Journal of Biological Chemistry 286, no. 15 (April 15, 2011): 13171–83. https://doi.org/10.1074/jbc.M110.197483.

Tharun, Sundaresan. “Roles of Eukaryotic Lsm Proteins in the Regulation of mRNA Function.” International Review of Cell and Molecular Biology 272 (2009): 149–89. https://doi.org/10.1016/S1937-6448(08)01604-3.

Tollervey, James R., Tomaž Curk, Boris Rogelj, Michael Briese, Matteo Cereda, Melis Kayikci, Julian König, et al. “Characterizing the RNA Targets and Position-Dependent Splicing Regulation by TDP-43.” Nature Neuroscience 14, no. 4 (April 2011): 452–58. https://doi.org/10.1038/nn.2778.

Torres, Pascual, Omar Ramírez-Núñez, Ricardo Romero-Guevara, Gisel Barés, Ana B. Granado-Serrano, Victòria Ayala, Jordi Boada, et al. “Cryptic Exon Splicing Function of TARDBP Interacts with Autophagy in Nervous Tissue.” Autophagy 14, no. 8 (August 3, 2018): 1398–1403. https://doi.org/10.1080/15548627.2018.1474311.

Tseng, Yu-Ling, Po-Chao Lu, Chi-Chang Lee, Ruei-Yu He, Yung-An Huang, Yin-Chen Tseng, Ting-Jen Rachel Cheng, Joseph Jen-Tse Huang, and Jim-Min Fang. “Degradation of Neurodegenerative Disease- Associated TDP-43 Aggregates and Oligomers via a Proteolysis-Targeting Chimera.” Journal of Biomedical Science 30, no. 1 (April 26, 2023): 27. https://doi.org/10.1186/s12929-023-00921-7.

Uchida, Tsukasa, Yoshitaka Tamaki, Takashi Ayaki, Akemi Shodai, Seiji Kaji, Toshifumi Morimura, Yoshinori Banno, et al. “CUL2-Mediated Clearance of Misfolded TDP-43 Is Paradoxically Affected by VHL in Oligodendrocytes in ALS.” Scientific Reports 6, no. 1 (January 11, 2016): 19118. https://doi.org/10.1038/srep19118.

Vandoorne, Tijs, Koen Veys, Wenting Guo, Adria Sicart, Katlijn Vints, Ann Swijsen, Matthieu Moisse, et al. “Differentiation but Not ALS Mutations in FUS Rewires Motor Neuron Metabolism.” Nature Communications 10, no. 1 (September 12, 2019): 4147. https://doi.org/10.1038/s41467-019-12099-4.

Volkert, Michael R., and David J. Crowley. “Preventing Neurodegeneration by Controlling Oxidative Stress: The Role of OXR1.” Frontiers in Neuroscience 14 (2020). https://www.frontiersin.org/articles/10.3389/fnins.2020.611904.

Walker, Adam K., Krista J. Spiller, Guanghui Ge, Allen Zheng, Yan Xu, Melissa Zhou, Kalyan Tripathy, Linda K. Kwong, John Q. Trojanowski, and Virginia M.-Y. Lee. “Functional Recovery in New Mouse Models of ALS/FTLD after Clearance of Pathological Cytoplasmic TDP-43.” Acta Neuropathologica 130, no. 5 (November 2015): 643–60. https://doi.org/10.1007/s00401-015-1460-x.

Wang, Peng, Jianwen Deng, Jie Dong, Jianghong Liu, Eileen H. Bigio, Marsel Mesulam, Tao Wang, et al. “TDP-43 Induces Mitochondrial Damage and Activates the Mitochondrial Unfolded Protein Response.” PLOS Genetics 15, no. 5 (May 17, 2019): e1007947. https://doi.org/10.1371/journal.pgen.1007947.

Wang, Wenzhang, Li Li, Wen-Lang Lin, Dennis W. Dickson, Leonard Petrucelli, Teng Zhang, and Xinglong Wang. “The ALS Disease-Associated Mutant TDP-43 Impairs Mitochondrial Dynamics and Function in Motor Neurons.” Human Molecular Genetics 22, no. 23 (December 1, 2013): 4706–19. https://doi.org/10.1093/hmg/ddt319.

Wen, Xinmei, Wenzhi Tan, Thomas Westergard, Karthik Krishnamurthy, Shashirekha S. Markandaiah, Yingxiao Shi, Shaoyu Lin, et al. “Antisense Proline-Arginine RAN Dipeptides Linked to C9ORF72- ALS/FTD Form Toxic Nuclear Aggregates That Initiate In Vitro and In Vivo Neuronal Death.” Neuron 84, no. 6 (December 17, 2014): 1213–25. https://doi.org/10.1016/j.neuron.2014.12.010.

Wicks, Paul. “The ALS Ice Bucket Challenge – Can a Splash of Water Reinvigorate a Field?” Amyotrophic Lateral Sclerosis and Frontotemporal Degeneration 15, no. 7–8 (December 1, 2014): 479–80. https://doi.org/10.3109/21678421.2014.984725.

Wijesekera, Lokesh C., and P. Nigel Leigh. “Amyotrophic Lateral Sclerosis.” Orphanet Journal of Rare Diseases 4, no. 1 (February 3, 2009): 3. https://doi.org/10.1186/1750-1172-4-3.

Wils, Hans, Gernot Kleinberger, Jonathan Janssens, Sandra Pereson, Geert Joris, Ivy Cuijt, Veerle Smits, Chantal Ceuterick-de Groote, Christine Van Broeckhoven, and Samir Kumar-Singh. “TDP-43 Transgenic Mice Develop Spastic Paralysis and Neuronal Inclusions Characteristic of ALS and Frontotemporal Lobar Degeneration.” Proceedings of the National Academy of Sciences of the United States of America 107, no. 8 (February 23, 2010): 3858–63. https://doi.org/10.1073/pnas.0912417107.

Winton, Matthew J., Lionel M. Igaz, Margaret M. Wong, Linda K. Kwong, John Q. Trojanowski, and Virginia M.-Y. Lee. “Disturbance of Nuclear and Cytoplasmic TAR DNA-Binding Protein (TDP-43) Induces Disease-like Redistribution, Sequestration, and Aggregate Formation *.” Journal of Biological Chemistry 283, no. 19 (May 9, 2008): 13302–9. https://doi.org/10.1074/jbc.M800342200. (a)

Winton, Matthew J., Vivianna M. Van Deerlin, Linda K. Kwong, Wuxing Yuan, Elisabeth McCarty Wood, Chang-En Yu, Gerard D. Schellenberg, et al. “A90V TDP-43 Variant Results in the Aberrant

Localization of TDP-43 In Vitro." FEBS Letters 582, no. 15 (June 25, 2008): 2252–56. https://doi.org/10.1016/j.febslet.2008.05.024. (b)

Wymer, James, Stephen Apple, Antoinette Harrison, and Bryan Alan Hill. "Pharmacokinetics, Bioavailability, and Swallowing Safety With Riluzole Oral Film." Clinical Pharmacology in Drug Development 12, no. 1 (2023): 57–64. https://doi.org/10.1002/cpdd.1168.

Xiao, Shangxi, Teresa Sanelli, Helen Chiang, Yulong Sun, Avijit Chakrabartty, Julia Keith, Ekaterina Rogaeva, Lorne Zinman, and Janice Robertson. "Low Molecular Weight Species of TDP-43 Generated by Abnormal Splicing Form Inclusions in Amyotrophic Lateral Sclerosis and Result in Motor Neuron Death." Acta Neuropathologica 130, no. 1 (July 1, 2015): 49–61. https://doi.org/10.1007/s00401-015-1412-5.

Xu, Lu, Tanxin Liu, Lili Liu, Xiaoying Yao, Lu Chen, Dongsheng Fan, Siyan Zhan, and Shengfeng Wang. "Global Variation in Prevalence and Incidence of Amyotrophic Lateral Sclerosis: A Systematic Review and Meta-Analysis." Journal of Neurology 267, no. 4 (April 1, 2020): 944–53. https://doi.org/10.1007/s00415-019-09652-y. (a)

Xu, Ya-Fei, Tania F. Gendron, Yong-Jie Zhang, Wen-Lang Lin, Simon D'Alton, Hong Sheng, Monica Castanedes Casey, et al. "Wild-Type Human TDP-43 Expression Causes TDP-43 Phosphorylation, Mitochondrial Aggregation, Motor Deficits, and Early Mortality in Transgenic Mice." The Journal of Neuroscience: The Official Journal of the Society for Neuroscience 30, no. 32 (August 11, 2010): 10851–59. https://doi.org/10.1523/JNEUROSCI.1630-10.2010.

Xu, Yichi, Ruanmin Zou, Jing Wang, Zhi-wei Wang, and Xueqiong Zhu. "The Role of the Cancer Testis Antigen PRAME in Tumorigenesis and Immunotherapy in Human Cancer." Cell Proliferation 53, no. 3 (February 5, 2020): e12770. https://doi.org/10.1111/cpr.12770. (b)

Xue, Yuanchao, Kunfu Ouyang, Jie Huang, Yu Zhou, Hong Ouyang, Hairi Li, Gang Wang, et al. "Direct Conversion of Fibroblasts to Neurons by Reprogramming PTB-Regulated MicroRNA Circuits." Cell 152, no. 1 (January 17, 2013): 82–96. https://doi.org/10.1016/j.cell.2012.11.045.

Yokoshi, Moe, Quan Li, Munetaka Yamamoto, Hitomi Okada, Yutaka Suzuki, and Yukio Kawahara. "Direct Binding of Ataxin-2 to Distinct Elements in 3′ UTRs Promotes mRNA Stability and Protein Expression." Molecular Cell 55, no. 2 (July 17, 2014): 186–98. https://doi.org/10.1016/j.molcel.2014.05.022.

Yoshino, Hiide, and Akio Kimura. "Investigation of the Therapeutic Effects of Edaravone, a Free Radical Scavenger, on Amyotrophic Lateral Sclerosis (Phase II Study)." Amyotrophic Lateral Sclerosis 7, no. 4 (January 1, 2006): 247–51. https://doi.org/10.1080/17482960600881870.

Zamani, Akram, Adam K. Walker, Ben Rollo, Katie L. Ayers, Raysha Farah, Terence J. O'Brien, and David
K. Wright. "Impaired Glymphatic Function in the Early Stages of Disease in a TDP-43 Mouse Model of Amyotrophic Lateral Sclerosis." Translational Neurodegeneration 11, no. 1 (March 15, 2022): 17. https://doi.org/10.1186/s40035-022-00291-4.

Zhang, Yingsha, ChangHui Pak, Yan Han, Henrik Ahlenius, Zhenjie Zhang, Soham Chanda, Samuele Marro, et al. “Rapid Single-Step Induction of Functional Neurons from Human Pluripotent Stem Cells.” Neuron 78, no. 5 (June 5, 2013): 785–98. https://doi.org/10.1016/j.neuron.2013.05.029. (a)

Zhang, Zhijun, Sandra Almeida, Yubing Lu, Agnes L. Nishimura, Lingtao Peng, Danqiong Sun, Bei Wu, et al. “Downregulation of MicroRNA-9 in iPSC-Derived Neurons of FTD/ALS Patients with TDP-43 Mutations.” PLOS ONE 8, no. 10 (October 15, 2013): e76055. https://doi.org/10.1371/journal.pone.0076055. (b)